SHOCK-WAVE AND HIGH-STRAIN-RATE PHENOMENA IN MATERIALS

EDITED BY
MARC A. MEYERS
LAWRENCE E. MURR
KARL P. STAUDHAMMER

CRC Press
Taylor & Francis Group

SHOCK-WAVE AND HIGH-STRAIN-RATE PHENOMENA IN MATERIALS

MECHANICAL ENGINEERING

A Series of Textbooks and Reference Books

Editor

L. L. Faulkner
Columbus Division, Battelle Memorial Institute
and Department of Mechanical Engineering
The Ohio State University
Columbus, Ohio

1. *Spring Designer's Handbook,* Harold Carlson
2. *Computer-Aided Graphics and Design,* Daniel L. Ryan
3. *Lubrication Fundamentals,* J. George Wills
4. *Solar Engineering for Domestic Buildings,* William A. Himmelman
5. *Applied Engineering Mechanics: Statics and Dynamics,* G. Boothroyd and C. Poli
6. *Centrifugal Pump Clinic,* Igor J. Karassik
7. *Computer-Aided Kinetics for Machine Design,* Daniel L. Ryan
8. *Plastics Products Design Handbook, Part A: Materials and Components; Part B: Processes and Design for Processes,* edited by Edward Miller
9. *Turbomachinery: Basic Theory and Applications,* Earl Logan, Jr.
10. *Vibrations of Shells and Plates,* Werner Soedel
11. *Flat and Corrugated Diaphragm Design Handbook,* Mario Di Giovanni
12. *Practical Stress Analysis in Engineering Design,* Alexander Blake
13. *An Introduction to the Design and Behavior of Bolted Joints,* John H. Bickford
14. *Optimal Engineering Design: Principles and Applications,* James N. Siddall
15. *Spring Manufacturing Handbook,* Harold Carlson
16. *Industrial Noise Control: Fundamentals and Applications,* edited by Lewis H. Bell
17. *Gears and Their Vibration: A Basic Approach to Understanding Gear Noise,* J. Derek Smith
18. *Chains for Power Transmission and Material Handling: Design and Applications Handbook,* American Chain Association
19. *Corrosion and Corrosion Protection Handbook,* edited by Philip A. Schweitzer

20. *Gear Drive Systems: Design and Application,* Peter Lynwander
21. *Controlling In-Plant Airborne Contaminants: Systems Design and Calculations,* John D. Constance
22. *CAD/CAM Systems Planning and Implementation,* Charles S. Knox
23. *Probabilistic Engineering Design: Principles and Applications,* James N. Siddall
24. *Traction Drives: Selection and Application,* Frederick W. Heilich III and Eugene E. Shube
25. *Finite Element Methods: An Introduction,* Ronald L. Huston and Chris E. Passerello
26. *Mechanical Fastening of Plastics: An Engineering Handbook,* Brayton Lincoln, Kenneth J. Gomes, and James F. Braden
27. *Lubrication in Practice: Second Edition,* edited by W. S. Robertson
28. *Principles of Automated Drafting,* Daniel L. Ryan
29. *Practical Seal Design,* edited by Leonard J. Martini
30. *Engineering Documentation for CAD/CAM Applications,* Charles S. Knox
31. *Design Dimensioning with Computer Graphics Applications,* Jerome C. Lange
32. *Mechanism Analysis: Simplified Graphical and Analytical Techniques,* Lyndon O. Barton
33. *CAD/CAM Systems: Justification, Implementation, Productivity Measurement,* Edward J. Preston, George W. Crawford, and Mark E. Coticchia
34. *Steam Plant Calculations Manual,* V. Ganapathy
35. *Design Assurance for Engineers and Managers,* John A. Burgess
36. *Heat Transfer Fluids and Systems for Process and Energy Applications,* Jasbir Singh
37. *Potential Flows: Computer Graphic Solutions,* Robert H. Kirchhoff
38. *Computer-Aided Graphics and Design: Second Edition,* Daniel L. Ryan
39. *Electronically Controlled Proportional Valves: Selection and Application,* Michael J. Tonyan, edited by Tobi Goldoftas
40. *Pressure Gauge Handbook,* AMETEK, U.S. Gauge Division, edited by Philip W. Harland
41. *Fabric Filtration for Combustion Sources: Fundamentals and Basic Technology,* R. P. Donovan
42. *Design of Mechanical Joints,* Alexander Blake
43. *CAD/CAM Dictionary,* Edward J. Preston, George W. Crawford, and Mark E. Coticchia
44. *Machinery Adhesives for Locking, Retaining, and Sealing,* Girard S. Haviland
45. *Couplings and Joints: Design Selection, and Application,* Jon R. Mancuso

46. *Shaft Alignment Handbook,* John Piotrowski
47. *BASIC Programs for Steam Plant Engineers: Boilers, Combustion, Fluid Flow, and Heat Transfer,* V. Ganapathy
48. *Solving Mechanical Design Problems with Computer Graphics,* Jerome C. Lange
49. *Plastics Gearing: Selection and Application,* Clifford E. Adams
50. *Clutches and Brakes: Design and Selection,* William C. Orthwein
51. *Transducers in Mechanical and Electronic Design,* Harry L. Trietley
52. *Metallurgical Applications of Shock-Wave and High-Strain-Rate Phenomena,* edited by Lawrence E. Murr, Karl P. Staudhammer, and Marc A. Meyers
53. *Magnesium Products Design,* Robert S. Busk
54. *How to Integrate CAD/CAM Systems: Management and Technology,* William D. Engelke
55. *Cam Design and Manufacture: Second Edition; with cam design software for the IBM PC and compatibles, disk included,* Preben W. Jensen
56. *Solid-State AC Motor Controls: Selection and Application,* Sylvester Campbell
57. *Fundamentals of Robotics,* David D. Ardayfio
58. *Belt Selection and Application for Engineers,* edited by Wallace D. Erickson
59. *Developing Three-Dimensional CAD Software with the IBM PC,* C. Stan Wei
60. *Organizing Data for CIM Applications,* Charles S. Knox, with contributions by Thomas C. Boos, Ross S. Culverhouse, and Paul F. Muchnicki
61. *Computer-Aided Simulation in Railway Dynamics,* by Rao V. Dukkipati and Joseph R. Amyot
62. *Fiber-Reinforced Composites: Materials, Manufacturing, and Design,* P. K. Mallick
63. *Photoelectric Sensors and Controls: Selection and Application,* Scott M. Juds
64. *Finite Element Analysis with Personal Computers,* Edward R. Champion, Jr., and J. Michael Ensminger
65. *Ultrasonics: Fundamentals, Technology, Applications: Second Edition, Revised and Expanded,* Dale Ensminger
66. *Applied Finite Element Modeling: Practical Problem Solving for Engineers,* Jeffrey M. Steele
67. *Measurement and Instrumentation in Engineering: Principles and Basic Laboratory Experiments,* Francis S. Tse and Ivan E. Morse
68. *Centrifugal Pump Clinic: Second Edition, Revised and Expanded,* Igor J. Karassik

69. *Practical Stress Analysis in Enineering Design: Second Edition, Revised and Expanded,* Alexander Blake
70. *An Introduction to the Deisgn and Behavior of Bolted Joints: Second Edition, Revised and Expanded,* John H. Bickford
71. *High Vacuum Technology: A Practical Guide,* Marsbed H. Hablanian
72. *Pressure Sensors: Selection and Application,* Duane Tandeske
73. *Zinc Handbook: Properties, Processing, and Use in Design,* Frank Porter
74. *Thermal Fatigue of Metals,* Andrzej Weronski and Tadeuz Hejwowski
75. *Classical and Modern Mechanisms for Engineers and Inventors,* Preben W. Jensen
76. *Handbook of Electronic Package Design,* edited by Michael Pecht
77. *Shock-Wave and High-Strain-Rate Phenomena in Materials,* edited by Marc A. Meyers, Lawrence E. Murr, and Karl P. Staudhammer
78. *Industrial Refrigeration: Principles, Design and Applications,* P. C. Koelet

Additional Volumes in Preparation

Mechanical Engineering Software

Spring Design with an IBM PC, Al Dietrich

Mechanical Design Failure Analysis: With Failure Analysis System Software for the IBM PC, David G. Ullman

SHOCK-WAVE AND HIGH-STRAIN-RATE PHENOMENA IN MATERIALS

EDITED BY
MARC A. MEYERS
University of California, San Diego
La Jolla, California

LAWRENCE E. MURR
University of Texas at El Paso
El Paso, Texas

KARL P. STAUDHAMMER
Los Alamos National Laboratory
Los Alamos, New Mexico

CRC Press
Taylor & Francis Group
Boca Raton London New York

CRC Press is an imprint of the
Taylor & Francis Group, an informa business

Library of Congress Cataloging-in-Publication Data

Shock–wave and high-strain-rate phenomena in materials / edited by
Marc A. Meyers, Lawrence E. Murr, Karl P. Staudhammer.
p. cm. – (mechanical engineering)
ISBN 0-8247-8579-7
1. Deformations (Mechanics) 2. Shock (Mechanics) I. Meyers,
Marc A. II. Murr, Lawrence E. III. Staudhammer, Karl P.
IV. Series: Mechanical engineering (Marcel Dekker, Inc.)
TA417.6.S46 1992
620.1'126–dc20 92-3830
CIP

This book is printed on acid-free paper.

MARCEL DEKKER, INC.
270 Madison Avenue, New York, New York 10016

Current printing (last digit):
10 9 8 7 6 5 4 3 2 1

PRINTED IN THE UNITED STATES OF AMERICA

Foreword John S. Rinehart Award

This award is being established to recognize outstanding effort and creative work in the science and technology of dynamic processes in materials. This encompasses the processes by which materials are welded, formed, compacted, and synthesized, as well as dynamic deformation, fracture, and the extreme shock loading effects. The award is named after a true pioneer who witnessed and actively contributed to the field for over forty years.

This award will be given every five years, at the occasion of the EXPLOMET conferences. The selection of the first two awards, announced in August 1990, was made by a committee composed of the EXPLOMET chairmen and Dr. J. S. Rinehart. In subsequent years, the awardees will chair the committee for future awards. A permanent committee is in such a way established to select the nominees. In selecting the individuals, special attention will be given to the balance between fundamental science and technological implementation.

John S. Rinehart has not only witnessed, but actively taken part in the development of the field of dynamic deformation. He has dedicated his life to the study of stress waves in solids; the results of these investigations have been published in over 130 technical articles and three books, two of them co-authored by John Pearson. *Behavior of Metals Under Impulsive Loads, Explosive Working of Metals* and *Stress Transients in Solids*, have been the *vade mecum* of all scientists and engineers throughout the world working in the field. The simple, no-nonsense, yet fundamentally correct approach used by Dr. Rinehart combines the rigorousness of the physicist with the practicality of the engineer. His fifty-year career has been divided between government and university, and he has frequently served as a consultant to industry. He has occupied many positions of high responsibility throughout his career. Director of Research and Development for the U.S. Coast and Geodetic Survey, Director of the Mining Research Laboratory of the Colorado School of Mines, which he founded, Assistant Director of the Smithsonian Astrophysical Observatory, Head of the Mechanics Branch at the Naval Ordnance Test Station, China Lake, Professor of Mechanical Engineering at the University of Colorado. Dr. Rinehart was associated with Dr. E. J. Workman's Ordnance Research Group before this activity became a division of the New Mexico Institute of Mining and Technology in the early 1950s.

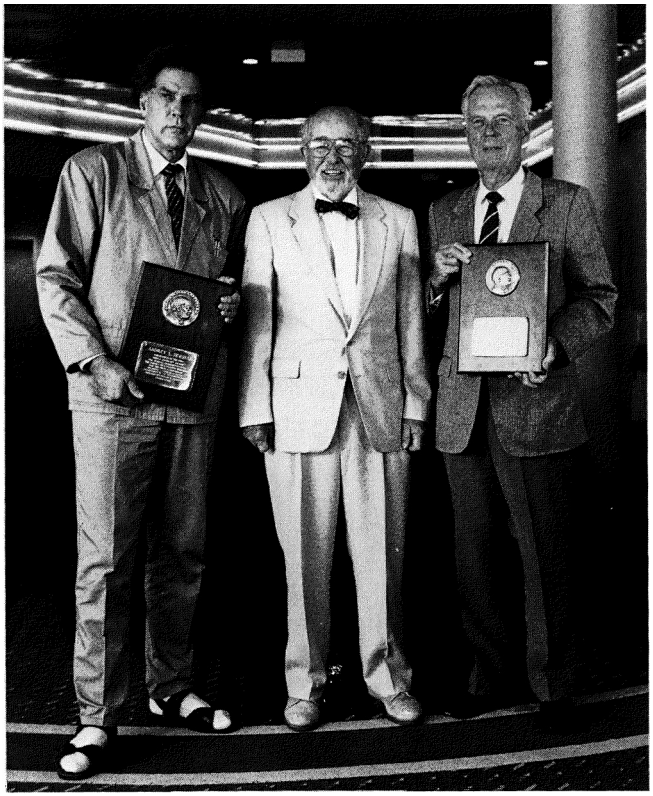

John S. Rinehart (center) personally gave the awards to the co-recipients Andrey Deribas (left) and Mark Wilkins (right).

INSCRIPTIONS

Andrey A. Deribas, co-recipient of the 1990 John S. Rinehart Award for seminal contributions to the theory of explosive welding, for the first experiments of shock synthesis and for leadership in the technological implementation of explosive fabrication. Mark L. Wilkins, co-recipient of the 1990 John S. Rinehart Award for seminal contributions to the development of hydrocodes, for their application to a multitude of dynamic problems and for leadership in the technological implementation of shock compaction.

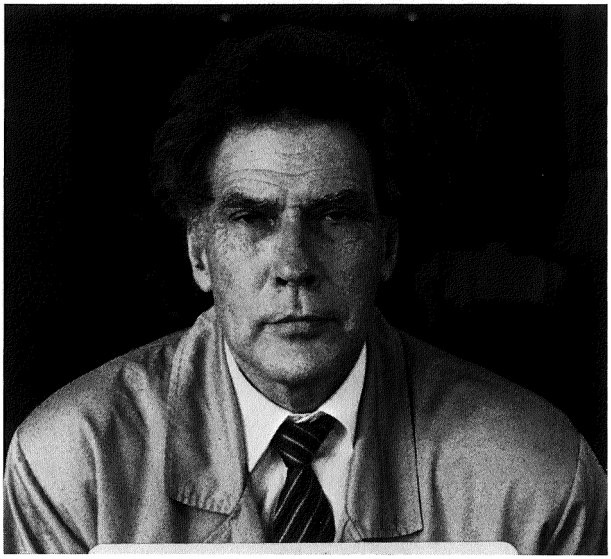

ANDREY A. DERIBAS

A.A. Deribas was born in 1931 in Moscow. He graduated from Lomonosov University in Moscow in 1953. His field of specialization is mechanics of continuous media. He initiated his research in the field of physics of explosions in 1956. He joined the Siberian Branch of the U.S.S.R. Academy of Sciences from the very beginning with his advisor, Academician Laverentiev, one of its founders. The first scientific results in the field of the explosive hardening of metals were obtained by him in 1960. Investigations on the explosive welding of metals have been carried out since 1961. His first results in the field of explosive compaction of powders and explosive synthesis of new materials took place in 1963. He was the head of the Laboratory of the Institute of Hydrodynamics in Novosibirsk. Research on the localization of explosion was initiated there and the metallic explosive chambers were created. He is the author of over 100 scientific papers and 25 inventions, and there have been two editions of his monograph "Physics of Explosive Welding and Hardening of Metals." Since 1976 he has been the Head of the Special Design Office of High-Rate Hydrodynamics in Novosibirsk. He has a Doctor of Science degree and is a Professor at the Electro-Technological School in Novosibirsk. He is a corresponding member of the U.S.S.R. Academy of Sciences. He was awarded the Lenin Prize for Science, the Prize of Council of Ministry of the U.S.S.R. for Science, and many other awards.

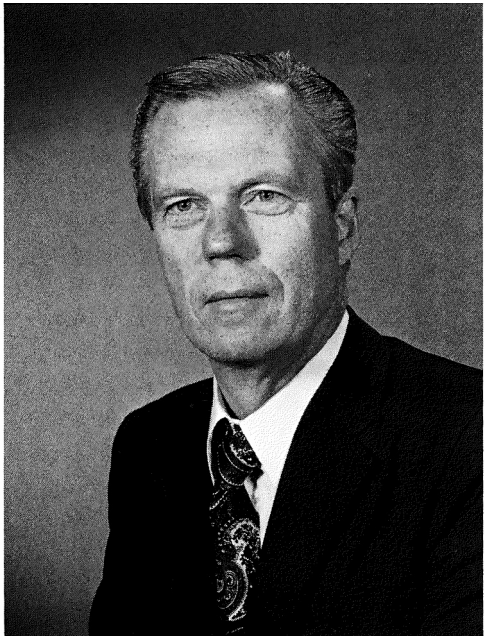

MARK L. WILKINS

Mark Wilkins joined the Lawrence Livermore National Laboratory (LLNL) in 1952, the year it was founded. He developed some of the major computer simulation programs used in the design of nuclear arms. He pioneered the application of large computers to simulate material behavior in the engineering application of materials. The numerical techniques are in current use world-wide. He has been a guest lecturer at some of the leading universities and laboratories in the United States, Europe, and Asia. During the early days of the space program he worked on modeling the effects of micrometeorite impacts. During the period 1967 to 1970, he led a research project sponsored by the Defense Advanced Research Projects Agency (DARPA) to develop a fundamental understanding of penetration mechanics. In 1973 he founded a new division in the Physics Department at LLNL for experimental and theoretical research on the behavior of materials. He has published over 70 scientific papers on modeling the behavior of materials and the simulation of physical phenomena.

Preface

This book contains the proceedings of EXPLOMET 90, the third of the EXPLOMET series. This quinquennial frequency is well suited for a realistic appraisal of progress in the field. Shock wave and high-strain-rate phenomena in materials are a vast subject that has, since World War II, evolved into a coherent body of knowledge with foundations in the basic sciences of physics, chemistry, and materials science, inputs from a variety of disciplines, and broad technological applications.

The expansion of this field and its redirection can be gauged by the evolution of participation and principal themes since the inception of EXPLOMET, in 1980. Concomitantly, the emphasis of the principal research thrusts has shifted throughout the years. A constant effort throughout this period has been the fundamental study of materials response under shock loading conditions.

This book is divided into ten sections in which the chapters have been organized in a logical sequence. Section I deals with high-strain-rate deformation, while Section II covers shock and combustion synthesis. Dynamic compaction is described in Section III. Section IV (shaped charge phenomena) presents a detailed and unique coverage of this important area. Shear localization (shear bands) is the subject of Section V; dynamic fracture is presented in Section VI. Another novel area of research, shock phenomena and superconductivity, is covered in Section VII. Section VIII deals with progress in shock waves and shock loading, while Section IX introduces a third novel topic of great importance: shock and dynamic phenomena in ceramics. Finally, the traditional topics of explosive welding and metal working are given in Section X.

The contents of this book, its organizational structure, and the emphasis on materials effects are intended to make it a useful research tool for practicing scientists and engineers, as well as a teaching tool in specialized curricula dealing with dynamic effects in materials. The contributors to this book represent thirteen countries in the world; over 40 percent of the contributors are from outside the United States. Therefore, these proceedings represent a global and up-to-date appraisal of this field.

The International Conference on the Materials Effects of Shock-Wave and High-Strain-Rate Phenomena, held at the University of California, San Diego in La Jolla, California, in August 1990 was sponsored by the U.S. Army Research Office, Materials Science Division (under contract ARO DAAL-03-90-G-0068), Los Alamos National Laboratory, Center of Excellence for Advanced Materials, and University of Texas at El Paso. We gratefully acknowledge this support. The chapters composing this book required retyping and editing to ensure a reasonably coherent format. Because of the extensive retyping it is likely that we may have missed typographical errors in our review process. We will assume responsibility for these remaining errors. We would like to thank Megan Harris and Faye Ekberg (University of Texas at El Paso), Debra Vigil and Carol Cole (Los Alamos National Laboratory), and Kay Baylor (UCSD) for their competent typing.

Marc A. Meyers
Lawrence E. Murr
Karl P. Staudhammer

Contents

SECTION IV: SHAPED CHARGE PHENOMENA

SHOCK-WAVE AND HIGH-STRAIN-RATE PHENOMENA IN MATERIALS

Section I
High-Strain-Rate Deformation

1

Dynamic Deformation and Failure

SIA NEMAT-NASSER

Center of Excellence for Advanced Materials
Department of Applied Mechanics and Engineering Sciences
University of California, San Diego
La Jolla, CA, USA, 92093

Dynamic deformation, flow, and fracture are integral parts of all dynamic processes in materials. At one extreme is ductile plastic flow with associated failure modes by shear banding or void nucleation, growth, and coalescence. At the other end are brittle fracturing, microcracking, and pulverization. A systematic scientific study of these phenomena, with a view toward a constitutive description and computational simulation of the involved processes, has been the focus of research at UCSD's Center of Excellence for Advanced Materials, over the last few years. This research has included the development of state-of-the-art dynamic probes for recovery experiments at strain rates ranging from quasi-static to $10^6/s$*, or greater, with associated time- and spatially-resolved data acquisition facilities and techniques. This has been paralleled by systematic material characterization and observation, and consequent physically-based micromechanical modeling with computational simulation of the dynamic response and failure modes. In the course of this effort, a number of novel experimental techniques have been developed, which provide powerful means of exploring and quantifying microstructural evolution in a variety of materials, from single and polycrystalline metals to ceramics and ceramic composites.*

This paper briefly reviews some of these experimental techniques and the associated diagnostics, focusing attention on novel Hopkinson bar techniques for recovery experiments. Application of these techniques to study, for example, void collapse in fcc and bcc metals, to probe material response at extremely high strains and strain rates, the phenomenon of adiabatic shear banding, and microcracking and phase transformation, are presented elsewhere in these proceedings.

I. INTRODUCTION

Dynamic processes refer to high-rate events generally associated with rapid deposition and/or transmission of energy through shock or other modes of wave motion. They can be used: (1) to develop fundamental understanding of material response under extreme pres-

sures, temperatures, and deformation and reaction rates; (2) to create new materials with unique microstructures and, hence, properties; and (3) to monitor dynamic events in materials and to probe and characterize the corresponding inelastic flow, fracture, and failure modes. These are necessary ingredients for developing physically-based mathematical and computational models for predicting synthesis, processing, structural changes, and response and failure modes over a broad range of pressures, temperatures, and deformation rates. At one extreme is ductile plastic flow with associated failure modes by shear banding or void nucleation, growth, and coalescence. At the other end is brittle fracturing, microcracking, and pulverization; see Fig. 1.

This conference addresses three main topics in dynamic processes in materials, i.e., dynamic synthesis and processing; dynamic deformation and fracture; and dynamic probing into materials; see Fig. 2. My comments are focused on *dynamic deformation and failure modes*. My basic aim is to outline some recent innovations, specifically developed to explore certain fundamental ingredients in the dynamic deformation and failure modes of materials. These are:

* Relation between microstructure and thermomechanical properties;
* Quantitative evaluation of response and failure modes;
* Physically-based constitutive models.

Central to a program which effectively implements these ingredients into an integrated research plan, are *dynamic recovery experiments*. In such experiments the microstructural evolution is related to the loading history, as well as to the thermomechanical response. Based on microstructural characterization, micromechanical models are developed and used to construct physically-based constitutive relations with quantitatively predictive capabilities. The constitutive models are then embedded through constitutive algorithms, into large-scale dynamic computer programs, to simulate the material response, the response of the structural elements made of these materials, as well as the synthesis and processing that lead to the creation of such materials. Figure 3a provides an outline emphasizing the key role that recovery experiments play in this sequence of events.

At the University of California, San Diego's (UCSD's) Center of Excellence for Advanced Materials (CEAM), we have made a number of key innovations over the past four years, which specifically focus on addressing the elements in Fig. 3a. While it will not be possible to examine all aspects of this activity, I will focus attention on some innovations in recovery experiments, particularly using the Hopkinson bar technique, and then comment on a breakthrough in computational algorithms for large-strain large-strain-rate rate-dependent, as well as rate-independent plastic flow of materials. Before doing this, I would like to point out that, in addition to the Hopkinson bar technique, we have made interesting innovations in the use of plate impact experiments for strain rates exceeding

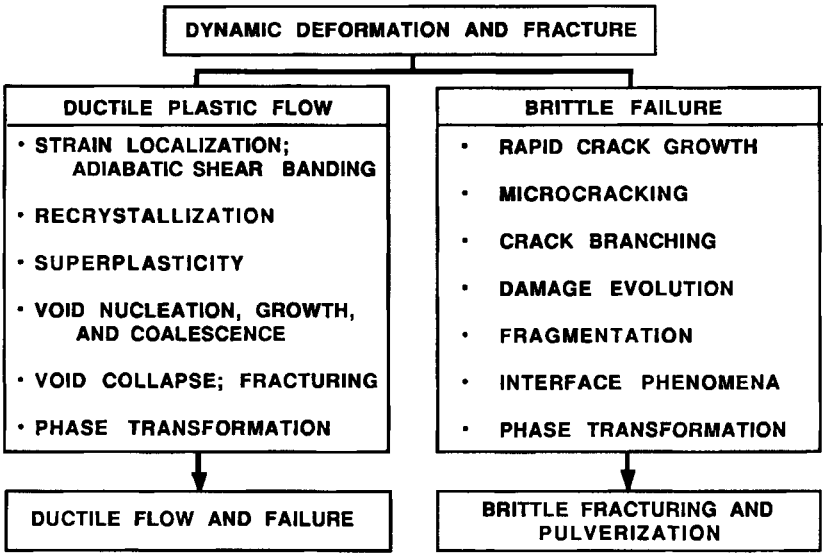

FIG. 1 *Major issues in dynamic deformation and failure modes of ductile and brittle materials.*

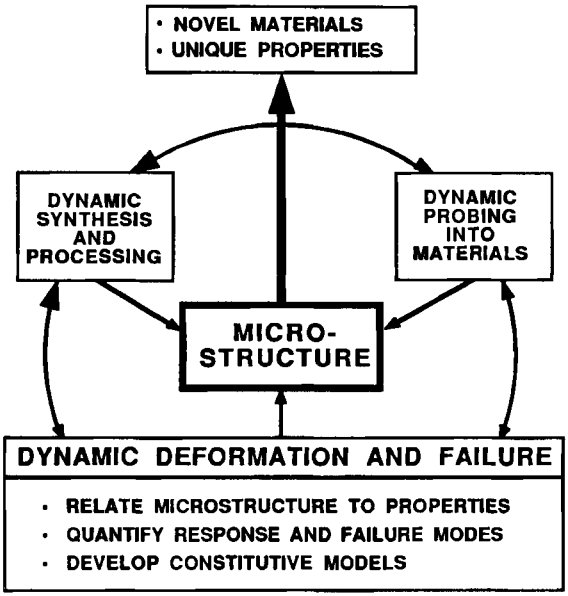

FIG. 2 *Dynamic processing in materials includes dynamic synthesis and processing, dynamic deformation and failure, and dynamic probing into materials: This conference addresses all three topics.*

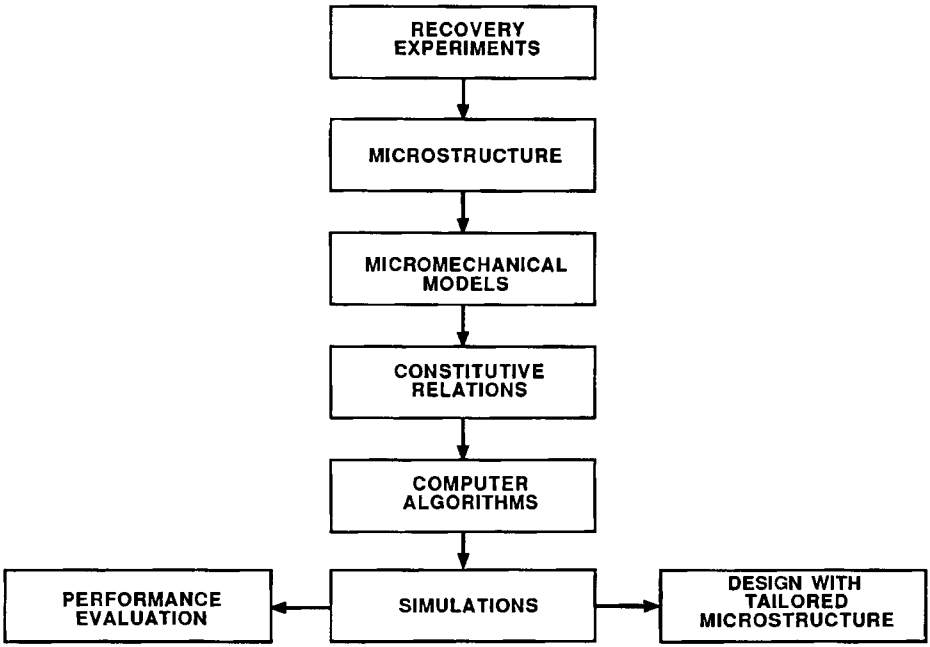

(a)

DYNAMIC RECOVERY EXPERIMENTS

- **NOVEL SPLIT HOPKINSON BAR TECHNIQUES**
  - Pulse-Shaping
  - Stress-Reversal
  - Full Pulse Trapping
  - Direct Multi-Axial Strain Measurements
- **PLATE IMPACT EXPERIMENTS**
  - Normal Plate Impact
  - Novel Configuration
  - Full Pulse Trapping
  - Oblique Plate Impact (Pressure-Shear)
  - Full Interferometric Measurements
- **LASER-INDUCED STRESS PULSE**
  - Very High Stress Amplitude
  - Very Short Pulse Duration
  - Full Pulse Trapping
  - Time-Resolved Measurements

(b)

FIG. 3 *(a) Dynamic recovery experiments play a central role in relating microstructure to dynamic properties, in developing micromechanical models for physically-based constitutive relations which can be used through constitutive algorithms in large-scale computer codes to simulate response and failure modes, to design microstructure for desired performance, and to evaluate materials and structural performance ; (b) UCSD's dynamic recovery techniques.*

$10^5/s$, and in the use of laser-induced stress pulses with extremely short--of the order of nanoseconds-- durations and high amplitudes. Figure 3b outlines these, and brief accounts can be found in Nemat-Nasser *et al.* [1], and Nemat-Nasser [2].

As illustrations of the application of these techniques, we note here our observations on plastic flow of fcc and bcc single and polycrystals, both at extremely high strains and strain rates with concomitant shear localization and fracturing, as well as phase transformation, dynamic fracturing, and microcracking of ceramics containing partially stabilized zirconia precipitates; see Nemat-Nasser and Chang [3], Rogers and Nemat-Nasser [4], Ramesh *et al.* [5], and Beatty *et al.* [6].

For ductile metals, the mechanism of void collapse has been used to probe material response at extremely high strains and strain rates, using the Hopkinson bar technique; see Chang and Nemat-Nasser [7]. It is observed that materials behave in a unique manner which has not been explored in these regimes. For example, when the void collapses under pure compression at high strain rates, dynamic recrystallization can take place in an extremely short period of time, and ductile materials such as pure single-crystal copper, can fracture in a seemingly brittle manner, with microcracks extending *normal to the applied compression* (a seemingly paradoxical result), into the newly formed crystals. This result brings into focus the importance of strain and strain rate histories in the mechanical response of crystalline solids. Because of this and related issues, innovative Hopkinson bar techniques developed at UCSD, which allow the subjecting of specimens to well-defined stress pulses for recovery experiments, are of central importance. For example, one is able to subject the sample to a single tension pulse, a single compression pulse, a compression pulse followed by a tension pulse, or any desired combination, with complete trapping for recovery analysis and characterization. The techniques also permit the study of microcracking in ceramics, with full recovery.

II. NOVEL TECHNIQUES FOR HOPKINSON BAR RECOVERY EXPERIMENTS

A. COMPRESSION EXPERIMENT

The split Hopkinson bar dynamic compression testing technique was invented by Kolsky in 1949, following the pioneering work of John and Bertram Hopkinson [8] [9] [10], and Davis [11].

In this approach, the dynamic stress-strain relation in uniaxial compression of a material is obtained by sandwiching a small sample between two elastic bars of common cross-sectional area and elasticity, called the *incident* bar and the *transmission* bar, respectively. An elastic stress pulse is imparted into the incident bar by striking it with a striker bar of given cross-sectional area and elasticity. By ensuring that all three bars remain elastic,

plastic deformation is induced in the (usually) ductile sample. The stress in the sample is obtained by measuring the transmitted pulse, and the strain of the sample is calculated from the pulse reflecting off the sample back into the incident bar, where it is measured by means of a strain gauge attached to this bar; see Fig. 4.

This classical Hopkinson bar technique is *not* suitable for recovery tests, since the reflected pulse in the incident bar is again and again reflected back into this bar, subjecting the sample to repeated compression loads. To remedy this major stumbling block in recovery experiments with the split Hopkinson bar, a novel fixture has been developed at UCSD's CEAM, which generates in the incident bar a *compression pulse followed by a tension pulse*. In this manner, once the tensile pulse, which tails the compression, reaches the interface between the sample and the incident bar, the sample is softly recovered, having been subjected to a known compressive pulse. As is discussed below, the shape and amplitude of this compressive pulse can be controlled, and hence the sample can be subjected to a pre-assigned stress history in this experiment.

UCSD's loading fixture for the *stress reversal Hopkinson bar* consists of an incident bar with a *transfer flange* at its loading end, and an *incident tube* resting at the one end against the transfer flange, and at the other end, against a *reaction mass*, as shown in Fig. 5a. The incident bar, the incident tube, and the striker are of the same material (maraging steel) and cross-sectional area, i.e., they have a common impedance. The striker and the incident tube have the same length. When the striker bar impacts the transfer flange of the incident bar, the same axial compression is generated in the incident bar, incident tube, and the striker. The pulse in the incident bar travels toward the sample at the longitudinal elastic wave velocity C_0, whereas the compression in the incident tube reflects back as *compression*, once it reaches the interface with the reaction mass. This compression travels back and loads the incident bar in tension, through the transfer flange. This tensile loading takes place at exactly the instant when the release tensile pulse, which has been reflected off the free end of the striker, reaches the interface with the transfer flange. The striker and the transfer flange begin to move at a third of the impact velocity opposite the impact direction, for a short time, until the striker separats from the transfer flange, bouncing back at a third of its initial impact speed. Figure 5b shows a typical stress pulse generated by this technique.

B. PULSE SHAPING

If the length of the sample is denoted by l, then it is easy to show that the strain rate in the sample is given by $\dot{\varepsilon} = -2\frac{C_0}{l}\varepsilon_r$, where ε_r is the strain reflected off the sample into the incident bar. A *constant* strain rate is attained by imparting a *rectangular pulse* to the incident bar.

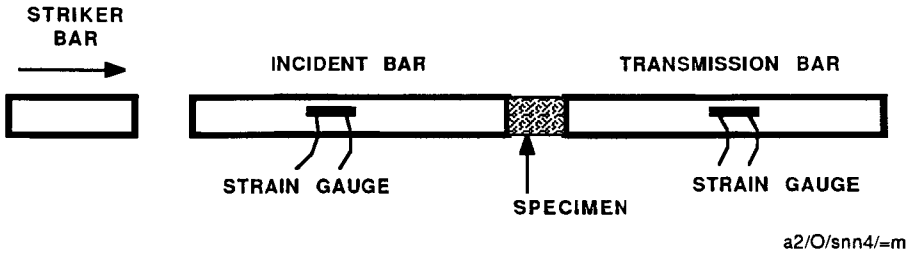

FIG. 4 *Classical compression Hopkinson bar: An elastic compressive stress pulse is imparted into the incident bar by striking it with a striker bar. The sample is subjected to repeated loading as the pulse reflects back and forth along the two bars.*

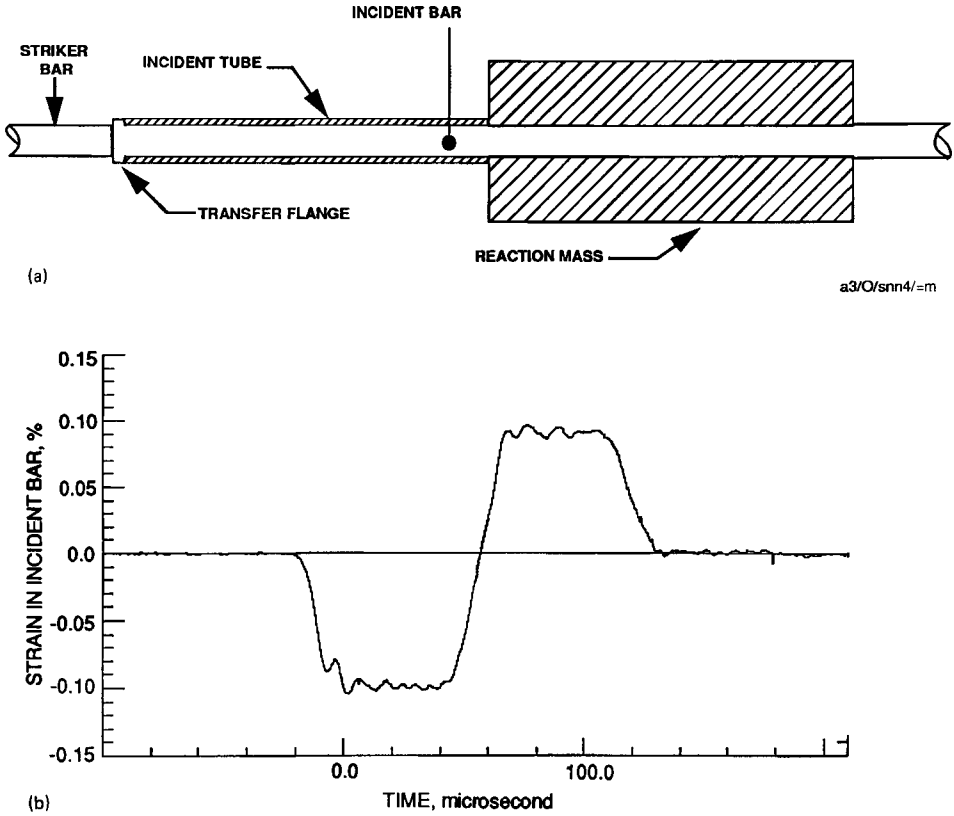

FIG. 5 *UCSD's stress reversal Hopkinson bar technique: (a) the loading fixture; (b) a typical stress pulse generated by this technique.*

For application to very hard brittle materials such as ceramics and their composites which undergo very small strains before failing, it is often desirable to apply stress pulses with a gentle rise, in order to allow more gradual stressing of the sample. The strain rate in the sample will no longer be constant. However, a complete record of the stress and strain in the sample, as functions of time, can be obtained; this can be related to the corresponding damage evolution in the sample through post-test sample characterization.

At UCSD, pulse shaping is attained by placing a suitable metal (usually OFHC) cushion between the striker and the transfer flange, attached to the latter. A detailed analysis of the plastic deformation of this kind of cushions has been given by Nemat-Nasser *et al.* [12]. Depending on the size of the cushion relative to the bars, and the velocity and the length of the striker, different pulse shapes can be generated. Figures 6a and b

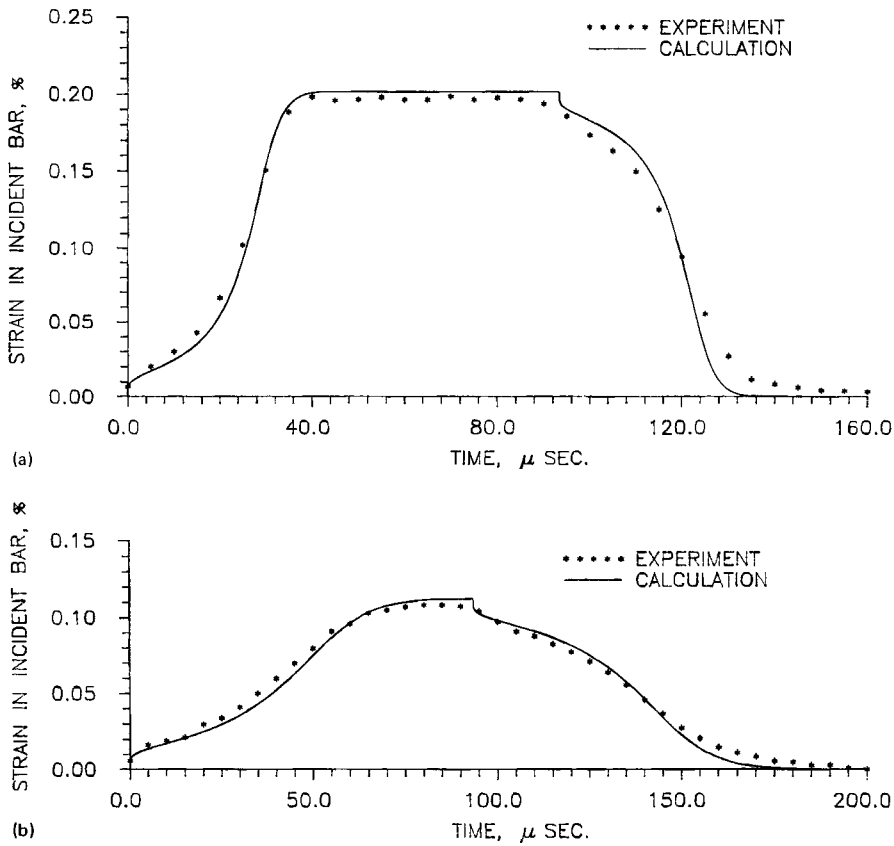

FIG. 6 *Pulse shaping: (a) for striker velocity of about 20 m/s; (b) for striker velocity of 11 m/s.*

show two extreme cases obtained using a copper cushion of 0.19" (4.8 mm) and 0.020" (0.51 mm) initial diameter and thickness, and a 3/4" (19 mm) striker of 9" (228.6 mm) length. Figure 6a is for a striker velocity of 19.72 m/sec, and Fig. 6b is for 11.02 m/sec. The theoretical prediction is based on incompressible, axisymmetric, rate-independent plastic flow of the cushion whose axial true stress, σ, and engineering (nominal) strain, ε, are related by a simple power-law, $\sigma = \sigma_0 \varepsilon^n$, where, for OFHC, direct experiments suggest $\sigma_0 \approx 570$ MPa and n=1/5.

An important point to bear in mind, in relation to dynamic testing of very hard and brittle samples, is that *the sample tends to indent the bars*, and, therefore, the reflected strain in the incident bar, ε_r, is *not* a measure of the strain rate in the sample.
At UCSD, we attach strain gauges to the sample and directly measure the axial as well as

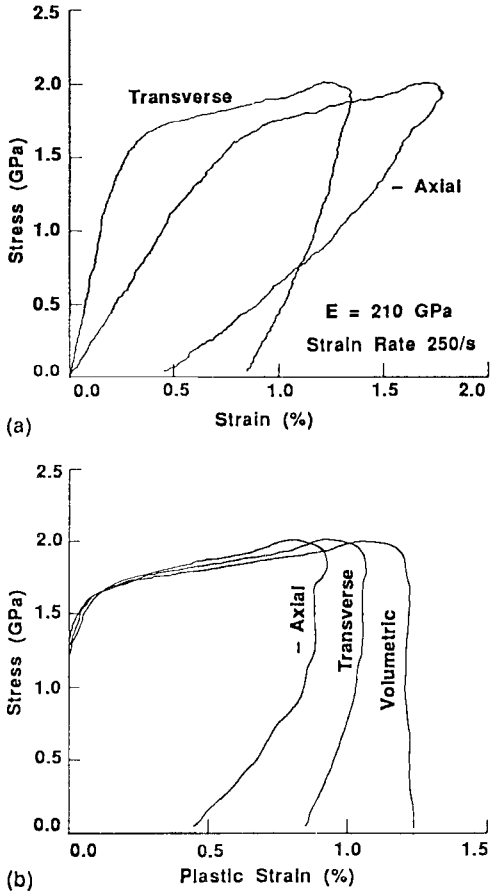

FIG. 7 *A typical result for Mg-PSZ; see Rogers and Nemat-Nasser (1990).*

the lateral strains of the sample as functions of time. A typical result for Mg-PSZ is shown in Fig. 7; see Rogers and Nemat-Nasser [4].

C. TENSION EXPERIMENT

The classical tension split Hopkinson bar has been used to obtain stress-strain relations of samples in unaxial stress, to *failure*; see Harding *et al.* [13] and Lindholm [14]. UCSD's novel technique allows for recovery experiments by trapping the compression pulse which reflects off the sample. The design of this apparatus is sketched in Fig. 8a. The loading fixture consists of a tubular striker riding on the incident bar which passes through a gas gun and terminates with a transfer flange at one end and the sample at the other end. A precision gap separates the transfer flange from a *momentum trap* bar. This gap is set such that when the striker has imparted to the incident bar the entire tensile pulse, the gap is

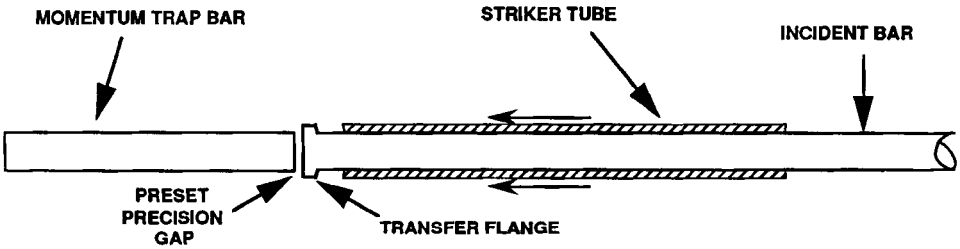

(a)

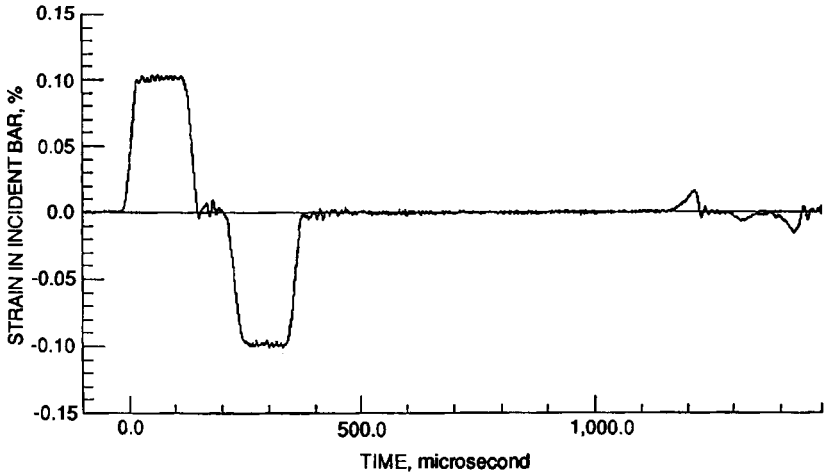

(b)

FIG. 8 *UCSD's momentum trapping technique for tension Hopkinson bar: (a) the loading fixture with momentum trap bar and precision gap; (b) a typical stress pulse generated by this technique (note that the pulse reflected off the sample is almost completely trapped).*

closed. Upon reflection as compression off the sample interface, this reflected pulse is then transmitted into the momentum trap bar and is trapped there. An example is shown in Fig. 8b.

In closing this section, we point out that it is also possible to perform *recovery* experiments with the sample having been subjected to a compression pulse *and* a tension pulse, using a modified version of the stress reversal Hopkinson technique. This requires redesigning the end of the transmission bar in contact with the sample such that, after the sample is subjected to compression and tensile pulses, it is pulled off the transmission bar; see Nemat-Nasser *et al.* [12] for details. This apparatus then allows study of the Bauschinger effect under dynamic loading.

III. MODELING AND COMPUTATION

A major component of UCSD's program is the development of physically-based constitutive models capable of predicting dynamic deformation, prior to and beyond failure. For dynamic flow of metals, this modeling includes effects such as strain rate, thermal softening, and workhardening due to plastic strain accumulation, and microstructural effects such as texture, crystal structure, precipitates, and voids or inclusions. In addition, through a series of careful experiments, attempts are made to include the *strain-rate history* effects which, up to now, have not been included in constitutive models used in large-scale codes. Recent experiments by Rashid [15] at UCSD have shown that the dislocation structures in single-crystal pure copper critically depend on the *strain-rate history*. Parallel with the above experiments and modeling, and as an important part of our program, has been the development of efficient and robust computer constitutive algorithms for implementation in dynamic computer codes.

Here we summarize the results of a recent breakthrough in explicit constitutive computational algorithms for finite-element calculations of large-deformation rate-independent and rate-dependent elastoplasticity, using a simple example based on the J_2 plasticity theory with isotropic hardening. The new algorithm provides a direct, explicit, and always nearly exact estimate of all stress components, and any internal variable that may be involved, for any prescribed deformation (or time) increment (large or small) in *one single step,* or in any desired number of substeps. The algorithm can accommodate nonsmooth yield surfaces (for rate-independent materials). This generalization is discussed elsewhere; Nemat-Nasser [2]. Here *as an illustration* we consider a *simple case* where the plastic part, $\boldsymbol{D}^p$, of the deformation rate, $\boldsymbol{D}$ is given by

$$\boldsymbol{D}^p = \dot{\gamma}\,\boldsymbol{\mu}, \tag{1}$$

where

$$\boldsymbol{\mu} = \boldsymbol{\tau}'/(\sqrt{2}\,\tau), \qquad \tau = (\tfrac{1}{2}\boldsymbol{\tau}':\boldsymbol{\tau}')^{1/2}, \qquad \boldsymbol{\tau}' = \boldsymbol{\tau} - \frac{1}{3}\boldsymbol{I}\,tr\,\boldsymbol{\tau}. \tag{2}$$

Clearly

$$\boldsymbol{\mu}:\boldsymbol{\mu} = 1, \quad \boldsymbol{\mu}:\dot{\boldsymbol{\mu}} = 0, \quad \dot{\gamma} = \boldsymbol{\mu}:\boldsymbol{D}^p. \tag{3}$$

The essential physics is embedded in the quantity $\dot{\gamma}$. As *an illustration*, consider the following power law

$$\dot{\gamma} = \dot{\gamma}_0 \left[\frac{\tau}{\tau_r}\right]^m, \tag{4}$$

where $\dot{\gamma}_0$ and τ_r are the reference strain rate and the associated reference flow stress. When m is very large, this model simulates rate-independent plasticity. For moderate values of m, the rate effect becomes dominant. For the rate-independent case, we consider the simple example of the yield condition,

$$f \equiv \tau - F(\gamma; \ldots). \tag{5}$$

In (4), τ_r, and in (5), F, represent the resistance of the material to plastic flow. They thus embody workhardening, temperature softening, and all related microstructural evolutions which have preceded the current state.

Models used for plasticity computations have generally been based on constitutive relations which do *not* include the effects of *strain-rate history* on the plastic flow of the material. In the present illustration, this means that, e.g., τ_r is regarded a function of only the accumulated plastic strain,

$$\gamma = \int_0^t \dot{\gamma}\, dt, \tag{6}$$

as well as the temperature, but not the strain-rate history. Although it is now generally accepted that hardening depends not only on the total plastic deformation, but also on the *deformation-rate history* experienced by the material, for simplicity we will not address this issue here.

To be specific, we consider the rate-independent model first, and then comment on the rate-dependent case. In either case, we write the deformation tensor as

$$\boldsymbol{D} = \boldsymbol{D}^e + \boldsymbol{D}^p, \quad or \quad D_{ij} = D^e_{ij} + D^p_{ij}, \tag{7}$$

where the elastic deformation rate tensor, $\boldsymbol{D}^e$, relates to an objective stress rate, $\overset{\circ}{\boldsymbol{\tau}}$, through the current elasticity tensor, $\boldsymbol{C}$, by

$$\overset{\circ}{\boldsymbol{\tau}} = \boldsymbol{C}:\boldsymbol{D}^e, \quad or \quad \overset{\circ}{\tau}_{ij} = C_{ijkl} D^e_{kl}. \tag{8}$$

In (8), $\overset{\circ}{\boldsymbol{\tau}}$ is defined by

$$\overset{\circ}{\boldsymbol{\tau}} = \dot{\boldsymbol{\tau}} - \boldsymbol{\Omega}\boldsymbol{\tau} + \boldsymbol{\tau}\boldsymbol{\Omega}, \qquad or \quad \overset{\circ}{\tau}_{ij} = \dot{\tau}_{ij} - \Omega_{ik}\,\tau_{kj} + \tau_{ik}\,\Omega_{kj}\,, \tag{9}$$

where $\boldsymbol{\Omega}$ is an appropriate spin; see Nemat-Nasser [2] [16] [17]. While a proper choice of the objective stress is important -- especially in kinematic hardening -- it has no bearing on the new algorithm.

Let the current stress state be on the yield surface. Define a hardening parameter by $H = dF/d\gamma = \dot{\tau}/\dot{\gamma}$, and from (1), (7), and (8), obtain

$$\overset{\circ}{\boldsymbol{\tau}} = \boldsymbol{C} : (\boldsymbol{D} - \dot{\gamma}\boldsymbol{\mu}). \tag{10}$$

Then, calculating $\boldsymbol{\mu} : \overset{\circ}{\boldsymbol{\tau}}$ from this equation, we arrive at

$$\dot{\tau}(\hat{t})/A + \dot{\gamma}(\hat{t}) = d(\hat{t}), \qquad t < \hat{t} \le t + \Delta t\,, \tag{11}$$

where

$$\tau(\hat{t}) = F(\gamma(\hat{t})), \qquad \gamma(\hat{t}) = \int_0^{\hat{t}} \dot{\gamma}(\theta)\,d\theta\,,$$

$$d = (\boldsymbol{\mu} : \boldsymbol{C} : \boldsymbol{D})/(\boldsymbol{\mu} : \boldsymbol{C} : \boldsymbol{\mu}), \qquad A = (\boldsymbol{\mu} : \boldsymbol{C} : \boldsymbol{\mu})/\sqrt{2}; \tag{12}$$

for isotropic $\boldsymbol{C}$, $A = \sqrt{2}G$ (where G is the shear modulus) and $d = \boldsymbol{\mu} : \boldsymbol{D}$.

Assuming continuing plastic or neutral loading, i.e. $d(t) \ge 0$, we integrate (11) over the time increment to obtain

$$\tau(t + \Delta t) - \tau(t) + A\,\Delta\gamma = A\,d^*\,\Delta t\,, \tag{13}$$

where d^* is an *estimate* of the average value of $d(\hat{t})$ over the considered time increment; see Nemat-Nasser [2] for details. The main step in our algorithm is to tentatively assign the deviatoric part of the *total deformation rate tensor*, i.e. $\boldsymbol{D}'$, *over the entire time increment* to be only due to plastic flow, i.e., set $\boldsymbol{D}^p = \dot{\gamma}(\hat{t})\boldsymbol{\mu}(\hat{t}) \approx \boldsymbol{D}'(\hat{t})$, $t \le \hat{t} \le t + \Delta t$, and then seek to correct the error that this assignment has introduced. With this assignment, the yield condition at $t + \Delta t$ is approximated by

$$\tau_A(t + \Delta t) = F(\gamma(t) + d^*\Delta t) \tag{14}$$

which includes the error

$$\Delta_e\tau = \tau_A(t + \Delta t) - \tau(t + \Delta t). \tag{15}$$

The error in the function $\dot{\gamma}(\hat{t})$ over the considered time interval is

$$\dot{\gamma}_{er}(\hat{t}) = d(\hat{t}) - \dot{\gamma}(\hat{t}), \qquad t \le \hat{t} \le t + \Delta t . \tag{16}$$

Then the error in the value of γ at $t + \Delta t$, denoted by $\Delta_e \gamma$, is given by

$$\Delta_e \gamma = \int_t^{t+\Delta t} \dot{\gamma}_{er}(\theta)\, d\theta = \dot{\gamma}^*_{er} \Delta t , \tag{17}$$

where $\dot{\gamma}^*_{er}$ is the mean value of $\dot{\gamma}_{er}(\hat{t})$ over the time interval t to $t + \Delta t$.

From (13) to (17) we have

$$\begin{aligned} \tau(t + \Delta t) - \tau(t) &= A\, \dot{\gamma}^*_{er}\, \Delta t \\ &= \tau_A(t + \Delta t) - \tau(t) - \Delta_e \tau \end{aligned} \tag{18}$$

which is exact. We estimate $\Delta_e \tau$, by

$$\Delta_e \tau \approx H\, \Delta_e \gamma \approx H\, \dot{\gamma}^*_{er}\, \Delta t , \tag{19}$$

and arrive at

$$\tau(t + \Delta t) = \frac{A\, \tau_A(t + \Delta t) + H\, \tau(t)}{A + H} , \tag{20}$$

$$\dot{\gamma}^*_{er} = \frac{\tau_A(t + \Delta t) - \tau(t)}{(A + H)\Delta t} , \tag{21}$$

$$\Delta\gamma = (d^* - \dot{\gamma}^*_{er})\Delta t . \tag{22}$$

Equation (20) is a near-exact estimate of the yield surface after the incremental loading associated with the prescribed deformation rate tensor $\boldsymbol{D}$, over time increment Δt.

For elastic-viscoplastic constitutive models, with *no yield surface*, we examine an example where the effective plastic strain rate $\dot{\gamma}$ is related to the effective stress τ by (4), with the following flow stress:

$$\tau_r = \tau_0 (1 + \frac{\gamma}{\gamma_0})^N , \tag{23}$$

where γ_0 is the reference strain, and N is a material parameter. We follow essentially the same procedure, but replace the hardening parameter H by η which is defined by

$$\eta = \frac{\tau(t)}{\sqrt{2}G}\left[\frac{1}{m\,d\,\Delta t} + \frac{N}{\gamma_0 + \gamma(t)}\right]. \tag{24}$$

Then,

$$\tau_A(t+\Delta t) = \tau_{rA}(t+\Delta t)\left[\frac{d}{\gamma_0}\right]^{1/m}, \qquad \tau_{rA}(t+\Delta t) \equiv \tau_0\left[1 + \frac{\gamma(t) + d\,\Delta t}{\gamma_0}\right]^N. \tag{25}$$

Nemat-Nasser and Chung [18] have compared the results of this algorithm with the explicit effective tangent moduli method proposed by Peirce *et al.* [19]. It is shown that the new algorithm predicts the near-exact solution in a single step, while the effective tangent moduli method may require thousands of steps for similar accuracy. In Fig. 9 we show a typical result based on the following values of the constitutive parameters: $\gamma_0/\sqrt{3} = \tau_0/E = 6.25\times10^{-3}$ (E = Young's modulus, with Poisson's ratio $\nu = 0.3$) and $N = 0.08$. The dimension of stress is arbitrary. As is seen, the size of the timestep for the new algorithm is immaterial: *the new algorithm is explicit, very accurate, and always stable, independent of the size of the time increment.*

For the rate-independent case, we consider $F(\gamma) \equiv \tau_r$, where τ_r is given by (23), with $N = 0.2$. Figure 10 shows the corresponding stress-strain curve, using the new algorithm.

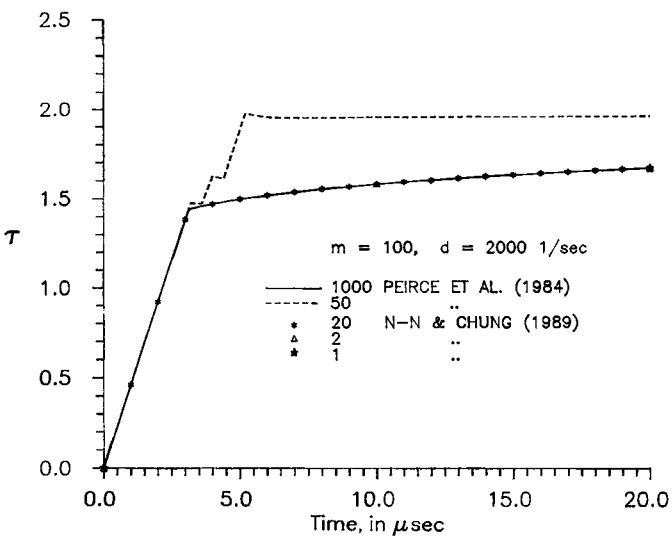

FIG. 9 *Performance demonstration of the new elastic-viscoplastic algorithm for power-law model (23) with m = 100 and flow stress (4); constitutive parameters are given after (25). The algorithm yields nearly exact results for any number of timesteps -- even one -- over the entire (unrealistically large) time increment.*

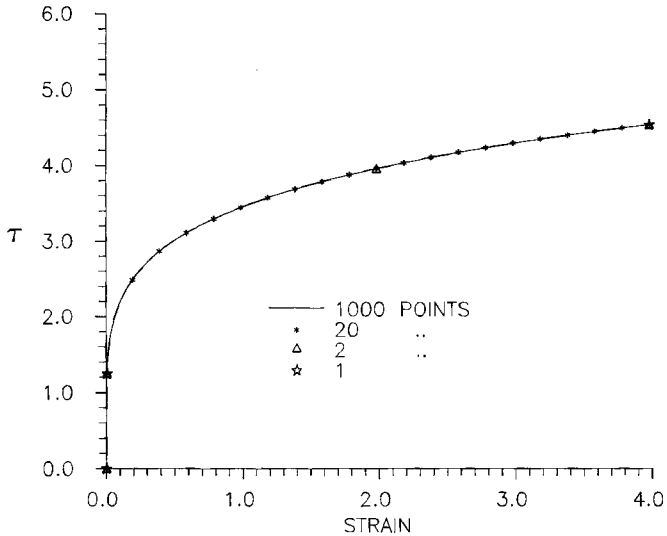

FIG. 10 *Performance demonstration of the new elastoplastic algorithm for power-law model (23). The algorithm yields nearly exact results for one, two, or any number of strain increments; strain of 4 corresponds to 640 times the initial yield strain, and the unit of stress is arbitrary.*

In this figure, the stress and strain units are arbitrary, but the strain of 4 corresponds to 640 γ_0, i.e. 640 units of the initial yield strain. As is seen, for an effective strain increment 640 times the yield strain, the exact point on the stress-strain curve is obtained in a *single strain increment* or in any desired number of strain increments. Nemat-Nasser [2] has extended this method to obtain near-exact stress components independently of the size of the time (or strain) increment.

ACKNOWLEDGMENT

The author wishes to thank Mr. Y.-F. Li for helping with the numerical illustrations. This work was supported by the U.S. Army Research Office under Contract No. DAAL-03-86-K-0169 with the University of California, San Diego.

REFERENCES

1. S. Nemat-Nasser, J. Isaacs, G. Ravichandran, and J. Starrett, Proceeding of TTCP TTP-1 Workshop on New Techniques of Small Scale High Strain Rate Studies, Australia (1989).
2. S. Nemat-Nasser, *Int'l J JSME,* Series 1, Japan Society of Mechanical Engineering, to appear (1991).

3. S. Nemat-Nasser and S.-N. Chang, *'90 Explomet Proceedings* (1991).
4. W. P. Rogers and S. Nemat-Nasser, *J. Amer. Cer. Soc.,* 73(1), pp. 136-39 (1990).
5. K. T. Ramesh, B. Altman, G. Ravichandran, and S. Nemat-Nasser, *Advances in Fracture Research,* ICF -7, pp. 811-817 (1989).
6. J. H. Beatty, L. W. Meyer, M. A. Meyers, and S. Nemat-Nasser, *'90 Explomet Proceedings* (1991).
7. S.-N. Chang and S. Nemat-Nasser, *'90 Explomet Proceedings* (1991).
8. B. Hopkinson, *Proc. Roy. Soc.* A, 74, p. 498 (1905).
9. B. Hopkinson, *Phil. Trans.* A, 213, p. 437 (1914).
10. J. Hopkinson, *Proc. Manch. Lit. Phil. Soc.,* 11, p. 40 (1872).
11. R. M. Davis, *Phil. Trans.* A, 2450, p. 3875 (1948).
12. S. Nemat-Nasser, J. Isaacs, and J. Starrett, in preparation (1991).
13. J. Harding, E. D. Wood, and J. D. Cambell, *J. Mech. Eng. Sci.,* 2, p. 88 (1960).
14. U. S. Lindholm, *J. Mech. Phys. Solids,* 12, p. 317 (1964).
15. M. Rashid, Ph.D. Thesis, University of California, San Diego (1990).
16. S. Nemat-Nasser, ASME *J. Appl. Mech.,* 50, pp. 1114-1126 (1983).
17. S. Nemat-Nasser, *Meccanica,* to appear (1990).
18. S. Nemat-Nasser and D.-T. Chung, *Comput. Methods in Appl. Mechanics and Eng.,* to appear (1991).
19. D. Pierce, C. F. Shih, and A. Needleman, *Comput. Struct.,* 18, 875-887 (1984).

2

Mechanical Behavior of Composite Materials Under Impact Loading

J. HARDING

Department of Engineering Science
University of Oxford
Parks Road, Oxford OX1-3PJ, U.K.

The problems of characterising the mechanical behaviour of composite materials under impact loading are discussed. Techniques for determining such behaviour for tensile, compressive and shear loading are described and some qualitative conclusions are drawn from the results obtained.

I. INTRODUCTION

The rate-dependence of the mechanical properties of metallic type materials may be determined using standard designs of test-piece. The macroscopic response of the bulk material, for well defined loading systems, may be related to data obtained in such tests and analytical functions, i.e. constitutive relationships, may be derived. These can then be used to describe the mechanical behaviour of structural components of different geometrical shapes and under more complex loading systems. For composite materials, however, where there are two or more phases present, several complicating factors arise. For example, the overall rate dependence of the composite will depend, to a greater or lesser extent, on the rate dependence of each of these various phases. Also of importance will be the reinforcement configuration, e.g. unidirectional, cross-ply or woven, and the type and direction of loading, e.g. tensile, shear or compressive. Thus for a unidirectionally-reinforced composite

under tensile loading in the fibre direction, where fibre fracture is likely to be the process controlling the failure of the composite, the fibre properties may be expected to determine the rate dependent behaviour. In contrast, for woven reinforced material loaded in compression in one of the principal directions of reinforcement, where a fibre buckling process is likely to control failure, the properties of the matrix will have a greater influence on the overall rate dependence.

A further complicating factor, however, for all multi-phase materials, is the presence of interfaces and hence the possibility of additional failure processes associated with the interface, for example, by deplying or interlaminar shear mechanisms. It becomes necessary, therefore, to consider whether the critical conditions under which such processes occur are also rate dependent.

In the light of these various factors it is clear that a full characterisation of the mechanical behaviour of composite materials at impact rates of straining is likely to require the use of a wider range of test configurations and test-piece designs than are commonly encountered in the testing of simpler single-phase metallic materials. The present review describes several of the techniques which have been used and discusses the results which have been obtained. Although in some of these tests it is difficult to distinguish between the various failure processes and their individual dependence on the rate of loading, so that a detailed interpretation of the results may not be possible, some general conclusions may be drawn.

II. REVIEW OF EXPERIMENTAL TECHNIQUES

Problems of data interpretation arise in all testing techniques used at impact rates of loading. For homogeneous isotropic metallic materials, however, these problems are least severe when the testing technique is based on the split Hopkinson pressure bar principle. For this reason all the experimental methods to be described here will also be based on this principle, although it is realised that for anisotropic multi-phase materials these difficulties may be greatly increased. Tensile, compressive and shear loading configurations will be considered, in each case with a design of test-piece intended to study, as far as possible, a single failure initiation process, although subsequent propagation of failure is likely to involve a complex interaction between several different failure processes.

In all Hopkinson-bar tests overall specimen dimensions need to be small, so as to

minimise radial inertia and wave propagation effects within the specimen, while care has to be taken in designing the method of load transfer between the specimen and the loading bars so as to avoid the introduction of a region of significant impedance mismatch which could introduce stress wave reflections and thus invalidate the Hopkinson-bar analysis. When composite specimens are to be tested the need for small overall specimen dimensions may conflict with the requirement for a specimen which is large relative to the scale of the reinforcement while the anisotropic nature of the composite material can complicate the design of the specimen/loading bar interface.

A. *TENSILE TESTING TECHNIQUES*

A tensile version of the Hopkinson-bar apparatus for use with composite specimens is shown schematically in fig. 1. A cylindrical projectile impacts the loading block and causes an elastic tensile loading wave to propagate along the loading bar towards the specimen and output bar. The thin strip specimen is waisted in the thickness direction and has a very slow taper so as to minimise stress concentrations due to free edge effects. The state of stress within the specimen has been investigated using a two-dimensional finite element analysis. It shows the biggest stress concentrations to be at the specimen/loading bar interface and to be significantly smaller than the controlling tensile stresses in the specimen gauge region which is in a state of uniform tension.

The specimen is fixed with epoxy adhesive into parallel-sided slots in the loading bars. Strain gauge signals from two stations on the input bar and one on the output bar allow the full dynamic stress-strain curve to be derived using the standard Hopkinson-bar analysis. However, since most composites fail at low or very low strains and may show a significant rate dependence of the initial elastic deformation, for the determination of which the Hopkinson-bar analysis is not very accurate, it is usual to make, in addition, a direct determination of the specimen elongation using a fourth set of strain gauges, attached to the specimen itself. A range of fibre reinforced polymeric materials have been tested in this way and the results compared with those obtained at lower rates of strain. Some of these results are summarised below and some tentative conclusions drawn.

Initial tests on a unidirectionally-reinforced carbon/epoxy material [1], loaded in

the reinforcement direction, at mean strain rates from ~0.0001/s to ~450/s, showed no effect of strain rate, see fig. 2a, on the tensile modulus, tensile strength or strain to failure; nor was there any effect of strain rate on the fracture appearance. Such behaviour is consistent with the conclusion that the tensile properties of the composite are entirely controlled by the carbon fibres the behaviour of which is entirely independent of strain rate. In contrast similar tests [2] on a plain coarse-weave carbon/epoxy material when loaded in a principal reinforcing direction, see fig. 2b, showed a small effect of strain rate on the initial tensile modulus and a more significant effect on the tensile strength and the elongation to failure. Here, however, the woven reinforcement geometry is likely to result in a stronger interaction with the matrix so that the rate dependent properties of the matrix play a more important role in the deformation process.

The rate dependence is much more marked when glass reinforcing fibres are used. Tensile stress-strain curves for a plain fine-weave glass/epoxy material [3] are shown in fig. 2c. The initial modulus and the tensile strength both increase very significantly with strain rate while, in contrast with the behaviour shown by the woven carbon/epoxy material, the overall elongation also increases with rate of loading. Part of this increased rate sensitivity may be due to a greater interaction with the matrix when a fine weave reinforcement is used. More important, however, is likely to be the rate dependent behaviour of the glass fibres themselves, the strength of which is expected to increase quite markedly at impact rates [4]. A direct confirmation of this in tensile tests on unidirectional glass/epoxy composites loaded in the reinforcement direction, however, did not prove possible. Although under quasi-static loading a tensile failure was obtained in the central gauge section of the specimen, under impact loading failure was invariably by the pull-out of glass-fibres from the matrix in the grip-regions of the specimen, see fig. 3, [5]. This implies that the ratio of the tensile strength of the glass fibres to the interfacial shear strength between the glass fibres and the epoxy matrix increases with increasing strain rate. This could be due either to an increase in the former or to a decrease in the latter.

Further evidence for the relative importance of the tensile to the shear strength in composite materials was obtained in tensile tests on some coarse satin-weave glass/polyester specimens, loaded in a principal reinforcement direction [6]. Here

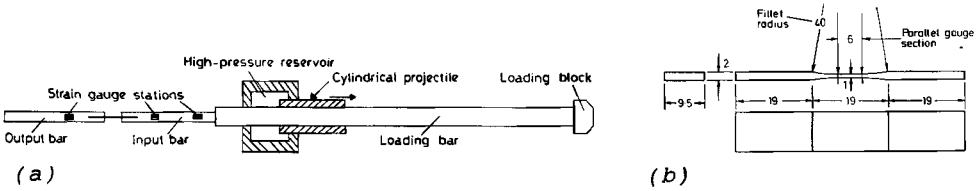

FIG. 1 *Tensile version of split Hopkinson bar (a) general assembly (schematic) (b) specimen design (dimensions in mm).*

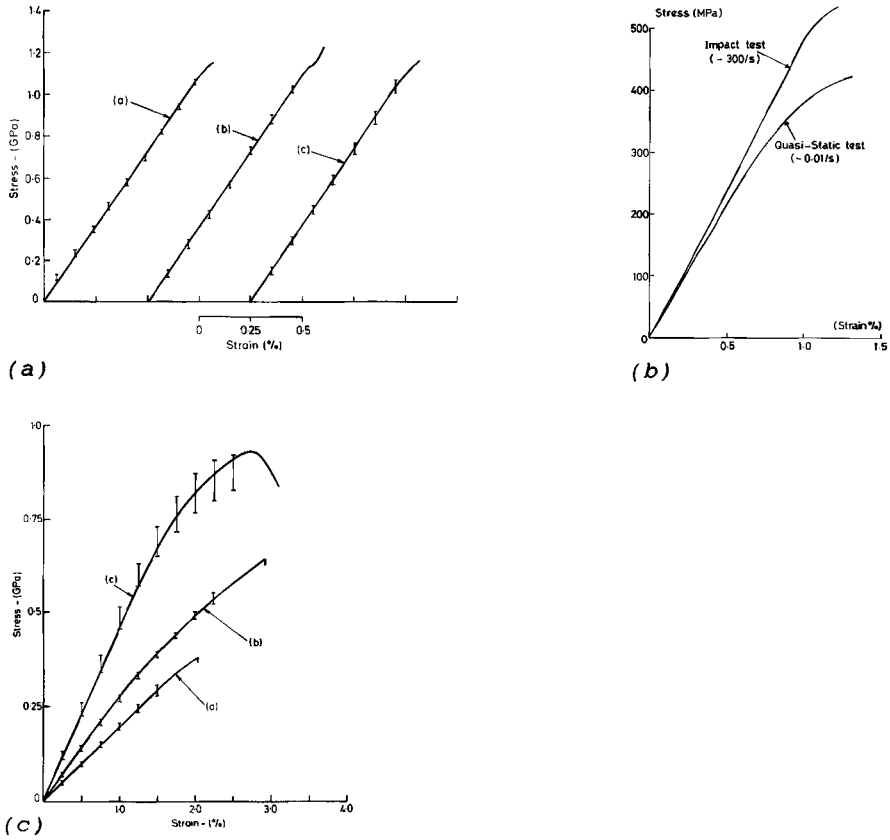

FIG. 2 *Effect of strain rate on tensile stress-strain curves for composite materials (a) unidirectional carbon/epoxy [mean strain rate (/s): a) - 0.0001; b) - 10; c) - 450;] (b) woven carbon/epoxy (c) woven glass/epoxy [mean strain rate (/s): a) - 0.0001; b) - 10; (c) - 900;].*

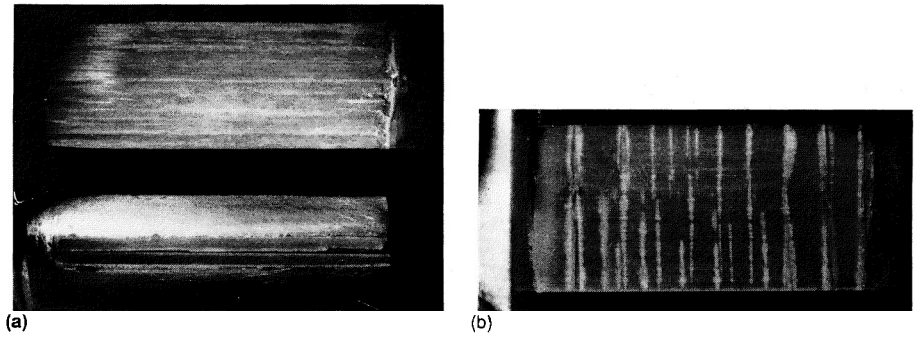

FIG. 3 *Tensile impact test on unidirectional glass/epoxy specimen (a) pull-out of fibre layer in grip region (b) unbroken gauge section showing debonding around matrix cracks.*

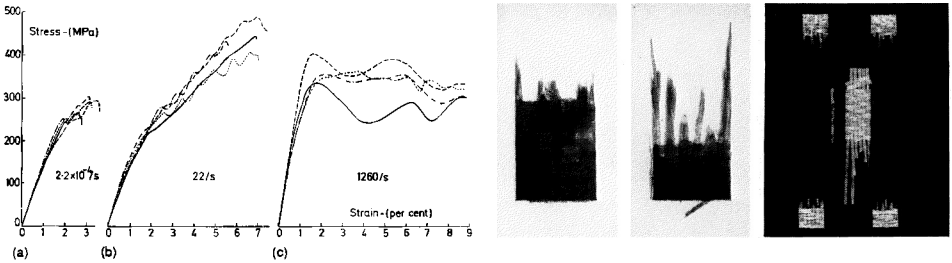

FIG. 4 Effect of strain rate on the tensile properties of a satin-weave glass/polyester composite at mean strain rates of (a) 0.0022/s; (b) 22/s; (c) 1260/s (a) stress-strain curves (b) fracture appearance.

there was a continuous change in both the stress-strain response, fig. 4a, and the fracture appearance, fig. 4b, from those observed at the quasi-static rate, where a tensile failure with limited fibre tow pull-out was obtained, to the medium rate, where a tensile failure was still obtained but fibre tow pull-out was very extensive and the overall strain to failure was quite high, ~7%, up to the impact rate, where failure was dominated by shear stresses giving pull-out of the whole central section of the specimen from the two ends with only limited tensile failure of individual fibre tows and an overall strain to failure of the order of 13%.

In the light of these results it is necessary to devise a technique for determining the effect of strain rate specifically on the shear strength of the composite specimen, i.e. both the interlaminar shear strength between adjacent reinforcing plies and the interfacial shear strength between fibre tows and the matrix.

B. SHEAR TESTING TECHNIQUES

Several techniques for determining the rate dependence of the interlaminar shear strength in composite materials have been devised. In two of these [7,8], both based on the torsional Hopkinson-bar, a very significant increase in shear strength with strain rate was observed for both woven and cross-ply glass/epoxy specimens. In contrast, a study of both the interlaminar and the transverse shear strength of a plain-weave carbon/epoxy laminate [9], using a test based on the double-notch shear version of the split Hopkinson-bar apparatus, showed no significant rate dependence. Unlike the previously described tensile tests, however, in none of these various shear tests was the specimen subjected to a well-defined stress system.

This problem has been tackled in a more recently developed test [10] which uses the "double-lap" shear specimen shown in fig. 5a. In this specimen, which has to be especially laid-up and cannot be cut from existing laminates, failure occurs on predetermined interlaminar planes. The strain distribution along one of these planes, as derived from a two-dimensional finite element analysis, gives the results shown in fig. 5b. It is clear that the shear strain on the interlaminar failure plane is very far from uniform. This is a problem common to most designs of shear specimen. It means that, although we may be able to determine the effect of strain rate on the critical load at which interlaminar shear failure occurs in the double-lap specimen, the corresponding shear stresses as estimated from the area of the interlaminar failure planes will only be representative values.

With this proviso it may be reported that all such measurements so far made, for a satin weave carbon/epoxy, a plain weave carbon/epoxy, a unidirectionally reinforced carbon/epoxy, a plain weave glass/epoxy and at the interface between plies of plain weave glass and a plain weave carbon in a hybrid carbon/glass/epoxy lay-up, showed a significant increase in the interlaminar shear strength at impact rates of loading. While these results clearly establish the general trend, the wide variations

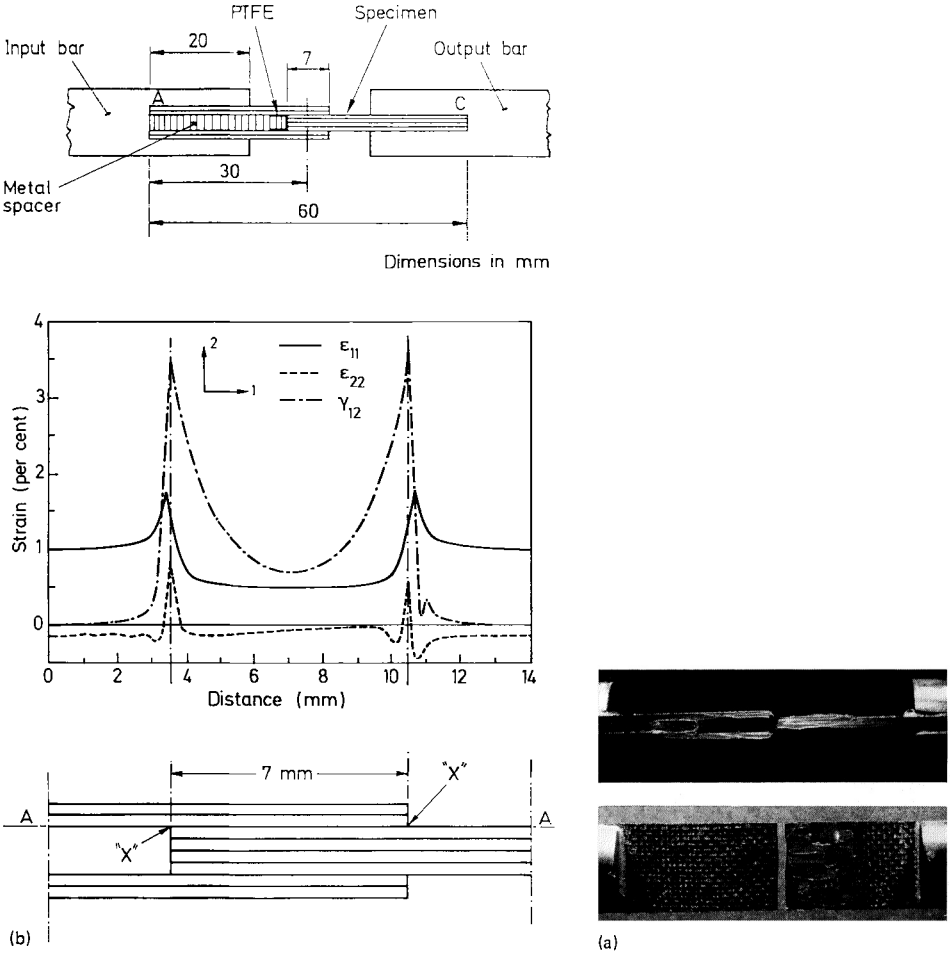

FIG. 5 *Interlaminar shear test (a) specimen design and fracture appearance (b) strain distribution on failure plane.*

in shear stress and shear strain along the interlaminar plane at failure make it difficult to determine from these tests a critical value of interlaminar shear stress for use in modelling damage accumulation processes in composites under impact loading.

C. COMPRESSIVE TESTING TECHNIQUES

The question of specimen design arises again when compressive impact testing of composite materials is considered. The standard design of specimen for use with the

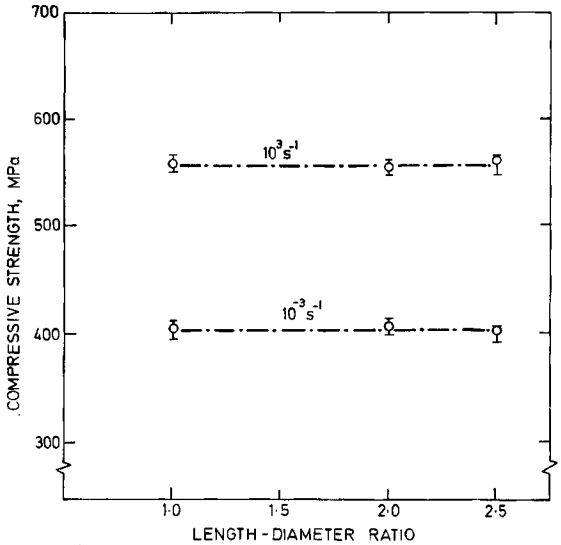

(a)

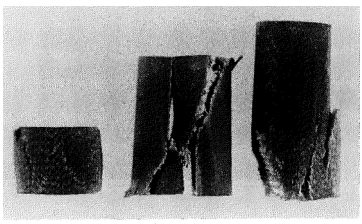

(b)

FIG. 6 *Effect of strain rate and specimen geometry on compressive behavior of woven glass/epoxy (a) ultimate compressive strength (b) quasi-static failure mode.*

compression Hopkinson-bar is a short cylinder of diameter slightly less than that of the loading bars. Most of the work on composite materials in the compression SHPB [11,12] has in fact used this design of specimen even though it is far from ideal for this type of material. In tests on a woven glass/epoxy laminate loaded in a principal reinforcing direction for specimens with different length to diameter ratio Parry [13] showed a significant increase in the ultimate compressive strength under impact loading, see fig. 6a. In the quasi-static tests failure was by a combination of shear and longitudinal splitting, see fig. 6b, with the possibility that failure was

initiated at the ends of the specimen. In the impact tests the specimens completely disintegrated preventing any conclusions from being drawn.

Some evidence that the initiation of compressive failure in woven glass/epoxy composites, at both quasi-static and impact rates, was by a shearing process was obtained in tests on cylindrical specimens reinforced with a single woven glass ply on a diametral plane [14]. The first sign of damage was a sudden drop in load on the stress-strain curve, see fig. 7a, corresponding to a shear failure across the axially-aligned fibre tow near the centre of the specimen, see fig. 7b. Nevertheless doubts clearly remain regarding the validity of data obtained using this design of specimen in the Hopkinson bar test.

However, since the specimen will only be subjected to transient loading, provided the loading bars are well aligned there is no reason why the waisted thin-strip tensile specimen of fig. 1b should not also be used in compression. It is close to the design recommended for the quasi-static compression testing of unidirectional carbon/epoxy specimens [15] and has the major advantage that failure is unlikely to be initiated by end effects at the specimen/loading bar interfaces.

Using this specimen design very marked increases in the compressive strength and the strain to failure under impact loading have been found [16] for both woven carbon and woven glass/epoxy specimens loaded in a principal reinforcing direction, see fig. 8. Failure initiates by shear across the central parallel region of the specimen on a plane inclined at ~45° to both the loading and the thickness directions, see fig. 9 for the glass/epoxy specimen. The damage zone is more extensive in the impacted specimens, corresponding to the much greater strain to failure.

III. DISCUSSION

Although considerable data are now becoming available on the impact mechanical response of fibre-reinforced composites, most of which show that there are quite significant effects which need to be taken into account, no clear picture is yet emerging on which to base a general approach, e.g. the development of some form of "constitutive relationship", which might be used to describe this behaviour. This may be for many reasons but perhaps primarily because the deformation of fibre reinforced polymers is essentially a damage accumulation process involving a large

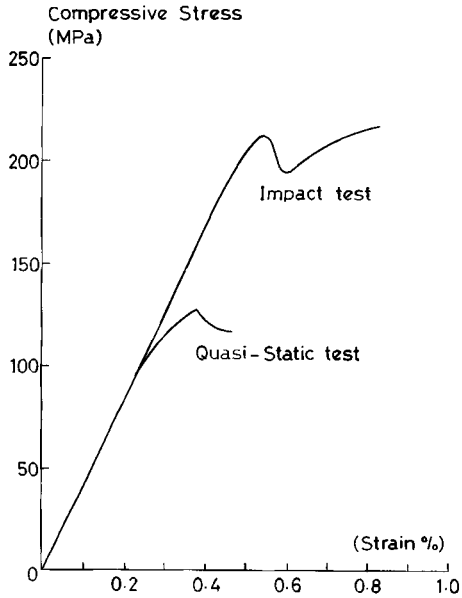

(a)

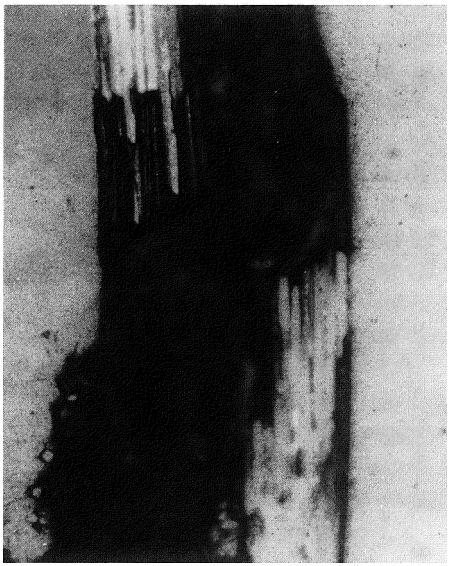

(b)

FIG. 7 *Initial compressive failure in single-layer reinforced glass/epoxy specimens (a) stress-strain curves (b) shear failure across axially-aligned roving.*

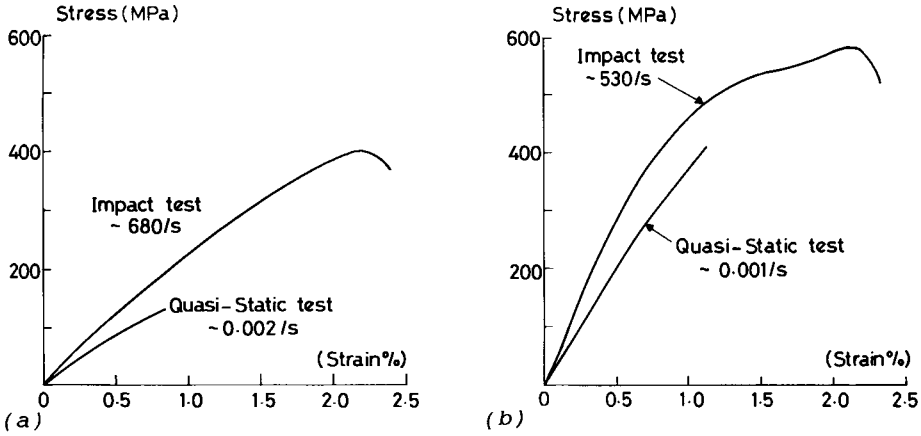

FIG. 8 *Effect of strain rate on the compressive stress-strain curves for thin strip specimens of (a) woven carbon/epoxy and (b) woven glass/epoxy.*

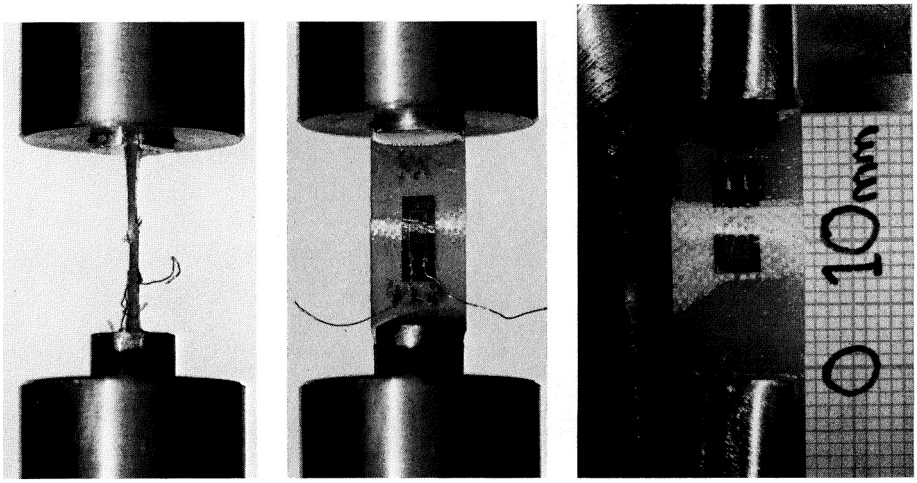

FIG. 9 *Effect of strain rate on compressive failure mode in thin strips specimens of woven glass/epoxy (a) quasi-static (b) impact*

number of different possible damage mechanisms. The testing techniques described above make some attempt to isolate and study some of these mechanisms. In other cases, e.g. in compression, the complex interaction between the fibres and the matrix make a detailed interpretation of the test data extremely difficult.

An attempt has been made [17] to apply finite element methods to the modelling of the tensile impact response of hybrid woven carbon/glass/epoxy laminates. Failure is assumed to initiate at an arbitrarily chosen site by the tensile fracture of an axially-aligned carbon tow and to be followed by limited delamination on adjacent interlaminar planes. The results obtained showed qualitative agreement with experiment but the technique cannot yet give a quantitative prediction of the hybrid impact behaviour.

IV. CONCLUSIONS

Testing techniques have been developed for studying the impact response of fibre-reinforced composites and for obtaining reliable data on their mechanical behaviour at high rates of strain. Care is required, however, in evaluating the data obtained if true "material properties" are to be derived and more work is needed if particular damage processes are to be isolated and their individual rate dependence determined.

V. ACKNOWLEDGMENT

Grateful acknowledgment is made to the Air Force Office of Scientific Research (AFSC), United States Air Force, from whom financial support was received, under Grant No. AFOSR-87-0129, during which much of the work reviewed above was performed.

REFERENCES

1. J. Harding and L. M. Welsh, in Proc ICCM IV, Fourth Int. Conf. on Composite Materials, Japan Soc. for Composite Materials, Tokyo, 1982, 845-852.
2. J. Harding, K. Saka and M. E. C. Taylor, Oxford University Engineering Laboratory Report No. 1654/1986
3. J. Harding and L. M. Welsh, J. Mater. Sci., 18, 1810-1826 (1983).

4. A. Rotem and J. M. Lifshitz, in Proc. 26th. Annual Tech. Conf. SPI, Reinforced Plastics/Composites Division, Society of Plastics Industry, New York, 1971, paper 10-G

5. L. M. Welsh and J. Harding, in Proc ICCM V, Fifth Int. Conf. on Composite Materials, TMS-AIME, 1985, 1517-1531.

6. L. M. Welsh and J. Harding, in Proc DYMAT 85, Mechanical and Physical Behaviour of Materials under Dynamic Loading, Jour. de Physique, Colloque C5, 1985, 405-414.

7. T. Parry and J. Harding, Colloque Int. du CNRS No. 319, Plastic Behaviour of Anistropic Solids, CNRS, Paris 1988, 271-288.

8. C. Y. Chiem and Z. G. Liu, in Proc IMPACT 87, Impact Loading and Dynamic Behaviour of Materials, DGM Informationsgesellschafft mbH, Oberursel, 1988, 2, 579-586.

9. S. M. Werner and C. K. H. Dharan, J. Comp. Mater., 20, 365-374 (1986)

10. J. Harding, Y. L. Li, K. Saka and M. E. C. Taylor, in Proc. 4th. Oxford Int. Conf. on Mech. Properties of materials at High Rates of Strain, Inst. of Phys. Conf. Series No. 102, Inst. of Physics, London and Bristol, 1989, 403-410.

11. L. J. Griffiths and D. J. Martin, J. Phys. D. Appl. Phys., 7, 2329-2341 (1974)

12. R. L. Sierakowski, G. E. Nevill, C. A. Ross and E. R. Jones, J. Comp. Mater., 5, 362-377 (1971)

13. T. Parry, Oxford University Engineering Laboratory (unpublished work)

14. Y. Bai and J. Harding, in Proc. Int. Conf. on Structural Impact and Crashworthiness, Elsevier Applied Science, London and New York, 1984, 2, 482-493

15. P. D. Ewins, RAE Technical Report No. 71217, 1971.

16. S. Shah, R. K. Y. Li and J. Harding, Oxford University Engineering Laboratory Report No. OUEL 1730/1988.

17. Y. L. Li, C. Ruiz and J. Harding, to appear in Composites Science and Technology.

3

New Directions in Research on Dynamic Deformation of Materials

GEORGE MAYER

Institute for Defense Analyses
Science and Technology Division
Alexandria, Virginia 22311, U.S.A

Progress in the development of new approaches to the analysis and experimental studies of the deformation, failure, and processing of structural materials under high loading rates has been reviewed. Advances in elucidation of the response of metals, ceramics, and polymeric materials to high loading rates, including the field of synthesis and processing, and directions of future work, will be considered.

I. INTRODUCTION

Studies of the dynamic loading and response of materials have multiplied during the past ten years, as exemplified by the host of papers presented at conferences and symposia which have been held on a regular basis (see for example, references 1-10). Because the area of dynamic loading is so broad, and due to the limitations of space in the proceedings and time at the present conference (and because of the limitations in my own knowledge), many topics, such as the treatment of detonations, shock phenomena relating to the earth, and hypervelocity studies, will be mentioned either not at all, or in passing. Suffice to say that significant attention is being devoted to these other important areas, and that they have been addressed regularly at the meetings already mentioned.

The two main areas of application discussed here which are reflected in the research activities, progress, and future directions of the field are armaments (armor, warheads, etc.) and synthesis and processing of materials. Hopefully, this bias can be overlooked, and more general extensions of the activities to be described will be seen by the reader.

AREAS OF APPLICATION
• ARMOR PROTECTION • PENETRATION PHENOMENA • SHOCK WAVE EFFECTS ON STRUCTURES • FRAGMENTATION • SPALLATION • SHAPED CHARGE JET FORMATION

FIG. 1 *Applications areas in armaments for dynamic loading phenomena*

In the decades of the Cold War, the U.S. Department of Defense became increasingly concerned about both the numbers and effectiveness of the conventional weaponry of the Soviet Union and their allies in the Warsaw Pact nations. The approach that was taken was to meet numbers of tanks and guns with smaller numbers of highly effective new weapons. On the research front of high loading rate phenomena, before embarking on new materials and other development programs, the state of understanding and areas of ignorance had to be established. The applications for new armaments were important, as is indicated in Figure 1. Thus, in 1977, the DoD asked the National Materials Advisory Board to study this problem, and a committee (the so-called Herrmann Committee) was established for this purpose. Their report "Materials Response to Ultra-High Loading Rates" (11) is still widely referenced, and the study was used as a guide by many DoD agencies for the support of research during the past decade.

With regard to shock synthesis and processing, the interests on the part of research sponsors stemmed from the possibilities of creating new materials thereto unknown, strengthening and hardening of materials by novel means, new joining methods, and less expensive routes to fabrication of advanced materials, such as intermetallics and ceramics.

II. REVIEW OF PROGRESS AND PROSPECTS

The broad impact of the Herrmann report and its recommendations can be realized from the progress which has been made in the ten years since the publication of the report. For example, one of the major issues at the time was the separation of the numerical modelling community from the sector dealing with dynamic material property measurements, and those involved with test firings. Much broader cooperation exists now, as seen by the development of more physically realistic constitutive models which interface well with complex hydrocodes. Some examples are discussed later in this paper. Such cooperative development has extended successfully into ceramic armor materials, with the Ceramics Modelling Working Group, organized in 1988 by G.E. Cort of the Los Alamos National Laboratory, and comprised of representatives of all three communities.

In 1980, a high priority for research was the elucidation of mechanisms of dynamic failure by brittle crack propagation, ductile void growth, and adiabatic shear banding, and the subsequent incorporation of these failure modes, through models, into hydrocodes. As an example of progress, there has been intense activity, both theoretical and experimental, into shear banding. Four widely different studies are described in references (12-15). For example, a model of shear banding was developed employing the concept of the energy dissipated by a moving dislocation (12). From direct observations of shear localization with high-speed photography, the energy dissipated in a band and the resulting temperature rise were estimated (13). Over the years, better resolution and sensitivity have been brought to the measurement of shear band temperatures, the most recent being done with an elaborate array of infrared detectors (16).

The development of new dynamic mechanical property tests for materials under well characterized and controllable loading conditions was also listed as a need in 1980. Many novel testing methods and equipment have been developed since that time, including a pressure-shear plate impact test (17) for shear strain rates greater than $10^5 s^{-1}$ and controllable levels of nearly hydrostatic pressure, a high-speed torsional testing machine (18), and a novel Taylor anvil impact test performed with an instrumented compression Hopkinson bar (19). On the subject of detection methods, a white light speckle method with high speed photography (21) and moire photography (21) have been employed to assess the dynamic displacement fields and dynamic stress intensity factors of fast cracks. A major new diagnostic tool for probing the internal events during projectile/target impact in thick sections of steels, ceramics, etc. has been successfully developed and applied at the Los Alamos National Laboratory (22). The system, called PHERMEX, is an acronym for pulsed high energy (30 MeV) radiographic machine emitting x-rays.

Studies of the characterization of dynamic brittle fracture in both metals and ceramics based upon a description of the nucleation, growth, intersection, and coalescence of cracks have only begun e.g. reference 23. Existing models, such as the SRI NAG/FRAG flaw nucleation and growth models (24) should be explored and possibly extended to include crack intersections and coalescence to failure.

Another subject which required attention within the dynamic loading of materials was the development of more detailed description of material behavior at ultrahigh rates of strain. The controlling micromechanisms and ranges where they dominate, should be identified. For this problem, it would seem ideal to develop a form of failure mechanism diagram, after Ashby's scheme (25). Figure 2 shows two examples developed for an alumina ceramic deformed in tension (a) and compression (b) The differences in the maps illustrate (over a range of fairly slow-strain rate) which failure mechanisms dominate and where they prevail. The information can be used in two ways: first, by specifying the stress, temperature, strain-rate, and load state (in these two cases, tension or compression) the map will provide

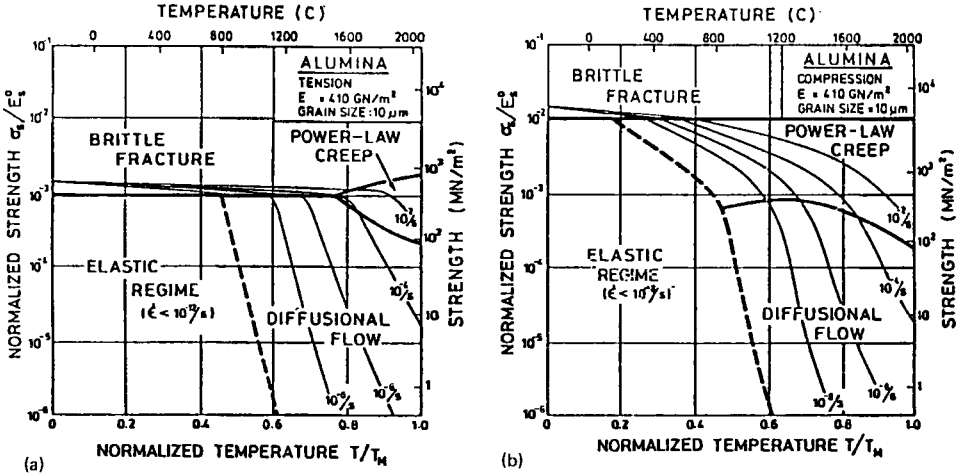

FIG. 2 *Failure-mechanism diagrams for a ceramic (alumina) loaded in (a) tension, and* (b) compression. *(from Cellular Solids Structure and Properties, 1988, by L.J. Gibson and M.F. Ashby, Courtesy of Pergamon Press)*

information of use for developing constitutive models. In addition, to avoid a particular failure mode, there may be flexibility in changing the grain size or other microstructural feature, altering the load or temperature, or limiting the strain-rate that the material experiences.

The foregoing are examples of topics within the broad field which have received concerted attention in the past decade in dynamic loading of materials. In order to systematically sort out our understanding in more comprehensive fashion, Figure 3 lists some important research areas which should receive continuing and new emphasis. Much progress has already been made on sorting out the roles of microstructure and defects and some of these results will be reported at this meeting (26, 27).

There has been recent interest in the behavior of ceramic materials under dynamic loading, e.g., on the role of pre-existing crack networks, their growth, and coalescence, and the behavior of pulverized and rubbelized ceramic and glassy materials under projectile impact. Figure 4 indicates topics which need additional attention.

Two subjects of major activity in dynamic loading deserve special mention. These are modeling and code development, and synthesis and processing of materials. The following sections address these topics.

RESEARCH AREAS FOR ADDED EMPHASIS
• DEVELOPMENT OF DATA BASES OF DYNAMIC PROPERTIES OF MATERIALS UNDER WELL-DESCRIBED, REPRODUCIBLE CONDITIONS
• CONTINUING STUDIES OF THE ROLES OF MICROSTRUCTURE AND DEFECTS IN DYNAMIC DEFORMATION AND FRACTURE
• CONSTRUCTION OF ASHBY DEFORMATION AND FRACTURE MAPS OVER A WIDE RANGE OF LOADING RATE AND TEMPERATURE REGIMES
• DETAILED STUDIES OF YIELD, DEFORMATION AND FAILURE AS A FUNCTION OF LOADING RATE FOR ADVANCED MATERIALS
• EXPANDED DIAGNOSTIC SPECTRUM OF IN-SITU DETECTION, WITH INCREASED SPEED, RESOLUTION, AND SENSITIVITY OF MEASUREMENT
• CONTINUING STUDIES OF THE ROLES OF MICROSTRUCTURE AND DEFECTS IN DYNAMIC DEFORMATION AND FRACTURE

FIG. 3 *Research areas for continuing and new emphasis in dynamic loading*

DYNAMIC LOADING ISSUES IN CERAMICS
• KINETICS OF CRACK NUCLEATION, GROWTH, AND INTERSECTION
• MECHANISMS OF CRACKING UNDER HIGH DYNAMIC COMPRESSIVE STRESSES
• DEVELOPMENT OF DAMAGE MODELS
• CONSTITUTIVE MODELLING OF PULVERIZED, CONFINED CERAMICS
• ENERGY DISSIPATION PHENOMENA
• EFFECTS OF PHASE TRANSFORMATIONS ON ENERGY DISSIPATION
• PROCESS ZONES IN CERAMICS
• METHODS FOR MEASURING DYNAMIC FRACTURE TOUGHNESS

FIG. 4 *Research issues in dynamic loading of ceramic materials*

A. *Materials Models and Code Developments*

Wider use of hydrocodes by the shock wave community has taken place over the past two decades because of the complexity of dynamic events, levels of pressure and temperature achieved, the novel new materials which are employed in the systems being used, and finally, because of the high and still escalating costs of full-scale testing in areas such as ordnance. The numerical simulations which undergird these codes have been facilitated by new supercomputers and by advanced methods, such as parallel processing. An excellent review of hydrocode concepts has been given by Anderson (28) and earlier by Zukas and colleagues (29, 30). The proliferation of codes has been a mixed blessing. On the one hand, some problems of increasing complexity under extreme conditions are being successfully addressed by individual codes; on the other hand, little compatibility exists between codes, and it is very costly and often restrictive (need for supercomputers, or restricted by classification) to maintain all of the codes in use today. Examples of some of the codes which have been popular are listed in Figure 5. The pros and cons of Lagrangian and Eulerian codes have been examined at length. For example, Lagrangian codes are generally more computationally efficient, need a smaller number of zones than Eulerian codes for equivalent accuracy, and avoid mixed material cell computations. The Lagrangian calculations allow the behavior at material interfaces (e.g., opening of voids) to be computed employing the concept of slidelines (31) and the Lagrangian approach allows superior treatment of material behavior (constitutive relations, strain hardening, etc.). On the negative side, large grid distortions create great problems for these codes, and users have often shifted to Eulerian codes for large deformation problems where there is extensive local flow, in high velocity impact regimes, for the collapse of shaped charges, in turbulent flows, etc. In recent years, codes have been adapted to account for intense localized failure modes, such as adiabatic shear and erosion (32). With the aid of such new capabilities, some Lagrangian codes (e.g., EPIC) can extend to treat "selected" large deformation problems. A general problem (more prevalent with Eulerian codes) is the need for large computer memories and long processing times, increasing the expenses of calculation.

EXAMPLES OF HYDROCODES	
Lagrangian (Finite Element)	Eulerian (Finite Difference)
HEMP	HULL
DYNA	JOY
PRONTO	CTH
EPIC	MESA

FIG. 5 *Some examples of hydrocodes used in numerical simulations*

Much progress has been made in developing better constitutive models for use in hydrocodes. The Johnson-Cook model (33) was widely accepted and updates for use in EPIC are periodically made. Other models which take into account specific materials parameters, such as microstructure and dislocation behavior are the Zerilli-Armstrong model (34) and the Mechanical Threshold Stress or MTS model of Follansbee (35). For brittle materials, Sandia National Laboratories have developed a mesocrack continuum damage model (36), based on the notion that many brittle materials contain pre-existing microcrack networks. The initiation, growth, and interaction of such cracks contribute to the nonlinear response of these materials and the latter are not predictable by classical fracture mechanics theories. This model has been useful in predicting the dynamic response of quasi-brittle materials under tensile loads.

More recently, significant advances have been made in developing a new generation of codes which combine the favorable aspects of Lagrangian calculations with limited Eulerian features for avoidance of mesh distortion (37). The techniques are Arbitrary Lagrangian Eulerian (ALE) and Free Lagrange. The ALE method has recently been extended to allow multimaterial zones, as well as nonoscillatory second-order-accurate advection routines, which are necessary for accurate computations. The key to making the ALE technique efficient was the development of automatic criteria (as measured by grid distortion) to switch a cell from Lagrangian to Eulerian.

Reducing the number of working hydrocodes seems to be a truly formidable task, in view of the range of problems addressed by these codes, from determining the response of structures to blast waves, to penetration , and to retorting of oil shale, etc. The trends to combine the best elements of different codes, such as ALE, and attempts to combine two and three-dimensional codes into one that treats both dimensions e.g., a new EPIC code (38), are promising directions. Figure 6 lists some continuing needs in the hydrocode arena. Although the list appears formidable, progress is being made on a number of fronts. For example, the advent of larger and faster computers has allowed three-dimensional versions of some hydrocodes to be formulated (39). Also, among new ventures into data bases, what appears to be a comprehensive effort is on-going at Sandia (40).

B. Shock Synthesis and Processing of Materials

The area of shock processing of materials (used in the broadest sense) has seen concerted interest during the past three decades. The broadening of the field is reflected from the book on Explosive Working of Metals by Rinehart and Pearson (41) to the fairly recent volume, Shock Waves for Industrial Applications, which was brought together by Murr in 1988 (8).

The early efforts in processing (Figure 7) employing shock waves were focused on explosive forming, often of large shapes, such as hemispherical sections or cones, on

HYDROCODE ADVANCES - SELECTED NEEDS
• Extend ALE to Three Dimensions
• Generalize Adaptive Mesh Refinement
• Narrow the Gap Between Practical Hydrocodes and Physically-based Models
• Anisotropic Materials Response
• Fracture Initiation Criteria (Ductile and Brittle Materials)
• Mechanism(s) and Models of Softening from Damage Accumulation (Ductile and Brittle Materials)
• Mechanisms and Models of Fracture Propagation (Ductile and Brittle Materials)
• Comprehensive Materials Property Data

FIG. 6 *Some future needs for the advancement of hydrocodes*

EARLY AREAS OF ACTIVITY
• Explosive Forming
• Explosive Welding
• Explosive Hardening
• Explosive Cladding

FIG. 7 *Early areas of activity in shock processing of metals*

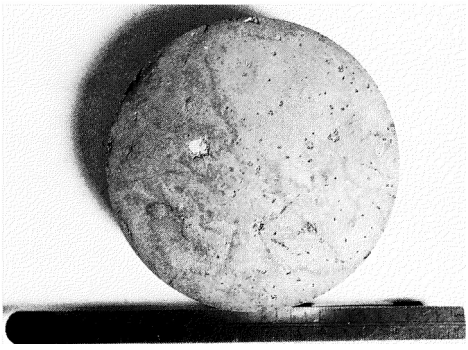

FIG. 8 *Specimen of titanium carbide fabricated by combustion synthesis and dynamic compaction (Courtesy of M.A. Meyers)*

surface hardening, and on explosive welding (42) and bonding or cladding. Interests in shock synthesis of diamond were spurred by the work of DeCarli and Jamieson (43) in 1961. DeCarli's patent (44) was followed by more patents and industrial applications of shock-synthesized diamond by the DuPont Company (45). Somewhat after his success with diamond, DeCarli demonstrated the successful shock synthesis of cubic BN from the hexagonal phase (46). Successful shock syntheses of hard materials and other materials of technological interest (e.g., intermetallics) have proceeded strongly in the U.S.S.R., Japan, and the U.S.A. during the past three decades, have been reported at the prior EXPLOMET meeting (4) and will be discussed at the present conference.

Dynamic processing and synthesis of materials have been of strong interest in the U.S.A., especially during the past decade, and this has been reflected in two studies of the National Materials Advisory Board (47, 48). Shock consolidation has been of interest for the densification of materials which are normally difficult to sinter, to avoid grain growth, and to seek a cost-effective industrial production method. More recently, dynamic consolidation has been combined with combustion synthesis (or self-sustaining, high-temperature synthesis) to yield ceramic and ceramic composite compacts close to full density (49, 50). Figure 8 shows a recent product which was dynamically compacted along with the combustion synthesis step. Figure 9 lists the more recent areas of activity in shock synthesis and processing.

Temperature predictions for shock processing have been made using hydrocodes (51) and thermal analysis models (52). Although careful and systematic approaches have been taken to explain the generation of dislocations and other defects during shock loading (53, 54), questions of defect nucleation mechanisms remain, and will be addressed at the present meeting (55). Figure 10 lists a series of areas that deserve future study. For example, transient and/or intermediate states that are generated during shock loading need to be treated both theoretically and experimentally. On a related topic, in an earlier work (56), diffusion coefficients under shock loading were reported to be 10^2-10^3 higher than normal, but no theoretical model was offered. The problem of mass transport over relatively large distances in short times has been difficult to explain. In a different vein, electrical phenomena have been reported in association with shock-related processing and fracture (57). It has also been reported that shock activation of catalyst materials can increase the reactivity of the catalysts by three orders of magnitude (48). This may represent an important practical effect, if it can be retained for a reasonable period of time.

III. FUTURE DIRECTIONS

The areas of on-going activity and need for increased understanding represent a base of opportunity for a rapidly widening field of research. In the future, more complex materials, such

RECENT AREAS OF ACTIVITY
• Powder Compaction
• Phase Transformations
• New Compound Synthesis
• Combustion Synthesis (SHS)
• Chemical Decomposition
• Polymerization and Cross-Linking
• Shock Modification and Activation

FIG. 9 *Recent activities in shock synthesis and processing of materials*

AREAS FOR FUTURE STUDY	
• Nucleation of Defects	• Nonequilibrium Temperatures in Shock Front
• Roles of Defects as Precursors	• Measurement of Temperature and Shear Stress in Dynamics Compression
• Void Collapse in Porous Materials	• Continued Emphasis on Tailoring of Shock Profiles and Containment Designs for Fracture Avoidance
• Transient or Intermediate States	
• Diffusion Phenomena	
• Electrical Phenomena Associated with Fracture	

FIG. 10 *Subjects in shock synthesis and processing which require new emphasis*

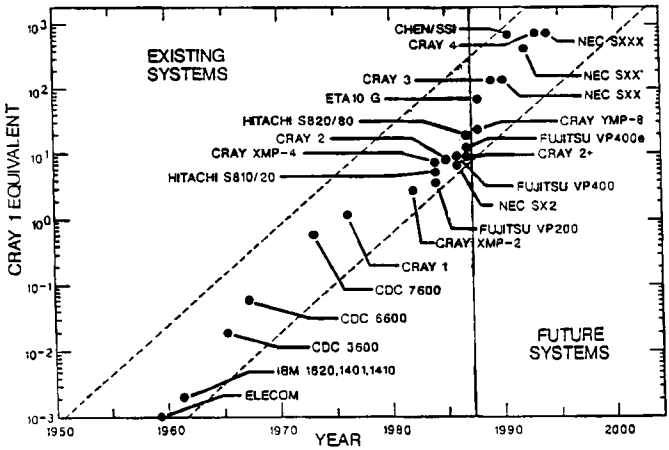

FIG. 11 *Trends in supercomputing capabilities (Courtesy of National Materials Advisory Board)*

as composites (metallic, ceramic, and organic), laminates, intermetallics, and hybrids will constitute special challenges for the high loading rate community.

Hypervelocity impact will receive new attention. Systems such as electromagnetic launchers (58) and multistage gas dynamic launchers (59) bring new experimental capabilities to this arena, which have broad applications from armament, to geosciences, and to space.

Finally, new computing capabilities on the horizon will enable computations that are impossible or impractical with machines that are available today (60) (Figure 11).

REFERENCES

1. *Shock Waves and High-Strain-Rate Phenomena in Metals,* M.A. Meyers and L.E. Murr (eds.) Plenum (1981).

2. *Shock Waves in Condensed Matter - 1983*, J.R. Asay, R.A. Graham, and G.K. Straub (eds.) North-Holland (1984).

3. *Proceedings of the Third Conference on the Mechanical Properties of Materials at High Rates of Strain 1984*, J. Harding (ed.) Institute of Physics (1984).

4. *Metallurgical Applications of Shock-Wave and High-Strain-Rate Phenomena,* L.E. Murr, K.P. Staudhammer, and M.A. Meyers (eds.) Marcel Dekker (1986).

5. *Shock Waves in Condensed Matter - 1985*, Y.M. Gupta (ed.) Plenum (1986).

6. *Hypervelocity Impact-Proceedings of the 1986 Symposium,* C.E. Anderson, Jr. (ed.) Pergamon (1987).

7. *Shock Waves in Condensed Matter 1987,* S.C. Schmidt and N.C. Holmes (eds.) North-Holland (1988).

8. *Shock Waves for Industrial Applications*, L.E. Murr (ed.) Noyes (1988).

9. *Proceedings of the International Conference on Mechanical and Physical Behavior of Materials under Dynamic Loading*, Journal de Physique, Tome 49, Colloque C3, Supplement No. 9 (Sept.. 1988).

10. *Shock Compression of Condensed Matter - 1989,* S.C. Schmidt, J.N. Johnson, and L.W. Davison (eds.) North-Holland (1990).

11. W. Herrmann, Chairman, Committee on Materials Response to Ultra-High Loading Rates, *Materials Response to Ultrahigh Loading Rates, NMAB-356*, National Academy of Sciences (1980).

12. C.S. Coffey, "Shear Band Formation and Localised Heating by Rapidly Moving Dislocations," *Mechanical Properties at High Rates of Strain 1984*, The Institute of Physics 519 (1984).

13. J.H. Giovanola, "Adiabatic Shear Banding Under Pure Shear Loading Part I: Direct Observation of Strain Localization and Energy Dissipation Measurements," *Mechanics of Materials 7*, 59 (1988).

14. T.W. Wright and S.C. Chou "Army Studies of Large Deformation Plasticity: *Proceedings of DoD/DARPA Coordination Meeting on Advanced Armor/Anti-Armor Materials and Advanced Computational Methods*, IDA D-576, G. Mayer (ed.) Institute for Defense Analyses, 1025 (March 1989).

15. T.J. Burns "A Mechanism for High Strain Rate Shear Band Formation," *Shock Compression of Condensed Matter - 1989*, S.C. Schmidt, J.N. Johnson, and L.W. Davison (eds.) North-Holland 345 (1990).

16. Y.C. Chi and J. Duffy "On the Measurement of Local Strain and Temperature During the Formation of Adiabatic Shear Bands in Steels" *Report No. 4, ARO Contract No. DAAL 03-88-K-0015*, (September 1989)

17. C.H. Li "A Pressure-Shear Experiment for Studying the Dynamic Plastic Response of Metals at Shear Strain Rates of $10^5 sec^{-1}$" *Ph. D. Thesis, Brown University*, Providence, RI (1981).

18. U.S. Lindholm, A. Nagy, G.R. Johnson, and J.M. Hoegfeldt "Large Strain, High Strain Rate Testing of Copper," *Jl. of Eng. Materials and Technology* (October 1980).

19. S. Nemat-Nasser, University of California at San Diego, personal communication (December 1989).

20. X.M. Hu, S.J.P. Palmer, and J.E. Field, "The Application of High Speed Photography and White Light Speckle to the Study of Dynamic Fracture," *Optics and Laser Technology*, 303 (December 1984).

21. J.M. Huntley and J.E. Field, "Application of Moire Photography to the Study of Dynamic Fracture," Proc. Seventh Intl. Conf. on Fracture (March 1989).

22. G.E.Cort, Los Alamos National Laboratory, personal communication (June 1990).

23. L.H. Leme Louro and M.A. Meyers, "Stress Induced Fragmentation in Alumina-Based Ceramics," *Shock Compression of Condensed Matter - 1989, S.C. Schmidt, J.N. Johnson, and L.W. Davison (eds.)*, North-Holland 465 (1990).

24. D.R. Curran, L. Seaman, and D.A. Shockey, "Dynamic Failure of Solids," *Physics Reports 147 (5 and 6)* 253 (1987).

25. L.J. Gibson and M.F. Ashby, *Cellular Solids-Structure and Properties*, Pergamon, 66-67 (1988).

26. J. Lankford, C.E. Anderson, and H. Coque "Microstructure Dependence of High Strain Rate Deformation and Damage Development in Tungsten Heavy Alloys," *International Conference on Shock-Wave and High-Strain-Rate Phenomena in Materials*, (1990).

27. B.O. Reinders, "Influence of Mechanical Twinning on the Deformation Behavior of Armco Iron," ibid.

28. C.E. Anderson, Jr., "An Overview of the Theory of Hydrocodes," *Int. J. Impact Eng. 5*, 33 (1987).

29. J.A. Zukas, G.H. Jonas, K.D. Kimsey, J.J. Misey, and T.M. Sherrick, "Three-Dimensional Impact Simulations: Resources and Results," *Computer Analysis of Large-Scale Structures*, K.C. Parck and R.F. Jones, Jr. (eds.), AMD, V. 49, ASME (1981).

30. J.A. Zukas, T. Nicholas, H.F. Swift, L.B. Greszczuk, and D.R. Curran, *Impact Dynamics*, Wiley (1982).

31. M.L. Wilkins, "Calculations of Elastic-Plastic Flow," *Methods of Computational Physics, 3*, B. Adler, S. Fernback, and M. Rottenberg (eds.) Academic (1964).

32. K.D. Kimsey and J.A Zukas, "Contact Surface Erosion for Hypervelocity Problems" *BRL-MR-3495*, U.S. Army Ballistics Research Laboratory (1986).

33. G.R. Johnson and W.H. Cook, "A Constitutive Model and Data for Metals Subjected to Large Strains, High Strain Rates, and High Temperatures," *Seventh International Symposium on Ballistics*, The Hague, The Netherlands (April 1983).

34. F.J. Zerilli and R.W. Armstrong "Dislocation Mechanics - Based Constitutive Relations for Material Dynamics Calculations," *Jl. App. Phys.* 61, 1816, (1987).

35. P.S. Follansbee, "Dynamic Deformation and Fracture in Armor/Anti-Armor Materials," *Proceedings of the DoD/DARPA Coordination Meeting on Armor/Anti-Armor Materials and Advanced Computational Methods, IDA-D-576*, G. Mayer (ed.), Institute for Defense Analyses, (March 1989).

36. E.P. Chen, Sandia Albuquerque National Laboratory, private communication (April 1990).

37. J.D. Immele (Chairman) *Report of the Review Committee on Code Development and Material Modelling LA-UR-89-3416,* (Los Alamos National Laboratory Report) Review Committee on Code Development and Materials Modelling, 15 (October 1989).

38. G.R. Johnson, Honeywell, Inc., private communication (December 1989).

39. W.E. Johnson and C.E. Anderson, Jr. "History and Application of Hydrocodes to Hypervelocity Impact," *Int. J. Impact Eng. 5*, 423, (1987).

40. J.S. Wilbeck, C.E. Anderson, Jr., J.C. Hokanson, J.R. Asay, D.E. Grady, R.A. Graham, and M.E. Kipp, "The Sandia Computerized Shock Compression Bibliographical Database," *Metallurgical Applications of Shock-Wave and High-Strain-Rate Phenomena*, L.E.. Murr, K.P. Staudhammer, and M.E. Meyers, (eds.) Marcel Dekker, 357, (1986).

41. J.S. Rinehart and J. Pearson, *Explosive Working of Metals*, MacMillan (1963).

42. G.R. Cowan and A.H. Holtzman, "Flow Configuration in Colliding Plates: Explosive Bonding," J. Appl. Phys. 34(4), 928, (1963).

43. P.S. DeCarli and J.C. Jamieson, "Formation of Diamond by Explosion Shock," *Science*, 133, 821 (1961).

44. P.S. DeCarli, "Method of Making Diamond," U.S. Patent 3,238,019, March 1, 1966.

45. O.R. Bergmann and N.F. Bailey, "Explosive Shock Synthesis of Diamond," in *High Pressure Explosive Processing of Ceramics*, R.A. Graham and A.B. Sawaoka (eds.) Trans Tech 65 (1987).

46. P.S. DeCarli, *Bull. Amer. Phys. Soc., 12,* 1127 (1967).

47. Committee on Dynamic Compaction of Metal and Ceramic Powders, *Dynamic Compaction of Metal and Ceramic Powders*, National Materials Advisory Board, National Research Council, Washington, DC, NMAB-394, (1983).

48. Committee on Shock Compression Chemistry in Materials Synthesis and Processing, *Shock Compression Chemistry in Materials Synthesis and Processing*, National Materials Advisory Board, National Research Council, Washington, DC, NMAB-414, (1984).

49. A. Niiler, T. Kottke, and L. Kecskes, "Shock Consolidation of Combustion Synthesized Ceramics," in *Proc. of First Workshop on Industrial Applications of Shock Processing of Powders*, CETR, New Mexico Institute of Mining and Technology (June 1988)

50. M.A. Meyers, University of California, San Diego, private communication (December 1989).

51. R.L. Williamson and R.A. Berry "Microlevel Numerical Modelling of the Shock Wave Induced Consolidation of Metal Powders" in *Shock Waves in Condensed Matter - 1985*, Y.M. Gupta (ed.), Plenum, 341, (1986).

52. T. Vreeland, Jr., P. Kasiraj, A.H. Mutz, and N.N. Thadhani, "Shock Consolidation of a Glass-Forming Crystalline Powder," in *Metallurgical Applications of Shock Waves and High Strain Rate Phenomena,* L.E. Murr, K.P. Staudhammer, and M.A. Meyers, (eds.) Marcel Dekker, 231, (1986).

53. J. Weertman, "Moving Dislocations in a Shock Front," *Shock Waves and High-Strain-Rate Phenomena in Metals*, M.A. Meyers, and L.E. Murr (eds.) Plenum, 469 (1981).

54. M.A. Meyers and L.E. Murr, "Defect Generation in Shock Wave Deformation," ibid., 487, (1981).

55. M.P. Mogilevsky, "Defect Nucleation under Shock Loading," *International Conference on Shock-Wave and High-Strain-Rate Phenomena* (August 1990).

56. S.V. Zemsky, Y.A. Ryabehikov, and G.D. Epshteyn, "Mass Transfer of Carbon Under the Influence of a Shock Wave," *Phys. Met. Metal. 46(1)*, 171, (1979).

57. J.T. Dickinson, L.C. Jensen, and A. Jahan-Latibari, "Fracto-emission: The Role of Charge Separation," *Jl. Vac. Sci. and Tech* (February 1984).

58. H. Fair, "Hypervelocity Then and Now," *Inst. Jl. Impact Eng. 5* 13 (1987).

59. L.A. Glenn, A.L. Latter, and E.A. Martinelli, "Multistage Gasdynamic Launchers," *Shock Compression of Condensed Matter - 1989*, S.C. Schmidt, J.N. Johnson, and L.W. Davison (eds.) North-Holland 977 (1990).

60. *The Impact of Supercomputing Capabilities on U.S. Materials Science and Technology - NMAB-451*, National Academy of Sciences (1988).

4

Constitutive Equations at High Strain Rates

L.W. MEYER

Fraunhofer-Institut für angewandte Materialforschung - IFAM
Lesumer Heerstr. 36, D-2820 Bremen 77, Germany

In this review is presented which forms of semiempirical or physically-based constitutive equations are useful for high strain rate applications, how they match the real behavior, and where are the limitations.

I. INTRODUCTION

"Constitutive Equations are the vehicle by which our knowledge of material behavior enters engineering design." This sentence from Kocks [1] illustrates very appropriately the goal: To solve mechanical problems with numerical methods where the quality of the results depends strongly on a sufficient description of the involved material behavior.

This restriction (to 'sufficient') is needed because the material behavior cannot be expressed in a general way. It is too complex to find complete solutions. Our understanding of the micromechanics certainly has made welcomed progress, but many questions are still open.

Therefore we have to concentrate on specific deformation or loading conditions, and on certain temperature- and strain-rate ranges. Hot working, creep, cyclic loading, unloading and history effects, i.e. are not

included. However cold working, monotonic straining transients, as well as temperatures between 50 and 500 K and strain rates between 10^{-5} to 10^{5} s^{-1} are considered in the following.

II. SEMI-EMPIRICAL EQUATIONS

One of the simplest forms of describing the material behavior is the Ludwik equation, [2]:

$$\sigma = A + B\,\epsilon^{n} \quad \text{or} \quad \tau = C + D\,\gamma^{n} \tag{2.1}$$

Using the constants A and B and the so called strain hardening parameter n it is often used to characterize the stress σ or τ as a function of the strain ϵ or γ at ambient temperatures and quasistatic loading. Ludwik claims that the strain hardening develops monotonically with a constant to the power n. Indeed, this is often true, at least beyond a transient for the very first plastic deformation, up to a saturation state of stress. To include the influence of temperature, T, and strain rate, $\dot{\epsilon}$, or $\dot{\gamma}$, the power law (2.1) was extended in several ways:

a) by Klopp, Clifton, Shawki [3] $$\tau = \tau_0\,\gamma^{n}\,T^{-\nu}\,\dot{\gamma}_p^{m} \tag{2.2}$$

with the strain rate hardening parameter m, and the temperature softening parameter ν, both as power laws,

b) by Litonski [4] $$\tau = C(\gamma_o+\gamma_p)^{n}\,(1-aT)(1+b\dot{\gamma}_p)^{m} \tag{2.3}$$

Here the strain is split up into a constant γ_o (which approximately represents the elastic part) and the plastic strain γ_p. The temperature influence is expressed linearly instead of as a power function. This assumes to a first approximation a linear-decrease of the stress with increasing temperature.

c) by Vinh et al. [5] $$\tau = F(\gamma)^{n}\,\left(\frac{\dot{\gamma}}{\dot{\gamma}_o}\right)^{m}\exp\left(\frac{W}{T}\right) \tag{2.4}$$

They found that an exponential expression of temperature provided a better fit to their results for aluminum, copper and mild steel.

d) Johnson/Cook [6,7] $\tau = [A+B\gamma^n][1+C\ \ln(\frac{\dot{\gamma}}{\dot{\gamma}_o})][1-(T^*)^m]$ (2.5)

where $T^* = (T-T_r)/(T_m-T_r)$

Johnson/Cook also used the Ludwik equation as a base and included strain rate and temperature influences. They chosed a logarithmic rate sensitivity with a constant C and normalized the strain rate with $\dot{\gamma}_o = 1\ s^{-1}$. Therefore, their constants of the Ludwik equation are related to a strain rate of $1\ s^{-1}$ and not to quasistatic loading. The temperature is included by a power expression of the homologous temperature T^*. Based on quasistatic and dynamic torsion and tension tests up to $\dot{\gamma} = 4 \times 10^2\ s^{-1}$, Johnson/Cook provided constants for 6 ductile and 6 less ductile materials, including Cu, Fe, brass, Ni, C-steel, tool steel, Al alloys, and DU. By this broad source of data, the Johnson/Cook equations are often used as constitutive equations for calculations.

e) Armstrong/Zerilli [8-10]

$$\text{bcc: } \sigma = \Delta\sigma_G+B_0\exp[(-\beta_0+\beta_1\ln\dot{\epsilon})T]+K_0\epsilon^n+k_\epsilon\ell^{-1/2} \tag{2.6}$$

$$\text{fcc: } \sigma = \Delta\sigma_G+B_1\epsilon^{1/2}\exp[(-\beta_0+\beta_1\ln\dot{\epsilon})T]+k_\epsilon\ell^{-1/2} \tag{2.7}$$

where $\Delta\sigma_0$, B_0, B_1, β_0, β_1, K_0, n, and k_ϵ are constants and ℓ is the average grain size. Armstrong and Zerilli distinguish between bcc and fcc materials. For fcc materials, as an important improvement, they coupled the strain hardening term with a temperature and strain rate dependence. The bcc materials are modeled similar to Clifton et al. and Johnson/Cook, where the strain or work hardening is independent from a temperature or strain rate influence. In a refinement [10], they included the effect of twinning at high strain rates and high strains, respectively, above a certain von Mises stress level, which leads to an increase of the Hall-Petch term of eq.(2.6 and 2.7):

$$\Delta(k\ell^{-1/2}) = k\ell^{-1/2}[(N+1)^{1/2}-1] \tag{2.8}$$

where N equals the average number of twins within the grains. With this improvement, they successfully modeled the Taylor-Impact of Johnson/Cook [7] for Armco iron without taking into account viscous drag. For copper,

indeed, Armstrong and Zerilli [9] included a viscous drag influence in the thermal stress

$$\sigma_e = \frac{1}{2}\,\sigma'\,[1+\sqrt{1+\frac{4C_0\dot{\epsilon}T}{\sigma'}}] \tag{2.9}$$

with σ' the T- and $\dot{\epsilon}$-dependent component of eq. (2.7):

$$\sigma' = B_1\,\epsilon^{1/2}\,\exp[(-\beta_0+\beta_1 \ln\dot{\epsilon})T] \tag{2.10}$$

They found good agreement with the results of Follansbee et al. [11] and Gourdin [12] on copper under compression and tensile loading.

Equations (2.1) to (2.5) were expressed mathematically as simply as possible or extended with some additional constants to meet the experimentally measured behavior as closly as possible. The advantage of such a point of view is that, with some effort, the mathematical curve fitting can meet the materials stress-strain behavior as close as the description allows. Sometimes the approximation gets close, as Vinh [5] or Campbell [13] demonstrated for fcc materials. In other cases, the curve fitting cannot approach the real behavior, because the strain hardening is not constant versus strain rate. Then a compromise has to be made (and it is on the mind of the user) in which strain rate region the empirical description has to fit best.

Another inherent restriction often is not noted: The description of the material behavior, the modelling and the named coefficients are based on test results determined up to a certain limited rate of strain. Therefore the users have to keep in mind, that only up to that strain rate the modelling is based on experimental results and that calculations of faster events are done as an extrapolation or as a guess, no more, no less.

It would be desirable if the semi-empirical equations could be established on a physical basis related to micromechanical behavior. But this is mostly not the case because the real behavior of a material is not a function of one state parameter, i.e. the strain. The reality is much more complicated. We have to consider that the material behavior is dependent on the evolution of the microstructure. This evolution depends on the initial structure and on the strain rate, respectively, the strain rate history and on the loading conditions such as compression or shear.

III. CONSTITUTIVE EQUATIONS BASED ON MICROSTRUCTURAL PROCESSES

The (external) stress σ leading to plastic deformation has to overcome the internal stresses from both far and short range obstacles. Written in a sum, one can assume

$$\sigma = \sigma_a + \sigma^* (T,\dot{\epsilon}) \tag{3.0}$$

Far range stress fields are determined mainly by the structure of the materials and less by the strain rate. Therefore, this part is called the athermal stress component, σ_a. The thermally influenced stress component, σ^* is related to the interaction between dislocations and short range obstacles which can be overcome with the help of thermal fluctuations. This includes the strong influence of the temperature, T and strain rate, $\dot{\epsilon}$.

With the Orowan equation for the dislocation velocity, the Arrhenius equation for the dislocation waiting time before an obstacle, and the equation for the free activation energy, the thermal activated stress σ^* is obtained:

$$\sigma^* = \hat{\sigma}\{1-[\frac{kT}{\Delta G_o} \ln (\frac{\dot{\epsilon}_o}{\dot{\epsilon}_p})]^n\}^m \tag{3.1}$$

Now σ^* can be expressed as a function of the external variables T and $\dot{\epsilon}_p$ and the constants $\hat{\sigma}$, ΔG_o, $\dot{\epsilon}_o$, n and m [14]. The importance of this expression is that it is based on micromechanics and that all the parameters have a physical background: the short range obstacles which can be overcome by the assistance of the thermal component σ^* are characterized by $\hat{\sigma}$= stress amplitude at T = 0 K, named mechanical threshold stress, ΔG_o = the activation energy at T = T_o, n or 1/q and m or 1/p determine the form of the force-distance-curves of mobile dislocations in the vicinity of specific short-range obstacles and $\dot{\epsilon}_o$ is specified by the microstructure. Known values of m, n and $\dot{\epsilon}_o$ for some metals are listed in Table 1. These equations are valid for one type or one dominant type of dislocation interaction with the microstructure, and the microstructure is assumed to be constant.

The concept of "threshold stress $\hat{\sigma}$", developed by Kocks [15], Follansbee [16-18] and Follansbee and Gray [19], uses the same fundamental description, but extends the application of the thermal activation theory

Table 1 Constants for eq. 3.1 to 3.4 for different materials

Materials	Ref.	Constants			$\hat{\sigma}$
		m=1/p	n=1/q	$\dot{\epsilon}_0$	
Aluminum (Pure)	[14]	1	1		
Some Hexagonal Metals	[14]	1	1		
Titanium Alloys	[14]	1	1/2	10^7	
	[45]	1	1/2	10^{10}	
Copper, Homogeneous Alloy	[14]	2	2/3		
	[42]	2	2/3		
	[16]	3/2	1		
Iron, Pure	[34]	1.5	1	10^8	
	[14]	2	1		
	[38]	2	1		
Steel Carbon	[14]	4	1		
0.46C, 1.5Mn	[36]	2	2/3	10^7	1690
0.45C	[38]	2	2/3	$10^{6.4}$	
0.45C	[38]	2	1/2	$10^{6.4}$	
0.45C	[38]	3	2	$10^{6.4}$	
Steel: 1Si and NiCrMo	[38]			10^7	
9Cr-3Si	[39]			10^7	
0.3C-3Ni-1Cr-0.5Mo	[36]	2	1/2	10^8	2120
Austenitic Steel	[37]			$2 \cdot 10^9$	
23Cr-17Ni-3Mo	[36]			10^{10}	
18Cr-Stainless Steel	[38]			10^8	
21Cr-16Ni-5Mn-3Mo	[35]	2	1/2	$8 \cdot 10^9$	2750
Nitronic 40	[34]	1.5		10^9	

to higher strains taking the evolution of the microstructure into account. With splitting the threshold stress $\hat{\sigma}$ into an athermal and thermal activated component (subscript "a" and "t", resp.), Follansbee and Kocks [16] use basically the same expression as eq. (3.1) to describe the kinetics s_i [in square brackets] or the flow stress σ, normalized with the temperature dependent Young's modulus $\mu(T)$:

$$\frac{\sigma}{\mu} = \frac{\hat{\sigma}_a+(\hat{\sigma}-\hat{\sigma}_a)}{\mu} \left\{1-\left[\frac{kT}{g_o\mu b^3} \ln\left(\frac{\dot{\epsilon}_o}{\dot{\epsilon}}\right)\right]^{1/q}\right\}^{1/p} \tag{3.2}$$

The evolution of the structure which determines $\hat{\sigma}$ is considered as the balance between dislocation accumulation (θ_0) and dynamic recovery (θ_r). To express that the strain is not assumed as a state variable, the strain hardening θ is described differentially

$$\frac{d\hat{\sigma}}{d\epsilon} = \theta = \theta_0 - \theta_r \quad \text{or} \quad \theta = \theta_0\left[1-F\left(\frac{\hat{\sigma}-\hat{\sigma}_a}{\hat{\sigma}_s-\hat{\sigma}_a}\right)\right] \tag{3.3, 3.4}$$

where the temperature and strain rate dependence is referred to the saturation threshold stress $\hat{\sigma}_s$. For fcc pure metals and alloys over wide ranges of temperatures but narrow ranges of strain rates, first it was assumed [20] that θ_0 is roughly constant with strain rate and is found to represent the strain hardening in stage II deformation. Follansbee and Kocks [16] indeed concluded (from tests at 76K and up to high true strains of ~1) that θ_0 must increase with strain rate in the following form

$$\theta_0 = C_1 + C_2 \ln(\dot{\epsilon}) + C_3 \dot{\epsilon} \tag{3.5}$$

in order to fit the experimental data to eq. (3.4) for accumulation and dynamic recovery. The determined strong increase of θ_0 above $\dot{\epsilon} = 10^3\ s^{-1}$ indicates that the dislocation accumulation θ_0 must increase dramatically above that range of strain rate. This observation might explain why frequently above $\dot{\epsilon} = 10^3\ s^{-1}$ a sharp increase in flow stress is reported.

On the other hand, the consideration of drag effects on the dislocation velocity is assumed as well to explain a sharp increase of stress-strain rate sensitivity [21]. At very high rates of strain for pure drag

and an ideal crystal, it is assumed that the dislocations move with a constant velocity and that the flow stress σ (which exceeds $\hat{\sigma}$) is directly proportional to the strain rate $\dot{\epsilon}$. For the transition range between thermally activated and drag controlled deformation ($\sigma<\hat{\sigma}$), both mechanisms may be operative. The drag influence can be included here by an influence on the running time t_r of the dislocations between the obstacles. Under this assumption, Hoge and Mukherjee developed a combined equation for the material behavior of tantalum which fits well with the measured behavior [22]. Burgahn et al. [23] showed that for a carbon steel C45 under the same assumption a similar relationship leads to a close agreement between predicted and measured behavior up to $\dot{\epsilon} = 10^3\ s^{-1}$ and that the expected higher rate sensitivity should reasonably influence the flow stress at $\dot{\epsilon} > 10^5\ s^{-1}$.

In all equations listed above, the temperature influence was not included in the work hardening or even when regarded by a separate linear, power or exponential term. Klepaczko [24,25] proposed not to neglect the temperature influence and included it in the basic double power expression

$$\tau = C(\theta)(\Gamma_o+\Gamma)^{n(\theta)}\ Z^{m(\theta)} + \langle\eta(\dot{\Gamma}-\dot{\Gamma}^*)\rangle \tag{3.6}$$

Furthermore, he combined a specific form of the Arrhenius relation with the strain rate sensitivity m

$$\tau = \hat{\tau}\left[\frac{\dot{\Gamma}}{\dot{\Gamma}_o}\ \exp\ \frac{\Delta H}{kT_m\theta}\right]^{m(\theta)} \tag{3.7}$$

with $\theta = T/T_m$ for the homologous temperature, T_m the melting temperature, Γ the true shear strain, $\dot{\Gamma}$ the true shear strain rate, $\dot{\Gamma}_o$ the frequency factor, ΔH the apparent activation energy, k the Boltzmann constant, and $\hat{\tau}$ the threshold stress. The expression in the brackets is the well-known Zener-Hollomon parameter, named Z. The functions $n(\theta)$ and $m(\theta)$ have to be chosen appropriate to the material behavior.

The complete set of constants reaches fifteen for bcc materials or thirteen for fcc materials. For three materials, polycrystalline pure aluminum, copper and a cold rolled 0.18 % carbon steel (1018), Klepaczko identified the material parameters from published results and found reasonable agreement. Of course, the determination of this large number of

constants requires some effort, but an important step is done: the inclusion of physical-based expressions.

Contrary to all models mentioned before, Steinberg and Colleagues [26] proposed a model to predict the yielding stress Y and the shear modulus G under uniaxial shock conditions. This model includes temperature and pressure influence, but neglects the strain rate. Based on experimental observations, it predicts reasonably well the material behavior at conditions of strong shocks. The constants used are given by Steinberg for more than 14 materials.

To cover also weaker shock conditions, where the strain rate influence cannot be neglected, Steinberg extended his model [27] with a thermal activated and a viscous drag term similar to Hoge and Mukherjee [22]. Consequently, the calculated and experimental curves, i.e. for Ta at 5 GPa, got much closer than with the rate independent model.

Under the assumption of small strains, Bodner/Partom [28] established a set of constitutive equations which may consider isotropic and directional hardening, thermal recovery of hardening, temperature dependence and an isotropic and directional damage development. Including all eftects, the number of material constants is large. Nevertheless, they can be obtained from standard uniaxial tests. For dynamic monotonic loading, only the basic rate dependence of plastic flow and isotropic hardening without thermal recovery is required.

The main equation governing the inelastic deformations is the kinetic equation D_2^p which is F (deviatoric stress invariants J_2) chosen essentially empirically, but mathematical flexible and with a physical basis to model different material behavior:

$$D_2^p = D_o^2 \exp[-(\frac{Z^2(1-\omega)^2}{3J_2})^n] \tag{3.7}$$

with D_0 the limiting strain rate in shear, $n = f(T,p)$, a material constant that controls rate sensitivity by temperature and pressure influence and the overall level of flow stress. Z is interpreted as a load history dependent parameter, corresponding in a general way to the yield stress, and ω is a history dependent damage parameter.

For the one dimensional stress case, eq. (3.7) can be developed to

$$\sigma = \frac{Z}{(2 \ln[\frac{2D_o}{\sqrt{3}\dot{\epsilon}_{11}^p}])^{\frac{1}{2n}}} \tag{3.8}$$

which is plotted in a normalized form in Fig. 1 for various values of n, [29].

Depending on the choice of n and D_o, from a nearly rate insensitive behavior ($n > 5$, $\dot{\epsilon}_p/D_o < 10^{-5}$) to a strong rate sensitive behavior ($n < 5$, $\dot{\epsilon}_p/D_o > 10^{-3}$), the flow stress can be modeled in close accordance to experimental results.

The dependence of the parameter Z on the plastic work W_p, generated from the initial state, is assumed to have the exponential form

$$Z(W_p) = Z_1 + (Z_o - Z_1)\exp\left(\frac{-m\,W_p}{Z_o}\right) \tag{3.29}$$

where Z_1 is a limiting, saturation value of Z to ensure that resistance to plastic flow is limited. $Z_o = Z_1 - \Delta Z$ is the initial value of Z_1, m is a constant related to the rate of hardening. Bodner showed that isotropic as

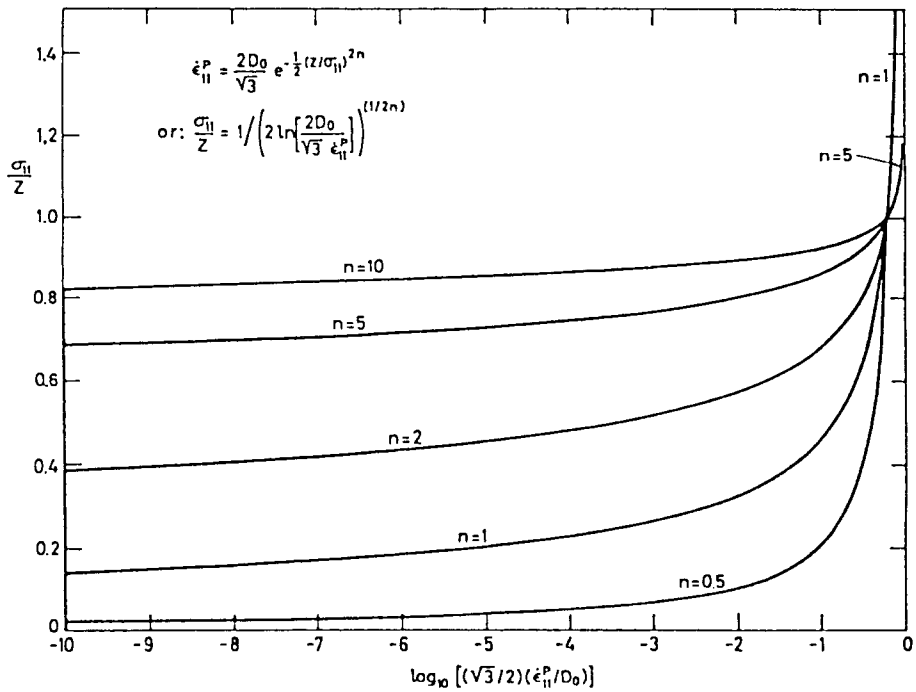

FIG. 1 *Dependence of the uniaxial flow-stress parameter on the strain rate parameter for different strain rate sensitivities n of the Bodner equation, after Bodner 1987.*

well as directional hardening and recovery at higher temperatures can be modeled rather well [29]. Anisotropic behavior is not included. For high strain rate application, only the basic dependence of plastic flow stress and isotropic hardening is required without thermal recovery. Then the following constants are needed: D_o, n, Z_o, Z_1, m and E. Rajendran, Bless and Dawicke [30] evaluated the material constants form Hopkinson-bar and flyer plate experiments for three initially isotropic materials. They showed that the Bodner-Partom modeling [28] successfully describes rate independent, rate sensitive, work hardening and non-work hardening material behavior.

IV. COMPARISON OF CONSTITUTIVE EQUATIONS WITH EXPERIMENTAL RESULTS

Clifton and co-workers [3] published shear stress data on pure aluminium from low to high rates of strain. Up to $\dot{\epsilon} = 10^4\ s^{-1}$ they found the rate sensitivity to be very low, but above $\dot{\epsilon} = 5 \cdot 10^4\ s^{-1}$, the rate sensitivity increases rapidly, up to 190 MPa per order of magnitude of strain rate, as shown in Fig. 2. This rapid stress increase at high rates of strain is also predicted from the Bodner-Partom equations. Bodner [31] compared his equation with these experimental results, Fig. 2. To satisfy the physical background of the equations, his comparison is done with using the yield stress at 0 K of 230 MPa as a value for the hardening parameter Z in its saturated state Z_s. This yields a very good agreement in the strain rate range below $\dot{\epsilon} = 10^4\ s^{-1}$. To match the data from experiments with extra thin, evaporated Al-film which leads to strain rates of about $10^7\ s^{-1}$, a limiting strain rate $2D_0$ of $5 \cdot 10^6$ or $10^7\ s^{-1}$ seems to be the best choice. With these assumptions, however the increased rate sensitivity of the bulk material at $\dot{\epsilon} = 10^5\ s^{-1}$ is not well predicted because the stronger stress increase by the equations starts later between 10^6 and $10^7\ s^{-1}$.

For the precipitation hardened Al alloy 6061-T6, the results of Hoggart and Recht [32] and Li [33,3] indicate that the rate sensitivity (with 60 MPa per order of magnitude of strain rate) is not as high as for the weaker pure aluminium, Fig. 3. To model these results, Bodner [31] named parameter of Z_s = 550 MPa, n = 5 and $2D_0 = 10^7\ s^{-1}$ for a reasonable agreement. Indeed, regarding the full range of strain rates, a choice of Z_s = 550 MPa, n = 3 and $2D_0 = 5 \cdot 10^5$ brings the behavior from low strain rates up to $\dot{\epsilon} = 10^5\ s^{-1}$ closer together, Fig. 3.

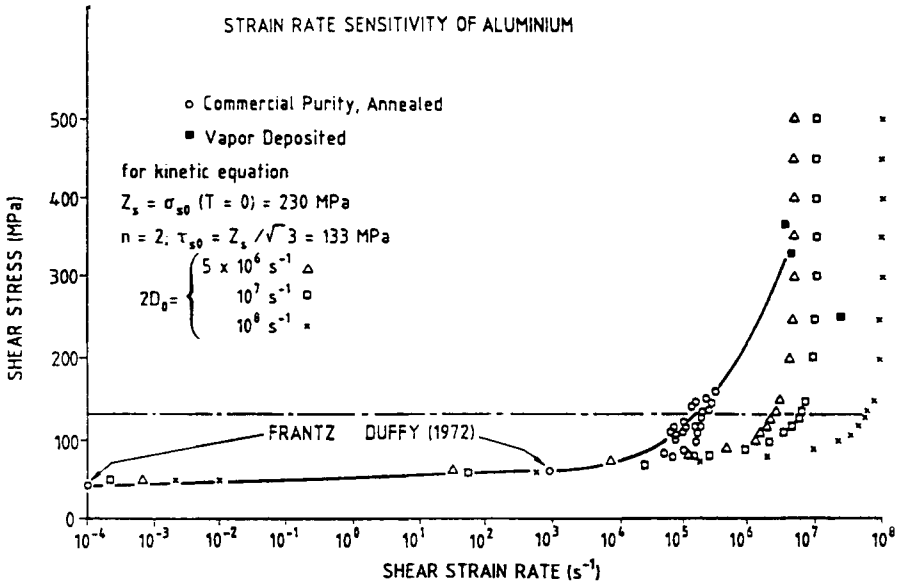

FIG. 2 *Comparison of the strain rate dependence of the flow stress of pure 1100-0 Aluminium, after Klopp, Clifton and Shawki 1985 and Bodner 1988.*

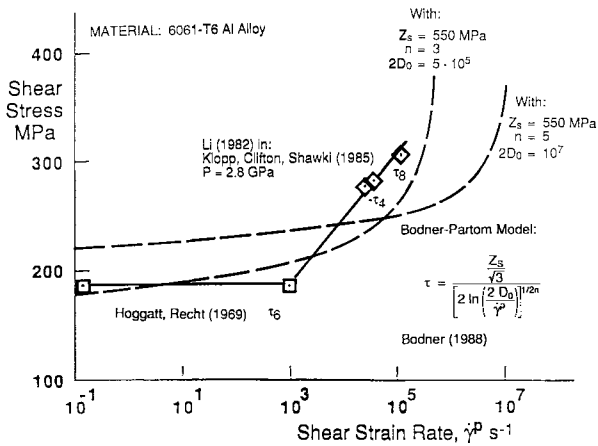

FIG. 3 *Comparison of the strain rate dependence of the flow stress of hardened 6061-T6 Aluminium-Alloy, Bodner 1988.*

It should be noted that the "limiting strain rate $2D_0$" and the frequency factor $\dot{\varepsilon}_0$ of the Arrhenius equation should not be interchanged. Of course, in both cases, a material-dependent saturation stress level is reached (so the physical background could be similar). Furthermore, for some metals like titanium, copper, carbon steels, the found frequency factors, Table 1, coincide with the value of 10^7 s^{-1} given by Bodner [31]. But for austenitic steels, the frequency factor ranges between 10^8 to 10^{10} s^{-1} [34-38,17-19]. Even in cases where the saturation stress at T=0 K and the frequency factor $\dot{\varepsilon}_0$ are not estimated, but evaluated from results of temperature- and strain rate-varied tests [35,36], the use of $2D_0 = 10^7$ s^{-1} leads to a better agreement than the use of $\dot{\varepsilon}_0 = 8 \cdot 10^9$ s^{-1} for 2 D_0 of a high strength austenitic steel [34], or the use of $\dot{\varepsilon}_0 = 5 \cdot 10^8$ s^{-1} for 2 D_0 of a low alloyed CNiCr-steel [36], Fig. 4.

The same CNiCr-steel with bcc structure was used here to apply the empirical equations and to compare their ability to describe the measured material behavior. From the engineering stress-strain curves, true stress data were developed and from ln/ln plots, the constants of the Ludwik, the

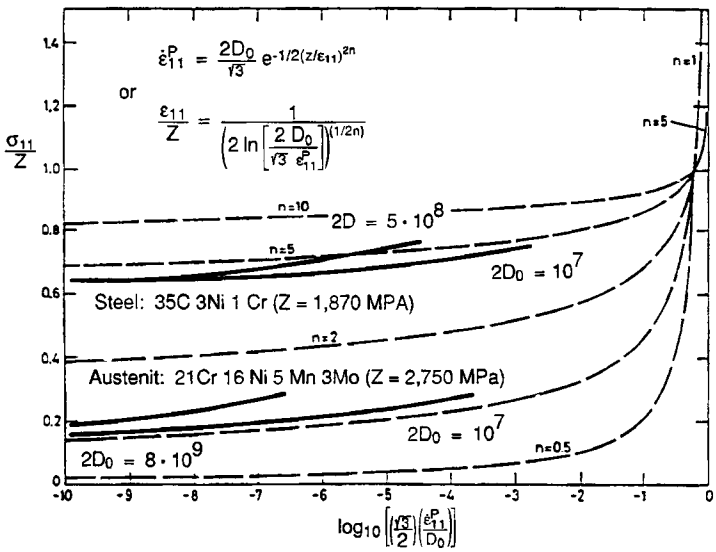

FIG. 4 *Comparison of the strain rate dependence of flow stress of a bcc- and fcc-steel (after Meyer/Staskewitsch, 1988 and Stiebler, et.al., 1989) with calculated values based on the Bodner-Partom Model (Bodner, 1988).*

Clifton, or Johnson/Cook equations are evaluated in order to get the best fit. The comparison at quasistatic loading between the measured and Ludwik-modeled behavior, Fig. 5, gives an excellent agreement from first yielding to 5 % strain and slightly under estimates, the stresses between 5 and 10 % strain. With increasing strain rates, the true flow stresses are initially insensitive up to $\dot{\epsilon} = 10^{-2} - 10^{-1}\ s^{-1}$, and then display a moderate rate sensitivity [36]. Assuming that the effect of rate sensitivity can be included by a simple power law theorem, the ln/ln plot should be a straight line. Indeed, this is the case, however they have different slopes, Fig. 6. Therefore, the rate sensitivity $m = d\ln(\sigma - A)/d\ln\dot{\epsilon}$ is not the same for different flow stresses, for m varies between 0.09 and 0.04. Dependent on which flow strength is be modeled, different constants must be used. In this comparison, an m of 0.064 was chosen for Clifton's modeling, marked with circles in Fig. 5. At low strains, the predicted stresses are too low; above 2 % strain, the predicted values are too high. A better correlation is reached with the Johnson/Cook eq. (2.5), but in the strict sense this holds only for this selected strain rate. The evaluation of the rate sensitivity parameter C shows that the constant C is a function of the yield strength and that it increases monotonically with strain rate $\dot{\epsilon}_p$, Fig. 7. In contrast to the original procedure [6,7] the constant $\dot{\gamma}_0$ is taken here to be $10^{-2}\ s^{-1}$, where the rate sensitivity for this steel appears. Fortunately, the stress variation of C with higher strains diminishes, but the rate influence remains. A certain value of C has to be selected to provide the best model for the particular strain rate region of interest. The same holds for the rate sensitivity constant β_1 of the Armstrong/Zerilli model (eq. 2.6) for the bcc steel: β_1 seems to be independent of strain, but drops down from about $10^{-3}\ K^{-1}$ at $\dot{\epsilon} = 10^0\ s^{-1}$, to $3{,}5 \cdot 10^{-4}\ K^{-1}$ at $\dot{\epsilon} = 10^4\ s^{-1}$, Fig. 8.

Regarding the material behavior at high rates of strain, there are no doubts that up to $\dot{\epsilon} = 10^3\ s^{-1}$, besides the athermal behavior, in many cases, thermally activated deformation mechanisms govern the flow stresses. For the range $10^3 < \dot{\epsilon} < 10^5\ s^{-1}$, the results are less clear, but there is strong evidence that the thermal activation still governs the main influence to $\dot{\epsilon} = 10^4\ s^{-1}$ [36,38-40], or even higher. In addition to our results with high strength steels [36,39], where the behavior up to $\dot{\epsilon} = 8 \cdot 10^3\ s^{-1}$ was found to be fully thermally activated, several other investigations support this opinion: The often cited example of Campbell/Ferguson [41], who found a remarkable change in strain rate sensitivity of the lower

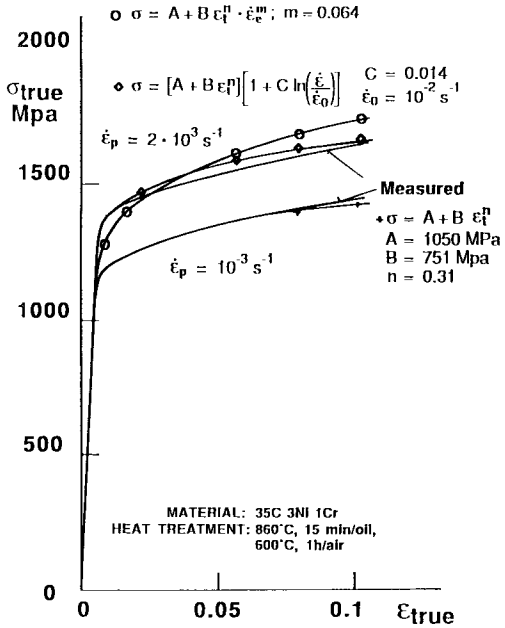

FIG. 5 *Comparison of measured material behaviour at low and high rate of strain with the prediction by Ludwik, double power and Johnson/Cook equations (material: HSLA-steel 35C 3Ni 1Cr).*

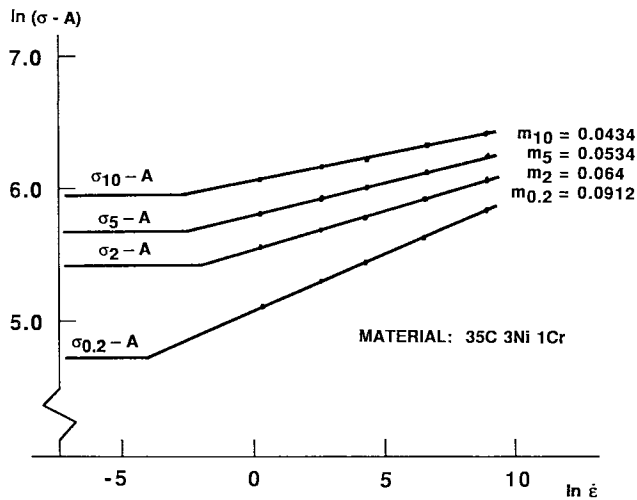

FIG. 6 *Strain rate sensitivity m of the double power equation for the .2, 2, 5 and 10 % flow-stress versus strain rate (Material: HSLA steel 35C 3Ni 1Cr).*

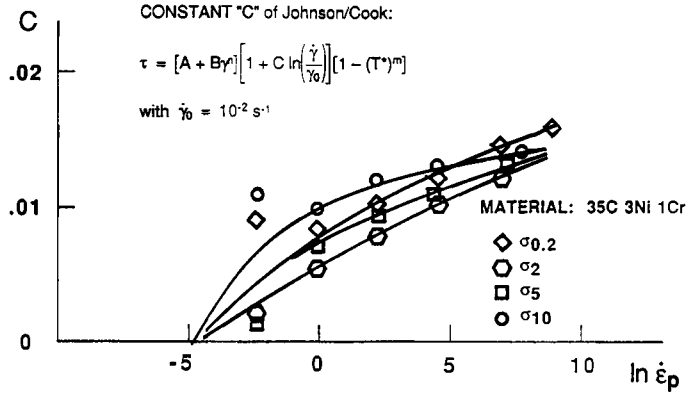

FIG. 7 *Strain rate sensitivity C of the Johnson/Cook equation for the .2, 2, 5 and 10 % flow stress versus strain rate (material: HSLA-steel 35C 3Ni 1Cr).*

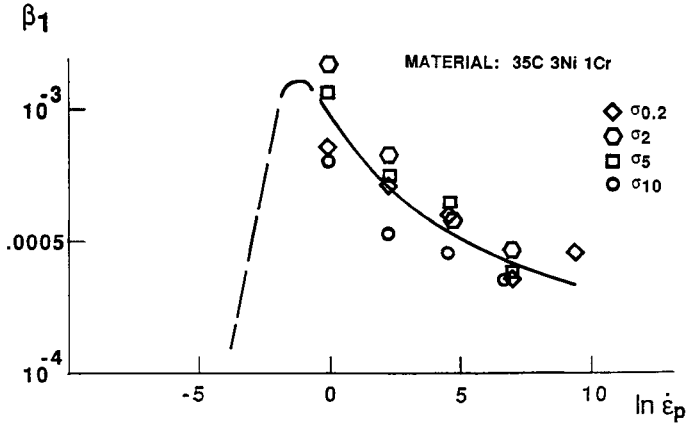

FIG. 8 *Strain rate sensitivity β_1 of the Armstrong/Zerilli equation for the .2, 2, 5 and 10 % flow stress versus strain rate (material: HSLA-steel 35 C 3Ni 1Cr).*

yield stress of mild steel above $\dot{\varepsilon} = 5 \cdot 10^3\ s^{-1}$, was re-examined by Nojima [38]. He analyzed different thermally activated dislocation mechanisms for carbon steel and found that, with the choice of structural parameters which are typical for these types of steels ($m = 1/p = 2$, $n = 1/q = 2/3$, $H_0 = 0{,}62$ eV), the yield stress of the carbon steels can be described very well with the thermal activation equation (3.1). In addition, and

that is important here, he showed that even up to the highest strain rate of $\dot{\epsilon} = 4 \cdot 10^4\ s^{-1}$, the flow stress of the 0.12 C-steel used by Campbell/Ferguson is properly modeled with an equation of pure thermal activation without the inclusion of drag effects [38]. The only difference is seen at T=195 K above $\dot{\epsilon} = 10^0\ s^{-1}$, where creations of twinning might have occurred.

Other examples are given by Follansbee [42] with the non-increasing strength at $\dot{\epsilon} = 10^4\ s^{-1}$, when the stress is measured under the condition of a constant threshold stress or a constant microstructure, or by Armstrong et al. [43] with the aforementioned alpha-uranium, where the measured rate sensitivity at $\dot{\epsilon} = 10^4\ s^{-1}$ is in accordance with a model description which is based solely on the thermal activation theory.

VI. SUMMARY

The semiempirical equations (eqs. 2.2 to 2.5) on the basis of the Ludwik expression separate the influence of strain rate and temperature from the strain hardening. In reality, the influences are coupled, especially in bcc materials. To make the equations agree with experimental results, the constants often have to be adjusted for the desired area of validity. The advantage of these simple equations is their easy implementation in computer codes.

Armstrong/Zerilli and Klepaczko improved the description by distinguishing between fcc and bcc materials and by introducing temperature-dependent coefficients. In both cases, the number of constants increased, with Klepaczko up to 12 or 15, but an important step towards a meaningful physical description has been accomplished.

The Bodner/Partom model uses less coefficients and has the possibility of being applicable to different loading conditions, including high rates of strain. Follansbee introduced the concept of the threshold stress, and by a model for the evaluation of state of the material structure, he overcame the old limits of the thermal activation theory. Of course this can only be achieved through an intensive test program. But from the viewpoint of material characterization, this is acceptable. In order to document the material behavior under dynamic conditions, no one may believe that with a few tests the complexity of real materials can be evaluated satisfactorily. From the viewpoint of modeling and computation, the opinion of Alexander [44], with respect to metal forming processes can be adopted with the same

intention for the high strain rate application: "Since even the classical theory requires sophisticated numerical computational techniques for the solution of all but the simplest of geometrical configurations, it seems worthwhile examining how [the procedure] can be modified to include the important effects [of real material behavior]."

Today this sounds more like an understatement. Let us assume, that everywhere the need for an accurate material description is accepted. The improvements in understanding will be worthwhile.

Acknowledgment

The assistance of the Fraunhofer-Gesellschaft München, the German Ministry of Defense, Bonn, both Germany, the Center of Excellence for Advanced Materials, and the Department of Applied Mechanics and Engineering, both at the University of California, San Diego, California, USA is greatly appreciated.

REFERENCES

1. U.F. Kocks, in Unified Equations for Creep and Plasticity, A.K. Miller (ed.), Elsevier Appl. Sci., N.Y., 1 (1987).
2. P. Ludwik, *Phys. Z.*, 10: 411 (1909).
3. R.W. Klopp, R.J. Clifton, T.G. Shawki, *Mech. Mat.*, 4: 375 (1985).
4. J. Litonski, *Bull. Acad. Pol. Sci.*, 25: 7 (1977).
5. T. Vinh, M. Afzali, A. Roche, in Mechanical Behavior of Material, Proc. ICM, K.J. Miller and R.F. Smith (eds.) Pergamon Press, Oxford & New York, 633 (1979).
6. G.R. Johnson et al., *J. Eng. Mat. Techn.*, 105: 42,48 (1983).
7. G.R. Johnson, W.H. Cook, in Proc. 7th Intl. Symp. on Ballistics, The Hague, 541 (1983).
8. F.J. Zerilli, R.W. Armstrong, *J. Appl. Phys.*, 61, No.5: 1816 (1987).
9. R.W. Armstrong, F.J. Zerilli, *J. d. Physique*, 49: C3-529 (1988).
10. F.J. Zerilli, R.W. Armstrong, in Shock Waves in Condensed Matter, S.C. Schmidt and N.C. Holmes (eds.), Elsevier Publ., Amsterdam, 273 (1988).
11. P.W. Follansbee, G. Regazzoni and U.F. Kocks, in 3rd Conf. on Mechanical Properties at High Rates of Strain, J. Harding (ed.), Inst. Physics, London, Conf.Ser.No.70: 71 (1984).

12. W.H. Gourdin, in Shock Waves in Condensed Matter - 1987, S.C. Schmidt, N.C. Holmes (eds.), Elsevier, Amsterdam, 351 (1988).

13. J.D. Campbell, A.M. Eleiche, and M.C.C. Tsao, in Fundamental Aspects of Structural Alloy Design, Plenum Publ. Corp., New York, 545 (1977).

14. O. Vöhringer, "Deformation Behaviour of Materials", Proc. Intl. Summer School, Univ. Nantes (France), Sept. 1989.

15. U.F. Kocks, *ASME J. Engrg. Mater. Tech.*, 98: 76 (1976).

16. P.S. Follansbee, U.F. Kocks, *Acta Metall.*, 36: 81 (1988).

17. P.S. Follansbee, in Proc. IMPACT'87 - Impact Loading and Dynamic Behavior of Materials, C.Y. Chiem, H.-D. Kunze, and L.W. Meyer (eds.), DGM Informationsges., Oberursel/Frankfurt, Vol. 1: 315 (1988).

18. P.S. Follansbee, in Shock Waves and Condensed Matter, S.C. Schmidt and N.C. Holmes (eds.), Elsevier Publ., New York, 249 (1988).

19. P.S. Follansbee, G.T. Gray III, *Met. Trans. A*, 20A: 863 (1989).

20. H. Mecking, U.F. Kocks, *Acta Metall.*, 29: 1865 (1981).

21. A. Kumar, F.E. Hauser, J.E. Dorn, *Acta Metall.*, 16: 1189 (1968).

22. K.G. Hoge and A.K. Mukherjee, *J. Mat. Sci.*, 12: 1966 (1977).

23. F. Burgahn, O. Vöhringer, E. Macherauch, Proc. Explomet 1990, this volume

24. J.R. Klepaczko, *J. Mechanical Working Technology*, 15: 143 (1987).

25. J.R. Klepaczko, P. Lipinski, and A. Molinari, in Proc. IMPACT-87 - Impact Loading and Dynamic Behavior of Materials, C.Y. Chiem, H.-D. Kunze, and L.W. Meyer (eds.), DGM Informationsgesellschaft, Oberursel/Frankfurt, Vol. 2: 695 (1988).

26. D.J. Steinberg, S. Cochran, and M. Guinan., *J. Appl. Phys.*, 51: 1498 (1980)

27. D.J. Steinberg and C.M. Lund, *J. de Physique*, 3, Sup.No.9, T49: C3-433 (1988).

28. S.R. Bodner and Y. Partom, *J. Appl. Mech.*, 42: 385 (1975).

29. S.R. Bodner, in Unified Equations for Creep and Plasticity, A.K. Miller (ed.), Elsevier, N.Y., 273 (1987).

30. A.M. Rajendran, S.J. Bless, and D.S. Dawicke, *J. Eng. Mat. Techn.*, 198: 75 (1986)

31. S.R. Bodner, in Proc. IMPACT'87 - Impact Loading and Dynamic Behaviour of Materials, C.Y. Chiem, H.-D. Kunze, and L.W. Meyer (eds.), DGM Informationsges., Oberursel, Vol. 1: 77 (1988).

32. C.R. Hoggatt and R.F. Recht, *Exp. Mech.*, 9: 441 (1969).

33. C.H. Li, Ph.D. Thesis, Brown University, Providence, RI (1982).

34. P.S. Follansbee, in 4th Conf. on Mechanical Properties at High Rates of Strain, J. Harding (ed.), Inst. Physics, London, Conf.Ser.No. 102: 213 (1989).

35. K. Stiebler, 4th Conf. on Mechanical Properties at High Rates of Strain, J. Harding (ed.), Inst. Physics, London, Conf.Ser.No.102: 181 (1989).

36. L.W. Meyer, E. Staskewitsch, in Proc. IMPACT'87 - Impact Loading and Dynamic Behaviour of Materials, C.Y. Chiem, H.-D. Kunze, and L.W. Meyer (eds.), DGM Informationsges., Oberursel/Frankfurt, Vol.1: 331 (1988).

37. R. Lagneborg, B.-H. Forsen, *Acta Met.*, 21: 781 (1973).

38. T. Nojima, in Proc. IMPACT'87 - Impact Loading and Dynamic Behaviour of Materials, C.Y. Chiem, H.-D. Kunze, and L.W. Meyer (eds.), DGM Informationsges., Oberursel/Frankfurt, Vol. 1: 357 (1988)

39. L.W. Meyer, 3rd Conf. on Mechanical Properties at High Rates of Strain, J. Harding (ed.), Inst. Physics, London, Conf.Ser.No. 70: 81 (1984)

40. T. Nicholas, *Exp. Mech.*, 138: 177 (1981).

41. J.D. Campbell and W.G. Ferguson, *Phil. Mag.*, 21: 63 (1970).

42. P.S. Follansbee, in Metallurgical Applications of Shock-Wave and High-Strain-Rate Phenomena. L.E. Murr, K.P. Staudhammer, and M.A. Meyers (eds.), M. Dekker, Inc., N.Y. 451 (1986).

43. R.W. Armstrong, P. Follansbee, and T. Zocco, in 4th Conf. on Mechanical Properties of Materials at High Rates of Strain, J. Harding (ed.), Inst. Phys. London, Conf.Ser.No. 102: 237 (1989).

44. J.M. Alexander, in Plasticity Today, A. Sawczuk, G. Bianchi (eds.), Elsevier Appl. Sci, Publ., London, 683 (1985).

5

Material Deformation at High Strain Rates

C. Y. CHIEM

Plasticité Dynamique, Laboratoire Matériaux
Ecole Nationale Supérieure de Mécanique
44072 Nantes Cedex 03, France

A brief review is presented of response of materials to various types of high strain rate loading.

Following collection of data from a large number of investigations, behavior of materials under the effect of strain rate and temperature will be discussed. This will include the correlation of mechanical properties to microstructures. Introducing micro-mechanisms of deformation will help to elucidate certain physical phenomena in this topic. Some models taking account of microstructural parameters will be discussed in order to clarify the range of applicability of each set of parameters. This will be discussed with various states of damage of materials.

I. INTRODUCTION

A wide range of engineering employ structural materials which are subjected to high or very high strain rate of loading such as impact of debris of aircraft composite panels or bird-strike on aero-engine, plastic flow close to fast propagating cracks, high speed metal-forming or machining processes and various military applications, etc. The way of approach in which this paper is developed is focalized in the illustration of the present state of research work in this domain. Progress in technology is continuously challenged by requirements of new technical performance. These requirements offer motivations for the development of mechanical testing of materials and structures under severe environment including fast development of numerical tools. In the past, many keynote lectures or review papers[1-5] are involved with structural response to high strain-rate loadings; and recently, more and more review papers comment on the material behavior at high

strain rate[6-12]. More recently, many non-metallic and composite materials including several reviews on these works have been published[13-15].

It is clear that most materials show a significant variation in the mechanical response underincreasing strain-rate loading or under temperature effects. Development of constitutive equations or equations of state which relate stress and strain to the usual conditions of strain rate and temperature allows techniques of numerical analysis to be applied in the modelling of structural design in function of known material properties. Recent progress shows the need to consider microstructural aspects or evolution in the material. Attempts have been made to introduce internal structure sensitive parameters and effects of initial structure and texture of the materials on the deformation mechanisms.

Extending those effects to high strain-rate processes becomes much more complex and the understanding of the dynamic response of materials is rendered much more difficult.

It is not possible for the time allotted to mention all the work realized by various scientists in this field of study. The choice is then made to describe this topic by selection of examples of important points and to refer to other sources cited in references to fill in the gaps.

II. HIGH STRAIN-RATE DEFORMATION OF METALLIC MATERIALS

A. *GENERAL CONSIDERATION*

Phenomenological theories including yield- and stability-criteria are not discussed in this review. We will only emphasize on deformation behavior of the materials and their metallurgical and physical effects. These latters are characterized mainly by the relationships between microstructures and residual mechanical properties and are resulted from the very complex correlations between stress, strain, stress and strain states, strain-rate and temperature. So, the major aim of doing experimental tests is to determine the stress required for a deformation to occur at strain-rate ε of the material of a specimen. This material has indeed a given structure s under fixed physical conditions such as temperature T and pressure P. By doing one of these parameters as a variable and the others as constant parameters, we set up a certain number of terms which help to describe as properly as possible a rather complex function which is:

$$\sigma = \sigma\ (\varepsilon, T, P, s) \tag{1}$$

This expression orientates mechanical modelling which has to describe changes in plastic stress. Mostly, mechanical tests are arranged to be under uni-axial stress or uni-axial strainconditions in order to simplify the expression and to facilitate the identification of the micromechanisms of deformation. Tendencies of the stress-strain behavior of materials versus strain-rate and temperature were discussed in [16,17].

This yields some constitutive equations which are developed by some authors referenced from [18] to [25].

It is clear that s from equation (1) is dependent on the initial structures of the materials (i.e., thermomechanical history prior to the test). The evolution of s during the test depends on the conditions of the test. This includes a range of microstructures such as planar dislocation arrays at lower strains which evolve into more dense arrays of dislocations at higher strains.

These different arrays can be composed of twin faults and α' martensite which occurs at the intersections of twin-fault bundles. The dislocation density changes are simply related to changes in stress (or strain) through the following kind of expressions:

$$\sigma = \sigma_0 + K\sqrt{\rho} \tag{2}$$

$$\rho = \rho_0 + M.\varepsilon \tag{3}$$

where σ_0, K and M are constants and ρ is the dislocation density (ρ_0 is the initial dislocation density), $\sqrt{\rho}$ being the average length of dislocation-segments. Under these considerations, constitutive equations using microstructural approach must take into account microscopic parameters such as: dislocation densities, twin densities, the mean value of dislocation cell size, the mean value of grain diameter, the mean distance between twins, the volume fraction of dislocation cells and twin-faults respectively.

B. STRAIN-RATE SENSITIVITY

One of the major problems which was noticed in 1961 is the rapid increase in strain-rate sensitivity of aluminum tested at strain-rate higher than 10^3 s^{-1} [26]. Similar phenomenon has been shown with other materials [27-30]. In solid mechanics point of view, some authors attribute this increased rate sensitivity to an inertia effect due to the rapid increase of strain-rate, while in the physical point of view, this rate sensitivity is attributed to a sudden transition from a thermally activated mechanism (low velocity) to a linear viscous mechanism (very high dislocation velocities with phonon and/or electron damping effects). This difference of points of view is well discussed in [9]. Nevertheless, the existing data seem inconclusive to define the transition behavior of the stress from low and medium strain-rates to high strain-rates around 10^3 $_s$-1.

Figure 1 shows an example of this strain-rate sensitivity through results obtained from investigations on a 3% Si-Fe single-crystal [31] which is b.c.c. This sudden transition as we can notice in Fig. 2 should be predominantly due to rapid increase of twin density versus strain-rate. Dislocation multiplication contributes also to rate sensitivity but much more smoothly in the case of b.c.c. materials. For f.c.c. materials, most have a higher stacking fault energy and have less

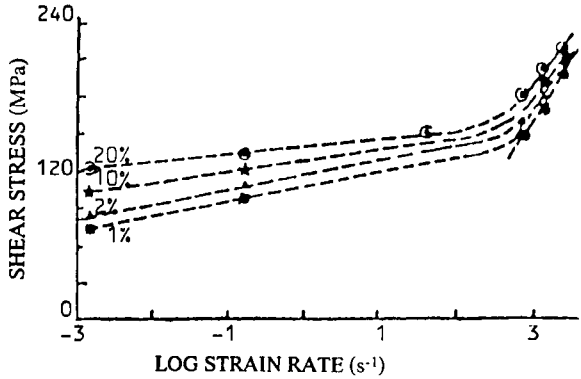

FIG. 1 *Strain-rate sensitivity of 3% Si-Fe single-crystals under high strain-rate shear loading [31].*

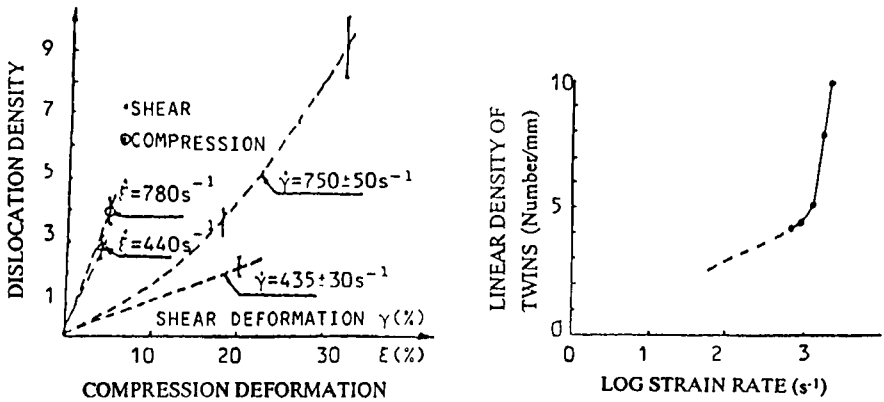

FIG. 2 *Results on uniaxial stress experiments of a 3% Si-Fe single-crystal subjected to rapid solicitations: dislocation density versus shear and compression strains at various strain-rates, linear density of twins versus strain rate [31] versus strain-rate.*

tendency to twin unless the temperature is decreased to very low value or the strain-rate is increased. At lower and medium strain-rates, f.c.c. materials as well as b.c.c. materials have more tendency to have dislocation cells as shown in Figs. 3 and 4.

C. *TWINNING AND DISLOCATION GLIDE*

Twinning is a rapid process which can occur only if pressure, shear stresses and temperature can reach together the required threshold conditions. In addition, crystallographic orientation, stacking fault energy, pulse duration, existing substructure and grain-size can also alter those conditions. The threshold stress of twinning [27] was proposed as:

$$\tau_c = \gamma_{fe} / nb \tag{4}$$

where γ_{fe} is the stacking fault energy of the materials, b, the Burgers vector of dislocations which generate the micro-twin and n, a stress concentration factor ($1<n<3$) as twinning is considered here as resulting from localized arrangement of dislocations. This localized phenomena can be observed macroscopically on the stress-strain curves of high strain-rate behavior of tungsten single-crystals shear-loaded in (112) planes as shown in Fig. 5. At high strain-rate, if all required conditions are satisfied, the stress concentration which is sufficient to generate twins is induced by microslip of dislocations in the early stage of deformation. Afterward, twinning occurs giving the serrated portion of the stress-strain curves [28].

Indeed, within the whole material, dislocation slip mechanism and twinning mechanism co-exist and are undergoing compromising arrangements in response to mechanical loading. Recent work [27] demonstrates this tendency as shown in Fig. 6 where the deformability of tungsten single-crystals is plotted versus ultimate shear stresses under three different strain-rates γ_1, γ_2, and γ_3 for the two tungsten single-crystals. The crystals are deformed at the initial predominance of either by slip of dislocations or by twinning. In the first case, the deformation augments with increasing strain-rate while in the case of twinning, it varies inversely with increasing strain-rate. This consequence shows the importance to take into account the rate of multiplication of dislocations and twins. By adding these two microstructural parameters to constitutive equations, the dynamic behavior of materials will be much more conveniently described.

To be consistent with this overall point of view, previous work in 3% Si-Fe single-crystals [25] proposed a derivation of the critical stress for twinning (Eq. 4) as follows:

$$\tau_{tw} = (1/n).\{(\gamma_{fe}/b_s) + (G.b_s/2r)\} \tag{5}$$

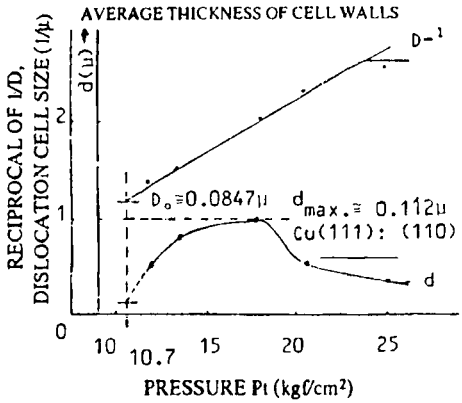

FIG. 3 *Reciprocal of dislocation cell size. 1/D and thickness of cell walls, d vs. pressure P_t induced by electromagnetic field in Cu single-crystal. The dislocation cell in the figure shows (---: mobile dislocations) and (_____: dislocations at the cell walls) [31].*

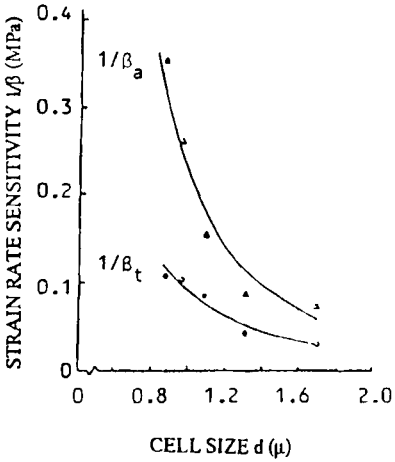

FIG. 4 *Apparent and true strain rate sensitivities as functions of dislocation cell size in Al single crystals [38,39].*

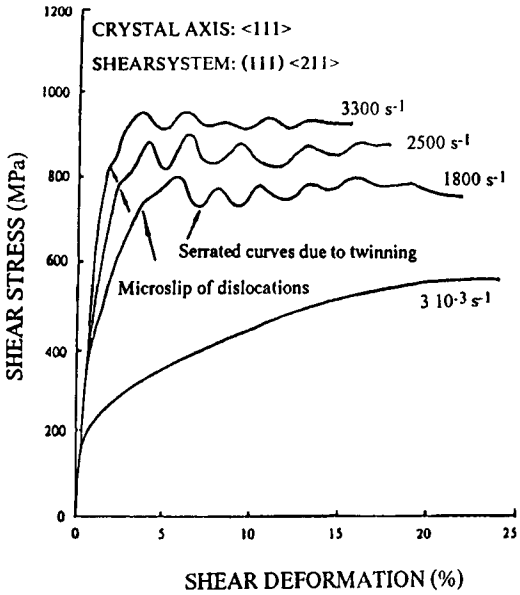

FIG. 5 *Stress-strain curves of a tungsten single-crystal of axis <111> subjected to various strain-rates of loading in shear. Serrated portion of the curves show twinning initiated by microslip of dislocations.*

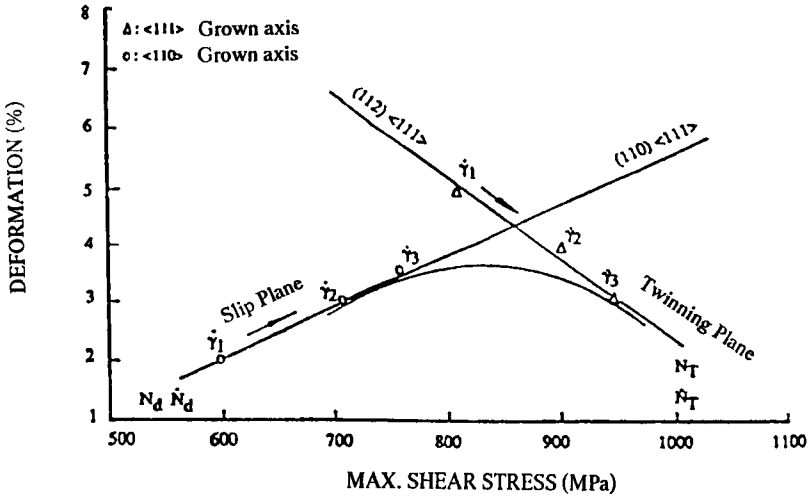

FIG. 6 *Deformability of the tungsten single-crystals with grown-axes <110> and <111> as a function of ultimate shear stress under three different strain-rates [34].*

with n as the coefficient of stress concentration at the tip of the twins, G, the shear modulus, b_s, the Burgers vector of screw-dislocations, γ_{fe}, the stacking-fault energy of the material and r, the radius of dislocation arc. This formula takes into account the twinning process as first components and the dislocation glide motion as second component. This approach allows for consideration of twinning as well as dislocation glide to be in permanent interactions.

III. STRAIN-RATE HISTORY EFFECTS AND MICROSTRUCTURES

History effects and temperature effects during high strain-rate deformation of materials have been studied in the aim of understanding material behavior and developing appropriate constitutive equations. It has been shown that two additional factors determining history effects are first, the lattice structure and then the development of the microstructure which is evolutive during straining. This supposes that two types of micromechanisms are involved in rate and temperature effects; one is the currently operating mechanisms of thermal activated motion of dislocations and the dynamic recovery of dislocations furnishing the physical "Storage-Flux-Annihilation" equilibrium of dislocation dynamics [35]. Experiments can be performed with a torsional Kolsky bar modified for simple shear loading of the specimens. Details of the test technique are mentioned in [38,39,55]. A recent review of history effects is presented in [56,57].

In this section only insight on the very few microstructural results are presented. The strain rate jump tests are generally viewed as particularly important in determining constitutive relations for dynamic plasticity because configurations are expected not to change significantly during the rise time of the jump in strain rate. Satisfactory correlation of experimental results with models [36,37] of the form suggested for thermally activated micromechanisms was shown. Results of incremental tests on aluminum single-crystals were presented in [38,39]. In Fig. 4 strain sensitivities are correlated to dislocation cell size; the later are important substructure related to dislocation densities and velocities, though effecting dislocation mobility. Saturation of cells formation induces a state of stability where all cells are having equal strength Burgers vectors. As reported in [40], the density of cell wall dislocations is approximately 50 times higher than the mobile dislocation density at the core of the cell. Evolution of dislocation cell wall thickness and cell size versus shock pressure generated by electromagnetic field [41] is shown in Fig. 3. One can notice the existence of a critical pressure for the cells to be nucleated and the cell wall thickness evolves to a maximum with pressure increase denoting a high level of work-hardening of the material. It was also shown that for high stacking fault energy metals, formation of dislocation cells and cross-slip of dislocations are easier.

IV. SHOCK INDUCED MICROSTRUCTURES AND MECHANICAL PROPERTIES

Microstructural observations of the recovered specimen of 3% Si-Fe single-crystals are done with TEM. In contrast to the normal microstructure after high strain rate testing, no twins are observed

in the recovered crystal. Impact testing with explosives on 3% Si-Fe single-crystals shows a very large density of twins. It is shown previously that twinning occurs only if a critical stress is reached. It is clear that conditions for the nucleation of twins depend on five parameters: the incubation time of twinning, the pressure and duration of the shock, the stacking-fault energy of the material which induces the interactions between twinning and dislocation glide motions and the temperature. Also all these are dependent on dislocation velocities; this later can increase or decrease the threshold stress of twin nucleation.

For this material, twins and stacking faults are the main micromechanisms responsible for the rapid strain rate sensitivity transition at 10^3 s^{-1}. This seems to be in good agreement with the transition zone mentioned in [42]. The mention of "rapid evolution" at the rate sensitivity transition point of this figure is also consistent with twinning because this latter is a very fast and sudden process (Propagation occurs at sound velocity).

A. *DISLOCATION MOBILITY*

Relationship between the resolved shear stress on a slip plane and the velocity of mobile dislocations on that slip plane is fundamental for the development of constitutive equations in the field of dynamic plasticity. The uniaxial strain experiments performed by plate impact recovery tests are aimed to contribute a little in this direction. Details on these experiments are already described in [43] with work done on 3% Si-Fe single-crystals. Results of these investigations on dislocation velocities are plotted together with results of many investigators in Fig. 7 [44-52]. The curves exhibit a general tendency of stress dependence that implies various mechanisms. Two regimes are existing: (a) a low velocity regime which is strongly stress dependent and where thermally activated mechanisms are predominant; (b) a high stress regime where high velocity is linearly dependent on stress and viscous drag is the rate controlling mechanism.

The treatment of thermally activated motion of dislocations past barriers such as impurities and intersecting dislocations seems quite well established [51,52]. At very low stresses, it is much more appropriate to use a stochastic approach as proposed in [56]:

$$V = (L\tau/B).(U_o/kT)^{1/2} \exp(-U_o/kT) \qquad (6)$$

for the case $\tau \leq 0.65\ kT/br_o l \simeq \tau$. In this relation B is the damping constant, Uo, the maximum of the bonding energy, L, the distance travelled for each activation, r_o, distance between defect and the glide plane, l, the dislocation segment length. At higher stresses where the dislocation velocity increases with increase in the resolved stresses. In this case the usual formula of the rate theory is only an approach:

$$V = L\nu_o(\tau).\exp\{-\Delta G_{(\tau)}/kT\} \qquad (7)$$

case where $\tau \leq 0.65\ Uo/br_o l$ and with a Debye frequency slightly dependent on stress, $\nu_{o(\tau)}$.

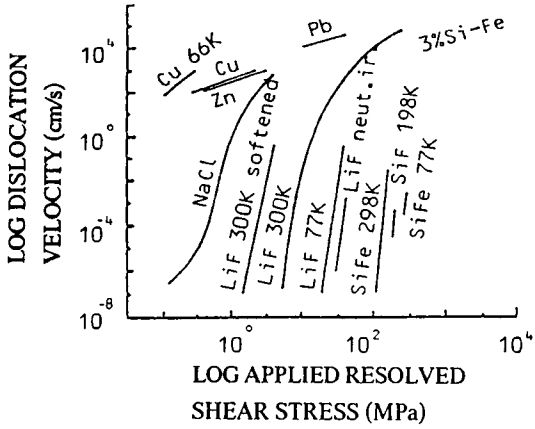

FIG. 7 *Dislocation mobility of various materials [38].*

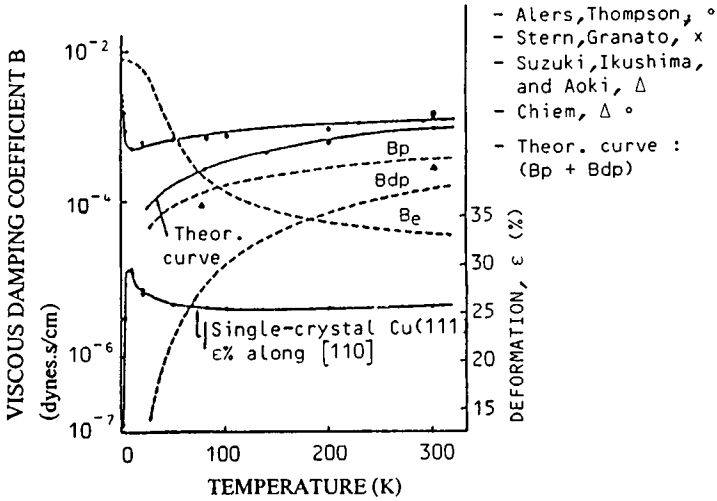

FIG. 8 *Temperature dependence of the viscous damping coefficient in copper single-crystal deformed by pulsed eectromagnetic field [41,53].*

At stress levels that are high enough to overcome the Peierls barrier associated with the periodic structure of the lattice, and low enough to cause dislocation velocities which are below elastic wave speeds for relativistic effects to be minimize, the resolved shear stress and the dislocation velocity then satisfy a linear viscous drag equation:

$$\tau b = BV_d \tag{8}$$

with the Burgers vector b as a lattice parameter that is equivalent of the displacement discontinuity of the dislocation and B is a drag coefficient. B is temperature dependent as shown in Fig. 8 [38,41,53]. At room or high temperature, interaction of thermal phonons and dislocations is responsible for viscous drag forces. When temperature is approaching the superconductivity transition point, mechanisms of electron drag become predominant. Phonon scattering is estimated to contribute to the drag coefficient. When materials are involved with very strong shock wave phenomena, evolution of the micromechanisms is also dependent on the type of waves as shown in Fig. 10[56]. We can summarize into four types of wave effects the metallurgical effects of the materials: *Behind the elastic waves, no imperfection; *Behind the plastic waves, generation of dislocations, stacking faults, twin boundaries and antiphaseboundaries; *Behind transformation waves (or plastic wave II), if the transformation $\alpha \Rightarrow \beta$ occurs, a new crystalline structure is formed containing the imperfections that were created by the preceding plastic wave and the transformation shear. If there is a reverse transformation, we have then ($\alpha \Rightarrow \beta \Rightarrow \alpha$); the imperfections are therefore due to double transformation by shear. It is difficult at the present to get better understanding in this field. More experimental work should be done at macroscopic level as well as at microscopic approach. Figure 9 shows the relationship between critical twinning pressure and stacking fault free energy for a number of f.c.c. metals and alloys as estimated and given from [57]. This again demonstrates the predominant effect of critical pressure (or stress) on the formation of twins or dislocation cells.

Many questions still exist in the region of very high dislocation velocities. Most of the work done has involved theoretical approaches regarding such phenomena as supersonic dislocations[41], the Smith shock interface [54] loading history dependent dislocation velocities[55] and dynamic nucleation of dislocations running at speeds higher than the Raleigh wave speed [62], etc. In contrast, very little work has been done in experiments of the dynamic of high velocity dislocation. This is mainly due to a lack of satisfactory means.

During the production of dislocations or other defects in the shock front, there is occurrence of heating. On the basis of work done on a solid during rarefaction, authors of ref.[58] obtained the following formula for the residual yield or flow stress of metals and alloys subjected to a "planar shock":

$$\sigma = \sigma_o + 2\alpha G\, b.\{\, C_R.\Delta T - \{(P_i + P_o).(V_o - V_i)\}/2 + \int_{V_i}^{V_f} P_{s(V)}\, dV \,\}^{1/2} \qquad (9)$$

where σ_o, α, C_R are constants for any particular material, G is the shear modulus, b is the Burgers vector, ΔT is the temperature change in the material, V_o, V_i and V_f are the initial, intermediate and final volumes, and P_o and P_i are the initial and intermediate pressures. Actually P_i and V_i are intermediate values associated with the peak shock pressure (P), and $P_{s(V)}$ is the isentropic relief path (considering the hydrodynamic theory [63]).

V. SOME WORDS ON HIGH POLYMERS

In the past two decades the mechanical behavior of high polymers subjected to high strain-rate loading have been extensively studied in experimental as well as fundamental research field. The viscoelastic behavior of the polymers is well described in [64, 65]; the high strain-rate behavior os some polymers has been studied experimentally by the use of torsional impact machine [66] and the torsional Hopkinson-bar apparatus [67] in which a modified Norton-Hoff constitutive relation was proposed. In [68] and [69], the authors tend to relate the macroscopic behaviors of polymers to the rupture of molecular chains and the influence of the distribution of the chemical compositions has been studied in [70].

The polymers consist of long molecular chains of covalently bonded atoms. The arrangement of the molecular chains presents two states: - The amorphous state which is considered to be a random tangle of molecules and the crystalline state named by the high orientation of molecules. The observation by means of some microscopic equipments shows that the semi-crystalline polymers have the structure of spherulites or in modelisation, the paracrystalline structure (Fig. 10(a) and (b)). An attempt of constitutive equation modelling was done in [71]. In this model, the crystalline part and the amorphous part are assumed to be cubes assembled in parallel and according to the amount of deformation a generalized modulus is defined which takes into account the shear modulii corresponding respectively to the crystalline and the amorphous oarts of the polymer, also, the coefficient of crystallinity. Thermally activated mechanisms of dislocations are supposed to be actived in the crystalline part and a thermodynamic visco-plastic model is applied to the amorphous part. After the use of identification technique, a simplified form of the constitutive equation which is written as:

$$\tau = A\ \ln(1 + \alpha\gamma).\gamma^{\beta}.\{1 + (\Delta T^{\theta}/T_g)\} \qquad (10)$$

where A is a constant of the material, α, the dislocation multiplication parameter, β, the strain-rate sensitivity, ΔT, the temperature increment during high strain-rate plastic straining due to localized

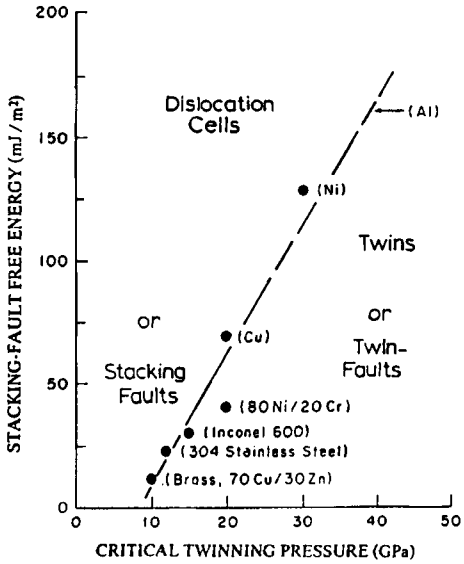

FIG. 9 *Critical twinning pressure versus stacking-fault free energy for a number of fcc metals and alloys. (Critical pressure values are estimated from shok-loading data of Ref. [57] stacking-fault free energy values are from [58]).*

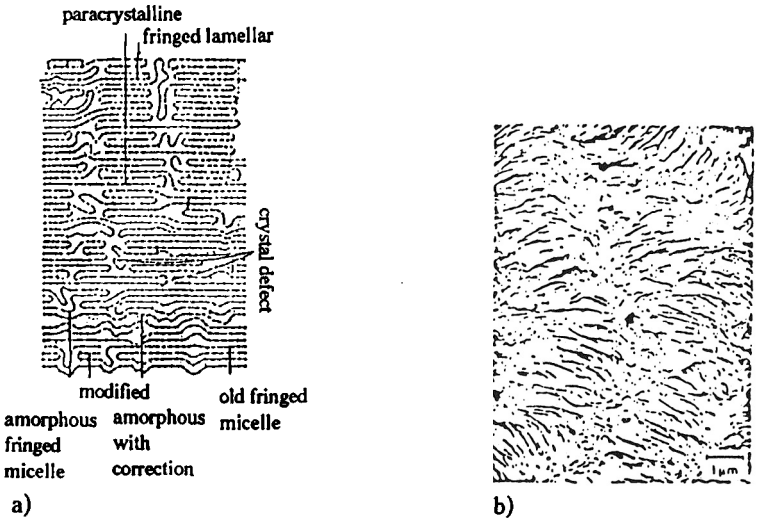

FIG. 10 *Microstructural model of high polymers: a) the model of paracrystalline structure; (b) an element of spherulite.*

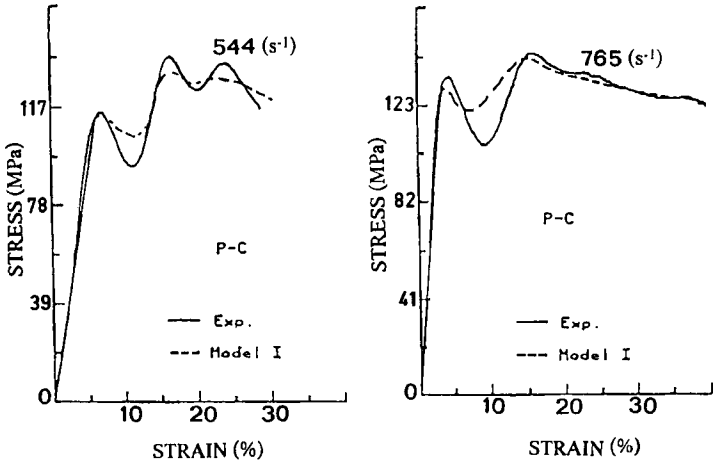

FIG. 11 *Attempt of modelisation on the stress-strain behavior of a polycarbonate PC deformed by dynamic torsion [71].*

adiabatic behavior of the polymers, T_g, the glassy transition temperature and θ, the stress sensitivity to temperature effects. All these parameters except A can be experimentally determined. An example of the model is applied to a polycarbonate [71] which is deformed at high strain-rate by torsion. Comparison of stress-strain curve obtained from the model and the curve given by experimental testing shows that this preliminary attempt gives a quite good agreement (Fig. 11).

VI. CONCLUSION

As previously mentioned, it is not possible to make a complete review under this topic and omission of results is expected; so the objective of this paper aims only to give a certain insight on the microscopic aspects of dynamic plasticity. The author wishes to give a certain warning in this occasion for the fact that tremendous efforts must be undertaken for microstructural studies if more powerful constitutive equations are wished. Progress is too slow in this field.

As the level of individual dislocations progress is sensitive on measurements of dislocation mobility but changes in mobile dislocation density during dynamic plastic deformation are still not understood. Influences of strain rate history, temperature, and shock pressure require further investigation as well as the role of the stacking fault energy of materials on twin nucleation, dislocation cell size formation and dislocation glide motion.

Until now most investigations have concentrated on metals, very few on single-crystals and almost none on composite materials or ceramics. Emphasis should be put to extend dynamic testing on the new trend of materials. Finally special care should be taken on the development of

physically based models of a wide range of applicability and the achievement of this requires good understanding of the micromechanisms of deformation that enables further progress in this field of research.

ACKNOWLEDGMENT

The author is indebted to his colleagues and friends for efficient help in the realization of all the results necessary for this review. My thanks are addressed to the French Ministry of Defence for their continual support to the studies performed in our Laboratory.

The author is also indebted to Dr. K. P. Staudhammer for discussions on this paper and Ms. D. Vigil for her help in realizing this manuscript. Both are members of the Los Alamos National Laboratory. Ms. Faye Ekberg at the University of Texas at El Paso typed the final, camera-ready manuscript.

REFERENCES

1. N. Jones and T. Wierzbicki, Editors, Structural Crashworthiness, Butterworths Press, London and Boston (1983).
2. W. Johnson and A. G. Mamalis, Crashworthiness of Vehicules, 1st Ed., Mechanical Engineering Publications, London (1978).
3. S. R. Bodner, Proc. Oxford Conference on "Mechanical Properties at High Rates of Strain," 70:451 (1984).
4. P. S. Symonds, H. Kolsky, and J. M. Mosquera, Proc. Oxford Conference on "Mechanical Properties at High Rates of Strain," 70:479, 1984).
5. C. Y. Chiem, "Crash et Collision de Structures", Proc. "Entretiens Sciences et Défense", Ministère de la Défense, Délégation Générale pour l'Armenent, Paris Mai (1990).
6. J. Mescall and V. Weiss, "Material Behaviour under High Stress and Ultrahigh Loading Rates," Proc. Sagamore Army Materials Research", Conf. 29 (1982).
7. J. Duffy, Proc. Oxford Conference on "Mechanical Properties at High Rates of Strain," 47:1 (1979).
8. L. E. Malvern, Proc. Oxford Conference on "Mechanical Properties at High Rates of Deformation," 70:1 (1984).
9. C. Y. Chiem, "Proc. International Conference "IMPACT 87" I:57, Bremen (1987).
10. K. P. Staudhammer, Proc. International Conference "IMPACT 87", 1:93, Bremen (1987).
11. R. J. Clifton, A. Gilat, C. H. Li, "Metallurgical Behaviour under High Stress and Ultra-High Loading Rates," Plenum Publishing Corp. (1983).
12. L. E. Murr, Proc. "Materials at High Stran Rates", Ed. T. Z. Blazinski, Elsevier Appl. Sci., London and New York (1987).
13. J. Harding, "Materials at High Strain Rates," Elsevier Applied Science Publishers, London, 133 (1987).
14. C. Y. Chiem and Z. G. Liu, Proc. Euromech Colloquium 214 on "the Mechanical Behaviour of Composites and Laminates," Kupari, Yugoslavia, (1986).

15. B. Hwaija, C. Y. Chiem, and J. G. Sieffert, "Strain-Rate History Effects on the Mechanical Behaviour of Microconcrete, "European Conf. on Structural Dynamics, Bochum (FRG), (1990).

16. U. S. Lindholm, "Review of Dynamic Testing Techniques and Material Behaviour," Institute of Physics, Serie No. 21, 3, (1974).

17. I. N. Ward, "Mechanical Properties of Solid Polymers," J. Wiley & Sons, Ltd. (1979).

18. P. Ludwik, "Elemente der Technologischen Mechanik," Berlin (1909).

19. G. R. Johnson and W. H. Cook, 7th International Symposium on Baltistics, the Hague; April (1983).

20. U. S. Lindholm, J. Neck. *Phys. Solids,* 12:317 (1964).

21. L. E. Malvern, *J. Appl. Mech., 18*:203 (1951).

22. P. Perzyna, *Quant. Appl. Math., 20*:321 (1963).

23. D. J. Steinberg, S. G. Cochran, and N. W. Guinan, *J. Appl. Phys., 51*:3 (1980).

24. F. J. Erzrilli and R. W. Armstrong, *J. Appl. Phys., 30*:129 (1959).

25. L. W. Meyer, "Constitutive Equations at High Strain-Rate," this Proceeding, (1990).

26. F. E. Hauser, J. A. Simmons, and J. E. Dorn, "Response of Metals to High Velocity Deformation," Ed., P. G. Shewman et V. F. Zackay, 93 (1961).

27. J. D. Campbell, *Mater. Sci. and Eng.* 12-9 (1973).

28. J. F. Adler and V. A. Philips, *J. Inst. Metals* 83-80 (1954).

29. J. W. Edington, *Phil. Mag.,* 1741 (1969).

30. A. R. Rasenfield et G. T. Hahn, Trans. ASM, 963 (1966).

31. J. P. Dubois, P. Blinot, and C. Y. Chiem, *J. de Physique,* C5-13: 46 (1985).

32. J. Friedel, "Dislocations," Pergamon Press, London (1964).

33. W. S. Lee, "Corrélation entre la microstructure et les propriétés mécaniques de matériaux à base de tungstene soumis au cisaillement à grande vitesse," Thèse de Doctorat, E.N.S.M./Université de Nantes (France), June (1990).

34. C. Y. Chiem, and W. S. Lee, *Mater. Sci. and Engr.,* (to be published).

35. J. Klepaczko, Proc. Oxford Conf., 283 (1989).

36. J. R. Klepaczko and C. Y. Chiem: *J. Mech. Phys. Solids 34* (1986) 29.

37. J. R. Klepaczko, A. Rouxel, and C. Y. Chiem: *J. de Physique, 46* (1985) C5-29.

38. C. Y. Chiem and J. Duffy, *Matls. Sci. and Eng.* 57 (1983) 233.

39. C. Y. Chiem, Dr.-es-Sci. d'Etata, ENSM, Univ. de Nantes, Juin (1980).

40. J. Shioiri, K. Satoh, and K. Nishimura: Proc. "High Velocity Deformation of Solids," K. Kawata and J. Shioiri, (Eds.), Springerverlag, N.Y. (1978) 50.

41. C. Y. Chiem, Dr.-Ing. Thesis, ENSM, Nantes, Janvier (1976).

42. P. S. Follansbee, "Impact 87" (1987).

43. C. Y. Chiem, R. J. Cliffon, P. Blinot, and P. Kumar: Technical Report ENSM/ETCA NoP M/D G V/83/X-1 (1983).

44. K. M. Jassby and T. Jr. Vreeland: *Phil. Mag. 21* (1970) 1147.

45. V. R. Parameswaran and J. Weertman: *Met. Trans. 2* (1971)1233.

46. D. P. Pope and T. Jr. Vreeland: *Phil. Mag. 20* (1969) 1163.

47. E. Y. Gutmanas, E. M. Hadgornyi, and A. V. Stepanov: *Soviet Phys. Sol. State 5* (1963) 743.

48. D. W. Moon, and T. Jr. Vreeland: *J. Appl. Phys. 39* (168)1766.

49. W. G. Johnston, and J. J. Gilman: *J. Appl. Phys. 30* (1959)129.

50. J. E. Flinn, and R. F. Tinder: *Scripta Met. 8* (1974) 689.

51. U. F. Kocks, A. S. Argon, and M. F. Ashby: *Progr. Mat. Sci. 19* (1975), 1-288.

52. V. L. Indenbohm, Yu, Z. Estrin, In M. Balarin (Eds.): Reinststoffprobleme 5 (1977). Akademie-Verlag, Berlin, 683.

53. C. Y. Chiem, and M. Leroy, C. R. Acad. Sce., Paris 282 C(1976) 323.

54. C. Y. Chiem, and J. Duffy: Brown University Report NSF ENG75-18532/9 (1979).

55. J. Duffy: "Material Behaviour Under High Stress and Ultrahigh Loading Rates Sagamore Army Materials Research Conference Proceeddings, J. Mescall and V. Weiss (1982) 21.

56. E. Hornborgen, "High Energy Rate Working of Metals," Sandsfjord and Lillehammer (Eds.), NATO, 14-25 Sept. (1964) 345.

57. L. E. Murr, "Shock Wave and High Strain Phenomena in Metals," ed. L. E. Murr and M. A. Meyers Plenum Press, NY, 1981, pp. 607.

58. L. E. Murr, and M. A. Meyers, "In Explosive Welding, Forming and Compaction," ed T. Z. Blazynski, Applied Science Pub., London 1983, p. 83.

59. J. Weertman: "Metallurgical Effects at High Strain-Rate," N. Y., Plenum (1973) 319.

60. C. S. Smith: *Trans. Met. Soc. AIME 212* (1958) 574.

61. Y. Y. Earmme, and J. H. Weiner: *J. Appl. Phys. 48* (1977)3317.

62. J. H. Weiner, and M. Pearl: *Phil. Mag. 31* (1975) 679.

63. J. M. Walsh, and R. H. Christian, Phys. Rev. 97 (1955) p. 1544.

64. J. D. Ferry "Viscoplastic properties of polymers" New York, London, Sydney, Toronto, 1970.

65. I. M. Ward "Mechanical properties of solid polymers" - John Willey & Son, LTD 1971.

66. T. Vinh and T. Kha "Adiabatic and viscoplastic properties of some polymers at high strain and high strain rate" - Conference Series n°70. Institute of Physics Bristol and London 1984.

67. C. Y. Chiem, J. P. Ramousse and Z. G. Liu. "Le comportement d'adhésifs et de matières plastiques soumis aux grandes vitesses de déformation". Rapport technique de l'E.N.S.M. n°CRB-85-AP/F 1985.

68. E. H. Andres "Developments in polymer fracture-1" Applied Science Publisher 1979.

69. H. H. Kausch "Polymer-fracture" Springer-Verlag Berlin Heidelberg, New York 1978.

70. D. W. Von Krevelen "Properties of polymers" - Elsevier 1976.

71. C. Y. Chiem and M. Y. Liu, Proc. Of the "International Symposium on Intense Dynamic Loading and its effects 574-583, Ed. Science Press, Beijing, China (1986).

6

Microstructure and Fracture During High-Rate Forming of Iron and Tantalum

M. J. WORSWICK,* N. QIANG,† P. NIESSEN,† and R. J. PICK†

*Defense Research Establishment Suffield
Medicine Hat, Alberta, Canada, T1A 8K6

†Department of Mechanical Engineering
University of Waterloo
Waterloo, Ontario, Canada, N2L 3G1

The evolved microstructure and damage resulting from high strain rate deformation of high purity iron and tantalum have been studied in Taylor cylinder specimens and Explosively Formed Projectiles (EFPs). In the iron, deformation occurred through slip and mechanical twinning while fracture was through adiabatic shear localization and ductile fracture along these shear bands. The tantalum exhibited remarkable ductility and very low hardening rates. Deformation was entirely by slip leading to necking and ultimate chisel-type rupture. TEM work showed the deformed specimens to have a very complex cell structure with numerous dislocation loops.

* *Current address: Department of Mechanical and Aerospace Engineering, Carleton University, Colonel By Drive, Ottawa, Ontario, Canada, K1S 5B6*

I. INTRODUCTION

The design of optimal high-rate metal deformation processes depends on the determination of both accurate material constitutive relations and failure criteria. As a first step in the determination of failure criteria, a study of the deformation and fracture mechanisms in high purity iron and tantalum was undertaken. Two high rate deformation processes were considered: the Taylor cylinder and the Explosively Formed Projectile (EFP). In the Taylor cylinder experiments, specimens of Armco Iron and tantalum were impacted at velocities sufficient to cause damage and then sectioned for metallographic examination. EFPs fabricated from Armco Iron were studied in order to compare the deformation mechanisms under explosive loading to those experienced in the Taylor test.

II. EXPERIMENT

The Taylor specimens were 9 mm in diameter and 33 mm in length. For the iron specimens, a symmetric configuration was used in which one cylinder was fired into an identical, stationary target cylinder. The impact velocities of 420 and 525 m/s were sufficient to cause damage. The tantalum cylinders did not remain symmetrical after impact since flow instabilities developed. Consequently, they were fired against a hardened steel anvil at velocities in the range 182-316 m/s.

Explosively Formed Projectiles (EFPs) were fabricated from Armco Iron. These devices consist of a dish shaped metal liner backed by high explosive. Upon

(a) 8 mm Wave Shaper *(b) 16 mm Wave Shaper*

FIG. 1 *Predicted final shapes of iron EFPs. Contours of temperature (°C) and equivalent plastic strain are plotted on left and right, respectively.*